Politecnico di Torino

Master Dissertation

Electrochemical Evaluation of Low-Platinum Catalysts for the Oxygen Reduction Reaction in Fuel Cell Applications

By

Mehdi Alipour

Supervisor(s):

Prof. Juqin Zeng

Co-tutors:

Prof. Candido Fabrizio Pirri

Dr. Giulia Gianola

Politecnico di Torino

2025 _ 2026

Table of Contents

Chapter 1 – Introduction

1.1 Energy Conversion, Sustainability, and Electrochemical Power Generation

The continuous growth of global energy demand, driven by industrialization, urbanization, and technological development, has intensified concerns related to climate change, environmental degradation, and the depletion of fossil fuel resources. Conventional energy systems based on coal, oil, and natural gas are associated with significant emissions of greenhouse gases, particularly carbon dioxide (CO_2), which is widely recognized as a major contributor to global warming [1]. The accumulation of CO_2 in the atmosphere enhances the greenhouse effect, leading to rising global temperatures and increasingly frequent extreme weather events [2].

In response to these challenges, international research and policy efforts have increasingly focused on the transition toward sustainable energy systems characterized by low carbon intensity, high efficiency, and long-term resource availability [3]. Among the various clean energy technologies under investigation, electrochemical energy conversion systems have attracted considerable attention due to their ability to convert chemical energy directly into electrical energy without intermediate combustion steps, thereby avoiding the efficiency limitations imposed by thermal cycles.

Fuel cells represent a key class of electrochemical energy conversion devices. They operate by converting the chemical energy of a fuel and an oxidant directly into electricity through electrochemical reactions occurring at two spatially separated electrodes. A typical fuel cell consists of an anode, a cathode, and an electrolyte that conducts ions while preventing electronic short-circuiting between the electrodes. When hydrogen is employed as the fuel and oxygen as the oxidant, the overall electrochemical reaction is [4]:

$$2H_2 + O_2 \rightarrow 2H_2O \tag{1,1}$$

The maximum electrical work obtainable from this reaction is determined by the Gibbs free energy change (ΔG) [5]. The theoretical reversible cell voltage (E^0) under standard conditions is given by:

$$E^0 = -\Delta G^0 / (nF) \tag{1.2}$$

where n is the number of electrons transferred per mole of reaction (n = 4 for the hydrogen–oxygen fuel cell) and F is the Faraday constant. Under standard conditions, this expression yields a reversible cell voltage of approximately 1.23 V. In real operating conditions, however, the actual cell voltage is lower due to various irreversible losses.

The operating voltage of a fuel cell can be expressed as:

$$E = E^0 - \eta\_act - \eta\_ohm - \eta\_mt \tag{1.3}$$

where η_act represents the activation overpotential associated with reaction kinetics, η_ohm accounts for ohmic losses arising from ionic and electronic resistances, and η_mt corresponds to mass transport limitations. Among these contributions, the activation overpotential at the

cathode is typically the dominant loss, mainly due to the intrinsically slow kinetics of the oxygen reduction reaction (ORR).

The ORR is a complex, multi-electron process involving several elementary steps and the breaking of the strong O=O bond, which has a bond dissociation energy of approximately 498 kJ mol^{-1}. Depending on the catalyst and the electrolyte environment, ORR can proceed through different reaction pathways. The desired pathway is the direct four-electron reduction of oxygen to water.

Alternatively, oxygen reduction may proceed via a two-electron pathway, leading to the formation of hydrogen peroxide or hydroperoxide species. In acidic media, this pathway is described by [6]:

$$O_2 + 2H^+ + 2e^- \rightarrow H_2O_2 \quad (1.4)$$

The formation of peroxide species is undesirable because it reduces the overall energy efficiency of the fuel cell and can lead to chemical degradation of catalyst layers and membranes. Consequently, the development of electrocatalysts that selectively promote the four-electron ORR pathway is a central objective in fuel cell research.

Electrocatalysts facilitate ORR by lowering the activation energy of the reaction through stabilization of key reaction intermediates, such as OOH, O, and OH, adsorbed on the catalyst surface. The catalytic activity is strongly dependent on the electronic structure of the active sites and their interaction with oxygenated species. According to the Sabatier principle, optimal catalytic performance is achieved when the adsorption strength of reaction intermediates is neither too strong nor too weak.

Platinum-based catalysts are currently considered the benchmark materials for ORR due to their favourable interaction with oxygen intermediates and high intrinsic activity. However, their high cost, limited abundance, and susceptibility to degradation under fuel cell operating conditions significantly hinder large-scale commercialization. These limitations have driven extensive research into alternative catalyst systems, including platinum alloys, low-platinum-loading catalysts, and platinum-free materials.

Among platinum-free catalysts, transition metal–nitrogen–carbon (M–N–C) materials, and in particular iron–nitrogen–carbon (FeNC) catalysts, have emerged as promising candidates. These materials exhibit high ORR activity in alkaline environments and have demonstrated increasingly competitive performance in acidic media when synthesized and processed appropriately.

Within this framework, the present thesis focuses on the synthesis, physio-chemical characterization, and electrochemical evaluation of FeNC catalysts and platinum-based reference systems. Special attention is devoted to understanding how synthesis routes, platinum loading, and catalyst structure influence ORR performance under both fundamental Ring Rotating Disc electrode (RRDE) and application-relevant Gas Diffusion Electrode (GDE) testing conditions.

1.2 Fuel Cells and Their Operating Principles

Fuel cells are electrochemical devices that convert the chemical energy of a fuel directly into electrical energy. Unlike conventional combustion-based systems, fuel cells do not rely on thermal cycles, which allows them to achieve higher efficiencies and lower emissions. When hydrogen is used as the fuel, the only reaction byproduct is water, making fuel cells particularly attractive for clean energy and transportation applications [4].

1.2.1 Types of Fuel Cells

Fuel cells can be classified according to the type of electrolyte and their operating conditions. Among the different technologies, low-temperature fuel cells are particularly relevant for this work.Proton Exchange Membrane Fuel Cells (PEMFCs) use a polymer electrolyte membrane that conducts protons. They typically operate at relatively low temperatures (below 100 °C) and offer high power density and fast start-up, making them suitable for automotive applications. However, PEMFCs strongly rely on platinum-based catalysts, especially at the cathode. In acidic media, four-electron reduction of oxygen to water can be written as [7]:

$$O_2 + 4H^+ + 4e^- \rightarrow 2H_2O \quad (1.5)$$

Alkaline Fuel Cells (AFCs) operate in alkaline environments and show faster oxygen reduction kinetics compared to acidic systems. This allows the use of non-precious metal catalysts. Nevertheless, alkaline systems can be sensitive to carbon dioxide contamination, which limits their widespread application. In alkaline media, the corresponding reaction is:

$$O_2 + 2H_2O + 4e \rightarrow 4OH^- \quad (1.6)$$

High-temperature fuel cells, such as solid oxide fuel cells, are mainly used for stationary power generation and are not the focus of this thesis.

1.2.2 Importance of the Oxygen Reduction Reaction

In low-temperature fuel cells, the ORR occurs at the cathode and is widely recognized as the main performance-limiting step. Compared to hydrogen oxidation at the anode, ORR proceeds more slowly and requires effective catalysts to achieve practical current densities.

The sluggish kinetics of ORR lead to energy losses in the form of overpotential, reducing the overall efficiency of the fuel cell. For this reason, improving ORR activity is a central objective in fuel cell research.

Platinum-based catalysts are currently considered the benchmark for ORR, particularly in acidic environments. However, their high cost and limited availability motivate the development of alternative catalysts with reduced platinum content or completely platinum-free compositions.

1.2.3 Motivation for Catalyst Research

To address the challenges associated with platinum catalysts, significant research efforts have been dedicated to developing advanced catalyst materials with high activity and improved

durability. Among these, Fe–N–C catalysts have attracted considerable attention due to their promising ORR performance, especially in alkaline media [8].

The performance of such catalysts is strongly influenced by their synthesis route, precursor selection, and thermal treatment conditions. Therefore, a detailed investigation of catalyst preparation methods and their impact on electrochemical behaviour is essential.

In this context, the present work focuses on the synthesis and characterization of FeNC catalysts and platinum-based reference catalysts, with particular emphasis on understanding their ORR performance using RRDE and GDE electrochemical techniques.

1.3 Oxygen Reduction Reaction (ORR)

ORR is a fundamental electrochemical process that occurs at the cathode of low-temperature fuel cells and plays a decisive role in determining their overall efficiency. Despite its importance, ORR is intrinsically slow compared to the anodic reactions, such as hydrogen oxidation, and therefore represents the main kinetic bottleneck in fuel cell systems. This sluggish behaviour results in significant overpotentials, leading to voltage losses and reduced power output [9].

From a mechanistic point of view, ORR involves the reduction of molecular oxygen to either water or hydrogen peroxide through multi-electron transfer processes. The complexity of this reaction arises from the need to break the strong O=O double bond and to manage multiple proton-coupled electron transfer steps. The reaction pathway followed depends strongly on the nature of the catalyst, the electrolyte composition, and the operating environment.

1.3.1 Kinetic Limitations and Overpotential

The slow kinetics of ORR originate from the multiple elementary steps involved, including oxygen adsorption, electron transfer, proton transfer, and desorption of reaction products. Each of these steps contributes to the overall activation energy of the reaction. As a result, a substantial overpotential is required to drive ORR at practical current densities.

In electrochemical measurements, this kinetic limitation is reflected in the difference between the thermodynamic equilibrium potential of ORR and the experimentally observed onset or half-wave potential. Improving ORR kinetics therefore requires catalysts that can optimize the adsorption strength of oxygenated intermediates, ensuring neither too weak nor too strong binding, in accordance with the Sabatier principle [10].

1.3.2 Role of Electrocatalysts in ORR

Platinum-based catalysts are widely recognized as the benchmark materials for ORR due to their high intrinsic activity and favourable reaction kinetics. In particular, Pt supported on carbon (Pt/C) has been extensively used as a reference catalyst in both acidic and alkaline environments [11]. Nevertheless, the high cost and limited availability of platinum motivate the development of alternative catalysts that can either reduce platinum loading or replace it entirely.

In this context, FeNC catalysts have emerged as promising platinum-group-metal-free materials for ORR. These catalysts typically contain iron atoms coordinated with nitrogen functionalities embedded in a carbon matrix [12]. Although their activity is generally lower than that of Pt-based catalysts in acidic media, FeNC materials often show competitive performance in alkaline environments and improved tolerance toward certain contaminants.

Understanding the ORR mechanism and selectivity on different catalyst systems is therefore essential for rational catalyst design. Electrochemical techniques such as rotating ring–disk electrode (RRDE) measurements are particularly valuable in this respect, as they allow simultaneous evaluation of ORR activity and selectivity by quantifying peroxide formation and electron transfer number [13].

1.4 Mechanics and Pathways of Catalyst-Driven ORR

The performance of fuel cells is strongly dependent on the nature of the electrocatalyst employed at the cathode, where the oxygen reduction reaction takes place. As discussed in the previous section, ORR is kinetically slow and requires highly active catalytic surfaces to proceed at practical current densities. For this reason, significant research efforts have been devoted to the development of efficient ORR electrocatalysts that combine high activity, durability, and economic viability.

1.4.1 Platinum-Based Catalysts

Platinum-based materials are widely regarded as the state-of-the-art catalysts for ORR. Their superior performance arises from an optimal interaction between platinum surfaces and oxygenated intermediates, which facilitates efficient electron and proton transfer while avoiding excessive adsorption that would block active sites. Among the various platinum configurations, platinum nanoparticles supported on high-surface-area carbon (Pt/C) are the most commonly used in both fundamental studies and practical fuel cell systems.

The use of carbon supports serves multiple purposes. First, it enables uniform dispersion of platinum nanoparticles, increasing the number of accessible active sites. Second, it enhances electronic conductivity within the catalyst layer. Finally, carbon supports allow significant reduction of platinum loading while maintaining high catalytic activity. For these reasons, Pt/C catalysts are typically employed as benchmark materials in electrochemical studies and are used as reference systems for evaluating alternative catalyst formulations.

Despite their excellent activity, platinum-based catalysts suffer from several drawbacks. The high cost and limited availability of platinum represent major barriers to large-scale commercialization. In addition, platinum catalysts are susceptible to degradation phenomena such as particle agglomeration, carbon corrosion, and dissolution under prolonged electrochemical operation. These limitations have motivated research into strategies aimed at reducing platinum usage, improving its utilization efficiency, or replacing it entirely with non-precious alternatives.

1.4.2 Platinum Loading and Catalyst Utilization

One of the most effective strategies to reduce the overall cost of Pt-based catalysts is to lower the platinum loading while preserving catalytic performance. This can be achieved by optimizing platinum dispersion, particle size, and metal–support interactions.

In electrochemical characterization, catalyst performance is often evaluated in terms of mass activity and specific activity. These parameters allow meaningful comparison between catalysts with different platinum loadings and highlight the importance of synthesis conditions in controlling catalyst structure and performance.

1.4.3 Platinum-Group-Metal-Free (PGM-Free) Catalysts

To overcome the limitations associated with platinum, platinum-group-metal-free (PGM-free) catalysts have attracted increasing attention. FeNC catalysts offer several advantages, including low cost, abundant raw materials, and good performance in alkaline media. Although their activity in acidic environments is generally lower than that of Pt-based catalysts, continuous improvements in synthesis strategies have led to significant enhancements in ORR activity and durability. Moreover, FeNC catalysts often exhibit high selectivity toward the four-electron ORR pathway in alkaline electrolytes, making them attractive for alkaline fuel cells and metal–air battery applications.

1.4.4 Motivation for Comparative Catalyst Study

Given the distinct advantages and limitations of Pt/C and FeNC catalysts, a direct comparison between these two systems is essential for understanding their relative performance and identifying optimal operating conditions. In this thesis, both Pt/C and FeNC catalysts were investigated using identical electrochemical methodologies in acidic and alkaline environments. Furthermore, platinum was deposited on FeNC supports at different loadings to explore the combined effect of platinum content and support properties on ORR activity.

By systematically studying Pt/C, FeNC, and Pt-decorated FeNC catalysts under controlled conditions, this work aims to provide insight into the relationship between catalyst composition, synthesis method, and electrochemical performance. This comparative approach forms the foundation for the experimental investigations presented in the following chapters.

1.5 Electrochemical Techniques for the Evaluation of ORR Catalysts

The electrochemical performance of (ORR) catalysts cannot be fully assessed by material characterization alone. Instead, reliable electrochemical techniques are required to quantify catalytic activity, reaction kinetics, selectivity, and stability under controlled conditions. For this reason, several electrochemical methods have been developed and standardized for ORR studies, each offering different levels of insight into catalyst behaviour.

In this work, a (RRDE), and gas diffusion electrode (GDE) techniques was employed. The use of multiple electrochemical configurations allows comprehensive evaluation of catalyst

performance, ranging from fundamental kinetic analysis to more application-relevant testing conditions [14].

1.5.1 Rotating Disk Electrode (RDE) Technique

The rotating disk electrode technique is one of the most widely used methods for fundamental ORR studies. In this configuration, a thin catalyst layer is deposited on a polished glassy carbon disk, which is rotated at a controlled speed during electrochemical measurements. Rotation induces a well-defined hydrodynamic flow, ensuring uniform mass transport of dissolved oxygen from the bulk electrolyte to the electrode surface.

The main advantage of the RDE technique lies in its ability to decouple kinetic and mass-transport contributions to the measured current. By performing linear sweep voltammetry at different rotation rates, it is possible to analyse the ORR kinetics under controlled diffusion conditions. The measured current density is governed by both the intrinsic reaction kinetics and the diffusion of oxygen, allowing extraction of kinetic parameters through appropriate electrochemical analysis like Cyclic voltammetry, linear sweep voltammetry and etc.

1.5.2 Rotating Ring–Disk Electrode (RRDE) Technique

The rotating ring–disk electrode technique represents an extension of the RDE method and provides additional insight into ORR reaction pathways. In the RRDE configuration, the working electrode consists of a central disk surrounded by a concentric ring electrode, electrically insulated from each other. While the disk is used to drive the ORR, the ring is held at a fixed potential to detect reaction intermediates produced at the disk surface.

One of the most important advantages of RRDE measurements is the ability to quantify hydrogen peroxide formation during ORR. By recording the current established at the ring we can have information about the peroxide yield and understand if producing water or hydroxide ions or producing hydrogen peroxide ions.

From simultaneous disk and ring current measurements, the peroxide yield and the average number of electrons transferred per oxygen molecule can be calculated. These parameters are critical for evaluating catalyst selectivity, as high peroxide production is generally undesirable due to reduced energy efficiency and membrane degradation [15].

In addition to selectivity analysis, 4-electrode measurements enable construction of Koutecky–Levich plots by combining data collected at multiple rotation speeds [16]. This analysis allows verification of kinetic control and provides further insight into the ORR mechanism. For these reasons.

1.5.3 Importance of Reproducibility in RRDE Measurements

Despite its advantages, RRDE & RDE measurements are sensitive to several experimental factors, including electrode surface quality, catalyst layer uniformity, and electrolyte purity. Variations in glassy carbon disk properties can significantly affect measured currents and lead to non-reproducible results if not properly controlled.

For this reason, particular attention must be paid to electrode preparation, electrochemical cleaning, and repetition of measurements. Performing multiple measurements under identical conditions and comparing the resulting curves is essential to ensure data reliability. In this thesis, reproducibility was systematically evaluated by repeating each RRDE test and directly comparing the results before selecting representative datasets for analysis taking into account that error ranges are included in the evaluation of the parameters.

1.5.4 Gas Diffusion Electrode (GDE) Technique

While RDE and RRDE techniques are well suited for fundamental studies, they do not accurately replicate the operating conditions of practical fuel cells. In real devices, oxygen is supplied in the gas phase rather than dissolved in the electrolyte, and the catalyst operates at much higher current densities.

The gas diffusion electrode technique was developed to address these limitations. In a GDE configuration, the catalyst layer is deposited onto a porous gas diffusion layer that allows gaseous oxygen to reach the catalyst directly through interconnected pores. This creates a three-phase boundary where gas, liquid electrolyte, and solid catalyst coexist, closely resembling fuel cell cathode conditions. GDE measurements enable evaluation of ORR performance at significantly higher current densities compared to RDE and RRDE.

1.5.5 Complementary Use of RRDE and GDE Techniques

Each electrochemical technique employed in this work serves a specific purpose. RRDE measurements provide detailed information on intrinsic activity, reaction kinetics, and selectivity under controlled conditions, while GDE measurements assess catalyst performance under gas-fed, high-current-density operation.

By combining RRDE and GDE methodologies, it is possible to establish a direct link between fundamental catalytic properties and application-relevant performance. This comprehensive electrochemical approach enables reliable comparison between Pt/C and FeNC catalysts and allows evaluation of synthesis strategies, platinum loading, and support effects under both idealized and realistic conditions.

The electrochemical techniques described in this section form the methodological foundation for the experimental investigations presented in the following chapters.

1.6 Scope and Objectives of the Thesis

The increasing demand for efficient, durable, and cost-effective electrocatalysts for energy conversion technologies has motivated extensive research into alternatives to conventional platinum-based materials. In particular, the oxygen reduction reaction (ORR) remains a critical bottleneck in fuel cell performance due to its inherently slow kinetics and strong dependence on catalyst properties. Within this context, the present thesis focuses on the synthesis, characterization, and electrochemical evaluation of both platinum-based and platinum-free catalysts for ORR applications.

The primary scope of this work is to investigate how different synthesis strategies and platinum loadings influence the structural, physicochemical, and electrochemical properties of ORR

catalysts. Special attention is devoted to iron–nitrogen–carbon (FeNC) materials, which represent a promising class of non-precious metal catalysts, as well as to conventional platinum-on-carbon (Pt/C) catalysts used as benchmark systems.

To achieve this goal, two distinct synthesis approaches were explored for both Pt/C and Pt-decorated FeNC catalysts. The first approach involves microwave-assisted synthesis, which offers rapid heating, reduced synthesis time, and potentially improved metal dispersion. The second approach relies on thermal treatment under hydrogen atmosphere, allowing controlled reduction of platinum precursors and providing a reference method for comparison. For each synthesis route, platinum loadings of 2 wt%, 5 wt%, and 10 wt% were investigated in order to evaluate the effect of metal content on catalyst performance and dispersion.

In addition to catalyst synthesis, a comprehensive characterization strategy was adopted. Physio-chemical techniques like FESEM, ICP and TGA were employed to analyse surface area, porosity, morphology, crystallinity, and thermal stability of the synthesized materials. These analyses provide essential information for understanding the relationship between catalyst structure and electrochemical behaviour.

Electrochemical characterization constitutes a central part of this thesis. Fundamental ORR activity and selectivity were evaluated using rotating disk electrode (RDE) and rotating ring–disk electrode (RRDE) techniques in both acidic and alkaline electrolytes. These methods allow detailed analysis of ORR kinetics, reaction pathways, and peroxide formation. To complement these studies and assess catalyst performance under more realistic operating conditions, gas diffusion electrode (GDE) measurements were also performed, enabling evaluation at higher current densities and under gas-fed conditions.The specific objectives of this thesis can be summarized as follows:

- To synthesize FeNC catalysts and Pt/C reference catalysts using microwave-assisted and hydrogen-purged thermal methods.
- To investigate the influence of platinum loading on catalyst structure and dispersion.
- To characterize the synthesized materials using physio-chemical techniques such as, FESEM, ICP and TGA.
- To evaluate ORR activity, selectivity, and reproducibility using RRDE measurements in acidic and alkaline media.
- To assess catalyst performance under practical conditions using GDE testing.
- To compare Pt-based and Pt-free catalysts and identify the most promising synthesis conditions for ORR applications.

By addressing these objectives, this thesis aims to provide a systematic and coherent analysis of how synthesis conditions affect ORR catalyst performance. The results obtained contribute to a deeper understanding of the potential and limitations of FeNC catalysts and offer insight into strategies for reducing platinum usage without compromising electrochemical performance.

Chapter 2 - Materials and Experimental Methods

2.1 Experimental Strategy

The pressing need to replace platinum-based catalysts due to cost and durability constraints has already been introduced. Among the alternative platinum-group-metal-free (PGM-free) systems, iron–nitrogen–carbon (FeNC) materials represent one of the most promising avenues owing to their high intrinsic activity derived from atomically dispersed FeN_x active sites [17].

Building upon these foundational concepts, this chapter introduces a novel, lab-made FeNC material designed to address the typical durability and activity limitations observed under demanding operational conditions. Specifically, we focus on the strategy and synthesis techniques employed to optimize its structure and enhance overall catalytic performance.

The experimental strategy of this work is based on the rational combination of FeNC catalysts with controlled platinum incorporation, aiming to exploit the synergistic effects between FeN_x sites and metallic Pt nanoparticles [18]. By replacing conventional Pt/C catalysts with FeNC based systems, it is possible to significantly reduce platinum content while preserving or even enhancing ORR performance. This hybrid approach offers a pathway toward cost-effective, high-performance electrocatalysts suitable for advanced electrochemical energy conversion devices.

A central aspect of this study is the systematic investigation of platinum loading, specifically 2 wt%, 5 wt%, and 10 wt% Pt, deposited onto FeNC and carbon supports. These loadings were deliberately selected to cover a wide range of Pt contents, enabling direct comparison between low-Pt, intermediate-Pt, and benchmark-like catalyst systems. This approach allows assessment of the minimum platinum amount required to achieve competitive ORR activity while maintaining favourable kinetics and mass transport properties.

To further strengthen the experimental design, two different synthesis methodologies were employed for platinum incorporation:

- microwave-assisted synthesis
- hydrogen-purged thermal reduction

Microwave synthesis offers rapid, volumetric heating and enhanced nucleation kinetics, which can lead to uniform Pt nanoparticle dispersion and reduced synthesis time. In contrast, hydrogen purge reduction provides a more conventional and controlled reduction environment, allowing careful evaluation of the influence of synthesis atmosphere and thermal history on catalyst structure and performance. Comparing these two approaches enables a deeper understanding of structure–property relationships in Pt-containing FeNC catalysts.

The FeNC catalyst itself was synthesized using a hard-template strategy based on SBA-15 mesoporous silica, selected for its well-defined pore structure, high surface area, and ability to direct carbon morphology during high-temperature pyrolysis [19]. This templating approach facilitates the formation of a porous, conductive carbon framework with homogeneously distributed active sites. Post-pyrolysis iron oxide or nanoparticles removal, combined with alkaline and acidic leaching steps, was carefully designed to eliminate non-conductive silica

residues and unstable iron species, ultimately yielding a purified and electrochemically active FeNC material.

Comprehensive physio-chemical characterization was carried out to establish a clear correlation between synthesis conditions, material structure, and catalytic behaviour. Techniques including, Field Emission Scanning Electron Microscopy (FESEM), Inductively Coupled Plasma (ICP) and thermogravimetric analysis (TGA) were employed to evaluate, morphology, compositional verification and thermal stability of the catalysts.

Electrochemical performance was assessed using both rotating ring–disk electrode (RRDE) and gas diffusion electrode (GDE) techniques. RRDE measurements were employed to investigate intrinsic ORR kinetics, electron transfer number, and peroxide formation under well-controlled mass transport conditions. In contrast, GDE measurements were used to evaluate catalyst performance under high current densities and realistic gas-fed conditions, bridging the gap between fundamental electrochemical testing and practical fuel cell operation. The combined use of RRDE and GDE provides a comprehensive and robust evaluation of catalyst activity, selectivity, and applicability.

Overall, this chapter presents the materials, synthesis routes, characterization techniques, and electrochemical methodologies employed in this work. The experimental framework was deliberately designed to ensure reproducibility, systematic comparison between catalyst systems, and meaningful interpretation of structure–performance relationships. The results obtained from this approach provide a solid foundation for the discussion presented in subsequent chapters.

2.2 Materials and Chemicals

All chemicals and materials employed in this work were of analytical grade or higher and were used as received without further purification unless otherwise specified. Particular attention was devoted to the selection of precursors and reagents in order to ensure reproducibility of the synthesis procedures and reliability of the electrochemical and physio-chemical characterization results.

2.2.1 Precursors and Reagents for SBA-15 Mesoporous Silica Synthesis

The synthesis of SBA-15 mesoporous silica requires the use of a structure-directing agent, a silica source, and an acidic medium to promote micelle formation and controlled hydrolysis–condensation reactions. All reagents were selected to ensure the formation of a highly ordered mesoporous structure with narrow pore size distribution and high thermal stability.

The triblock copolymer Pluronic P123 was employed as the structure-directing agent. This non-ionic surfactant self-assembles in aqueous acidic media to form cylindrical micelles, which act as templates for the formation of the mesoporous silica framework [19]. P123 was chosen due to its well-established ability to produce SBA-15 with long-range hexagonal ordering and uniform pore channels [20].

Tetraethyl orthosilicate (TEOS) was used as the silica precursor. TEOS undergoes acid-catalysed hydrolysis and subsequent condensation reactions, forming a silica network around

the P123 micellar structure. The use of TEOS ensures controlled silica polymerization and high structural integrity of the final SBA-15 material.

Hydrochloric acid (HCl) was employed to create a strongly acidic environment, which is essential for stabilizing the P123 micelles and regulating the kinetics of TEOS hydrolysis. The acidic medium promotes ordered self-assembly and prevents premature silica precipitation.

Deionized water was used as the solvent for dissolving the surfactant and facilitating the hydrolysis–condensation reactions. The purity of the water plays a crucial role in achieving reproducible pore structure and high surface area.

Following synthesis, template removal was achieved via thermal calcination, during which the organic P123 surfactant is decomposed and removed, leaving behind the ordered mesoporous silica framework. The resulting SBA-15 material exhibits a high specific surface area, well-defined mesopores, and excellent thermal stability, making it suitable as a hard template for Fe–N–C catalyst synthesis.

2.2.2 Precursors for FeNC Catalyst Synthesis

The synthesis of the FeNC catalyst was based on a hard-template approach using mesoporous silica, combined with molecular iron and nitrogen-containing precursors to promote the formation of FeN_x active sites embedded within a conductive carbon matrix.

Mesoporous silica SBA-15 was employed as a sacrificial template due to its high surface area, ordered hexagonal pore structure, and excellent thermal stability at high temperatures. SBA-15 acts as a structure-directing agent during carbonization, enabling the formation of a porous carbon framework with controlled morphology. The non-conductive nature of silica necessitates its complete removal after pyrolysis to obtain an electrochemically active material.

Iron nitrate ($Fe(NO_3)_3$) was used as the iron source. This salt was selected due to its high solubility in polar solvents, homogeneous dispersion capability within the precursor mixture, and effective decomposition during pyrolysis, which facilitates the formation of iron-coordinated nitrogen sites. Iron plays a critical role in the generation of catalytically active FeN_x which are widely recognized as primary active centres for ORR in FeNC catalysts.

1,10-Phenanthroline was employed as both nitrogen and carbon precursor. This heterocyclic aromatic compound was chosen due to its strong chelating ability toward iron ions, which promotes intimate Fe–N coordination prior to pyrolysis [21]. During high-temperature treatment, phenanthroline decomposes and contributes nitrogen functionalities to the carbon matrix, enhancing both electrical conductivity and ORR activity. In this work, the unhydrated form of phenanthroline was used, and precursor masses were adjusted accordingly to maintain stoichiometric consistency.

Solvent systems consisting of deionized water (H_2O) and ethanol (EtOH) were used during precursor impregnation and mixing steps. The mixed solvent system ensured adequate dissolution of iron nitrate and phenanthroline while promoting uniform dispersion of SBA-15 particles.

2.2.3 Chemicals for Template Removal and Catalyst Purification

Post-pyrolysis purification steps are critical for obtaining an electrochemically active FeNC catalyst. For this purpose, sodium hydroxide (NaOH) was used to selectively dissolve the silica template. NaOH effectively attacks the Si–O–Si network of SBA-15, enabling complete removal of the non-conductive silica framework while preserving the carbonaceous structure formed during pyrolysis. Due to the corrosive nature of NaOH, all alkaline treatments were conducted in polytetrafluoroethylene (PTFE, Teflon) containers.

Hydrochloric acid (HCl, 37 wt%) was employed for acid leaching to remove unstable iron species, residual inorganic impurities, and iron nanoparticles not coordinated within the FeN_x framework. Acid treatment improves catalyst durability and selectivity by eliminating species that may promote parasitic reactions or degrade under electrochemical operation.

Additional washing steps were performed using deionized water and ethanol to remove residual acids, bases, and soluble by-products, ensuring the chemical purity of the final catalyst.

2.2.4 Materials for Platinum Deposition

Platinum deposition onto FeNC and carbon supports was carried out using appropriate platinum precursors, solvents, and reducing environments. Although the fundamental support materials differed (FeNC versus carbon black), the platinum loadings were systematically fixed at 2 wt%, 5 wt%, and 10 wt% in all cases to enable meaningful comparison between synthesis routes and catalyst compositions.

For comparative purposes, commercial carbon black (40%Pt/Vulcan) was used as a reference support material for the synthesis of Pt/C catalysts. This allowed direct benchmarking against conventional platinum-based ORR catalysts synthesized under identical conditions [22].

Two distinct synthesis environments were employed for platinum deposition:

- Microwave-assisted synthesis, using polar solvents to enable rapid heating and homogeneous nucleation.
- Hydrogen-purged thermal reduction, where molecular hydrogen acted as a reducing agent under controlled temperature conditions.

The choice of synthesis route was intentionally designed to evaluate the influence of reduction kinetics, thermal history, and gas atmosphere on platinum particle dispersion and catalytic performance.

2.2.5 Materials for Electrochemical Measurements

Electrochemical characterization was conducted using high-purity reagents to minimize contamination and ensure reproducibility.

Electrolytes included 0.1 molar alkaline and acidic solutions, such as potassium hydroxide (KOH)(3.3 gr KOH pellet plus 0.5l water) and perchloric acid ($HClO_4$) (4.3 ml $HClO_4$ plus 0.5 l deionized water), prepared using ultrapure water. These electrolytes were selected to

investigate ORR performance under different pH environments and to assess catalyst stability across a wide operational range.

Nafion® solution was used as an ionomer and binder in catalyst ink formulations. Nafion promotes mechanical adhesion of the catalyst layer to the electrode surface while providing ionic conductivity within the catalyst film.

Isopropyl alcohol (IPA) and deionized water were employed as solvents for ink preparation, ensuring adequate dispersion of catalyst particles and uniform film formation during electrode fabrication.

For RRDE measurements, glassy carbon disk electrodes and platinum ring electrodes were used. Gas diffusion electrodes (GDEs) were employed for high-current-density testing under gas-fed conditions, providing a more realistic evaluation of catalyst performance.

2.3 Synthesis of SBA-15 Mesoporous Silica

Mesoporous silica SBA-15 was synthesized via a surfactant-templated sol–gel method under strongly acidic conditions [23]. This synthesis route was selected due to its ability to produce materials with a highly ordered two-dimensional hexagonal pore structure, large surface area, and thick pore walls, ensuring sufficient thermal and mechanical stability for subsequent high-temperature FeNC catalyst synthesis.

2.3.1 Reagents

The synthesis of SBA-15 was carried out using the following precursors:

- Pluronic P123 : structure-directing agent
- Tetraethyl orthosilicate (TEOS): silica source
- Hydrochloric acid (HCl, 37 wt%): acidic medium and hydrolysis catalyst
- Deionized water: solvent

In a typical synthesis, 10 g of Pluronic P123 was used as the surfactant template. The acidic medium consisted of 340 mL of deionized water and 48.8 mL of hydrochloric acid (37 wt%), providing the strongly acidic conditions necessary for micelle stabilization and controlled silica condensation. 24 g of TEOS was employed as the silica precursor.

2.3.2 Surfactant Dissolution and Micelle Formation

Pluronic P123 (10 g) was added to a mixture of deionized water (340 mL) and concentrated HCl (48.8 mL, 37 wt%) in a 1 litre Teflon Reactor. The solution was heated to 35–40 C° and magnetically stirred for approximately 5-6 hours, until a clear and homogeneous solution was obtained. This step is critical to ensure complete dissolution of the triblock copolymer and uniform formation of cylindrical micelles, which ultimately dictate the pore architecture of SBA-15.

The acidic environment promotes protonation of the ethylene oxide chains, stabilizing the micellar structure and preventing premature phase separation.

2.3.3 Silica Condensation and Aging

Once complete dissolution of P123 was achieved, 24 g of TEOS was added dropwise to the surfactant solution under continuous stirring.

After TEOS addition, the mixture was stirred continuously at 35–40 C° for 20 hours to allow acid-catalysed hydrolysis and initial condensation of the silica species around the P123 micelles. During this period, the formation of an ordered organic–inorganic mesostructured takes place.

Following the stirring step, the reaction mixture was transferred to a sealed container and subjected to a static aging treatment at 100 °C for 24 hours. The aging process promotes further condensation of the silica framework, increases pore wall thickness, and enhances long-range mesostructural ordering.

2.3.4 Recovery and Drying

After aging, the solid product was recovered by filtration and thoroughly washed with deionized water several times to remove residual hydrochloric acid and unreacted species. The filtered material was then dried at 60–80 C° overnight under ambient atmosphere to eliminate physically adsorbed moisture. At this stage, the material consists of silica containing the embedded organic P123 template and is not yet mesoporous.

2.3.5 Calcination and Template Removal

To remove the organic surfactant and obtain the final mesoporous silica structure, the dried solid was subjected to calcination in air. The temperature was increased at a controlled heating rate of 2 $C°\cdot min^{-1}$ to a final temperature of 550 C°, which was maintained for 10 hours.

This slow heating program is essential to prevent structural collapse and to ensure complete decomposition and removal of the P123 template. During calcination, the organic surfactant is oxidized, and the silica framework becomes fully condensed and mechanically robust.

The resulting SBA-15 material appears as a fine white powder and exhibits a highly ordered mesoporous structure with uniform pore size distribution and high specific surface area.

2.4 Synthesis of FeNC Catalyst

The FeNC catalyst was synthesized using a hard-template strategy based on SBA-15 mesoporous silica, combined with iron and nitrogen precursors. This approach enables precise control over the morphology, porosity, and distribution of catalytically active sites within the carbon matrix. The synthesis procedure involves precursor impregnation, controlled solvent evaporation, high-temperature pyrolysis under inert atmosphere, chemical removal of the silica template, and acid leaching to obtain the purified FeNC catalyst.

2.4.1 Precursors and Reagents

The following materials were used for the synthesis of the FeNC catalyst:

- SBA-15 mesoporous silica: 500 mg (hard template)
- Iron nitrate ($Fe(NO_3)_3$): 400 mg (iron source)
- Phenanthroline-1,10 (unhydrated): 492 mg (nitrogen and carbon source) *(If hydrated phenanthroline were used, the corresponding mass would be 540 mg; however, in this work the unhydrated form was employed.)*
- Deionized water (H_2O): solvent
- Ethanol (EtOH): co-solvent

2.4.2 Preparation of Precursor Solutions

To ensure homogeneous distribution of all components, the precursors were initially dissolved and dispersed in two separate solutions.

In the first beaker, 500 mg of SBA-15 was added to a mixture of 10 mL deionized water and 10 mL ethanol. The suspension was placed on a magnetic stirrer and stirred for several minutes until uniform dispersion of the silica particles was achieved.

In a second beaker, 400 mg of iron nitrate ($Fe(NO_3)_3$) and 492 mg of unhydrated 1,10-phenanthroline were dissolved in 5 mL deionized water and 5 mL ethanol. This solution was magnetically stirred for several minutes to ensure complete dissolution and complexation between the iron ions and the phenanthroline molecules. The use of phenanthroline promotes strong Fe–N coordination prior to pyrolysis, which is essential for the formation of FeN_x active sites.

2.4.3 Combined Mixing and Aging

After complete dispersion of the SBA-15 suspension, the entire content of the first beaker was slowly added to the second beaker containing the iron nitrate and phenanthroline solution. The combined mixture was magnetically stirred for several minutes to ensure thorough mixing and uniform impregnation of the SBA-15 template with the FeNC precursors.

The beaker was then covered with aluminium foil, and several small holes were pierced in the foil to allow controlled solvent evaporation. The covered beaker was placed on a hot plate and maintained at 75 C° for 24 hours. During this aging period, slow evaporation of the water–ethanol solvent promotes infiltration of the precursors into the mesopores of SBA-15 and facilitates intimate contact between iron, nitrogen, and carbon sources.

At the end of the aging step, the solvent had completely evaporated, and a dry precursor powder remained in the beaker.

2.4.4 Pyrolysis under Nitrogen Atmosphere

The dried precursor powder was carefully collected and transferred into a tubular furnace for high-temperature pyrolysis. The furnace was purged continuously with nitrogen gas (N_2) to establish and maintain an inert atmosphere throughout the thermal treatment.

The temperature was increased at a controlled heating rate of 5 C°/min up to a final temperature of 900 C°. Once the target temperature was reached, the system was maintained at 900 C° for 3 hours. This dwell time ensures complete carbonization of the phenanthroline-derived carbon, decomposition of the iron nitrate, and formation of FeN_x active sites embedded within the carbon matrix.

The nitrogen atmosphere prevents oxidation of the carbon framework and preserves the structural integrity of the material during pyrolysis. After completion of the thermal treatment, the furnace was allowed to cool naturally to room temperature under continuous nitrogen flow. The resulting material appeared as a black powder.

2.4.5 Alkaline Removal of SBA-15 Template

To remove the non-conductive silica template and obtain a conductive carbon material, the pyrolyzed powder was subjected to alkaline treatment using sodium hydroxide.

The black powder was transferred into a Teflon (PTFE) beaker, and a washing solution consisting of 80 mL deionized water, 80 mL ethanol, and 12.8 mg sodium hydroxide (NaOH) was added. The use of 2 molar NaOH enables dissolution of the silica framework of SBA-15, which is essential because silica is electrically insulating and would otherwise hinder electrochemical performance. The reaction between silica and NaOH can be represented as follows [24] [25] [26]:

$$SiO_2+2NaOH \rightarrow Na2SiO_3 \text{ (soluble silicate)}+2H_2O \quad (2.1)$$

The mixture was allowed to react, after which the solid–liquid separation was performed using centrifugation.

2.4.6 Centrifugation and Washing Procedure

The suspension was centrifuged at maximum rotational speed (5000 rpm) for 10 minutes. A total of four centrifugation cycles were carried out.

- First cycle: the original NaOH–water–ethanol mixture was centrifuged, and the supernatant containing dissolved silica was discarded.
- Second to fourth cycles: fresh deionized water was added to the solid, followed by centrifugation at maximum speed for 10 minutes and decantation of the supernatant after each cycle.

These repeated washing steps ensure complete removal of residual NaOH and dissolved silica species.

2.4.7 Acid Leaching and Final Purification

After alkaline treatment and washing, the catalyst was transferred to a clean beaker for acid leaching. Hydrochloric acid (37 wt%) was added to reach a total volume of 100 mL, and the suspension was magnetically stirred for 3 hours. This acid treatment removes unstable iron

species, residual inorganic impurities, and iron nanoparticles not coordinated within the FeN_x structure. The reaction is as follows [25] [27]:

$$Fe+2HCl \rightarrow FeCl_2+H_2 \quad (2.2)$$

$$Fe_2O_3+6HCl \rightarrow 2FeCl_3+3H_2O \quad (2.3)$$

$$Fe_3O_4+8HCl \rightarrow FeCl_2+2FeCl_3+4H_2O \quad (2.4)$$

Following acid leaching, the suspension was centrifuged to remove the acidic supernatant. The solid was then washed twice with deionized water and once with ethanol, each time followed by centrifugation and decantation.

2.4.8 Final Drying

The washed catalyst was transferred to a suitable container, covered with aluminium foil, and perforated to allow solvent evaporation. The sample was placed in an oven and dried until complete evaporation of residual solvents was achieved.

After drying, a fine black powder was obtained, corresponding to the purified FeNC catalyst, which was used for subsequent physio-chemical and electrochemical characterization.

2.4.9 Second Pyrolysis Treatment

To further enhance the structural stability, electrical conductivity, and formation of active FeN_x sites, the dried FeNC powder obtained after chemical purification was subjected to a second thermal treatment. The dried catalyst powder was carefully transferred into a tubular furnace and uniformly distributed within the heating zone. Prior to heating, the furnace was purged with nitrogen gas (N_2) at a pressure of 500 psi to ensure an inert atmosphere and prevent oxidation during thermal treatment. The temperature was increased at a controlled heating rate of 5 C°/min up to a final temperature of 900 C°, identical to the conditions employed during the first pyrolysis step. Once the target temperature was reached, the sample was maintained at 900 C° for 3 hours. This second dwell period promotes further graphitization of the carbon matrix, improves electrical conductivity, and stabilizes the FeN_x active sites by eliminating residual functional groups and volatile species. Throughout the thermal treatment, a continuous nitrogen flow was maintained to preserve the chemical and structural integrity of the catalyst. After completion of the dwell time, the furnace was allowed to cool naturally to room temperature under nitrogen atmosphere.

The resulting material was collected as a fine black powder and represents the final FeNC catalyst used for subsequent physio-chemical characterization and electrochemical evaluation [28].

2.5 Microwave-Assisted Deposition of Platinum on Carbon and FeNC Supports

2.5.1 Experimental Rationale and Optimization Strategy

Prior to platinum deposition on FeNC catalysts, a systematic optimization study was conducted using carbon-supported platinum (Pt/C) catalysts. This preliminary investigation was designed to identify the most suitable microwave synthesis parameters in terms of target temperature and dwelling time, with the objective of achieving homogeneous platinum dispersion while minimizing nanoparticle agglomeration.

Excessive platinum agglomeration leads to a reduction in electrochemically active surface area and promotes Ostwald ripening, which is detrimental to catalytic performance [29]. Therefore, optimizing microwave synthesis conditions was a necessary step before extending the method to FeNC–supported catalysts.

2.5.2 Materials and Precursor Preparation

Hydrogen hexachloro platinate(IV) hydrate 90% ($H_2PtCl_6 \cdot xH_2O$) (*sigma aldrich*) was employed as the platinum precursor. Commercial black carbon was used as the support material for the optimization study. Ethylene glycol served both as solvent and reducing agent, due to its strong microwave absorption and ability to reduce platinum ions under thermal treatment [30].

All initial Pt/C syntheses for parameter screening were carried out at a fixed platinum loading of 10 wt%, allowing the effect of microwave temperature and dwelling time to be isolated without introducing compositional variability.

The platinum precursor (12.5 mg) was first dissolved in 20 mL of ethylene glycol, while black carbon (45 mg) was separately dispersed in 25 mL of ethylene glycol. Each suspension was magnetically stirred independently until complete homogenization was achieved. Subsequently, the two solutions were combined and stirred to ensure uniform mixing prior to microwave treatment.

2.5.3 Microwave Synthesis Parameter Screening on Pt/C

Microwave-assisted reduction was performed to deposit platinum nanoparticles onto the carbon support. A constant ramp time of 1 minute was applied in all experiments, while the target temperature and dwelling time were varied to assess their influence on platinum dispersion. Four different microwave synthesis conditions were investigated:

- 140 °C, ramp time 1 minute, dwelling time 10 minutes
- 140 °C, ramp time 1 minute, dwelling time 5 minutes
- 120 °C, ramp time 1 minute, dwelling time 5 minutes
- 140 °C, ramp time 1 minute, dwelling time 2 minutes

These conditions were selected to evaluate the effects of both thermal energy input and exposure time on platinum nucleation and growth. Shorter dwelling times were expected to

limit particle coalescence, while lower target temperatures were investigated to minimize excessive nanoparticle growth.

After microwave treatment, each synthesized suspension was transferred into Falcon tubes and centrifuged to separate the solid catalyst from the ethylene glycol. The supernatant was discarded, and the solid powders were washed three times with deionized water, followed by a final washing step with ethanol. The washed catalysts were then dried in an oven for 24 hours.

2.5.4 FESEM Analysis and Selection of Optimal Microwave Conditions

The dried Pt/C catalysts were transported to the Politecnico di Torino laboratory for field-emission scanning electron microscopy (FESEM) analysis. FESEM imaging was employed to evaluate platinum nanoparticle size, dispersion uniformity, and degree of agglomeration.

Among the investigated conditions, the microwave synthesis performed at 120 °C with a dwelling time of 5 minutes resulted in the most homogeneous platinum dispersion on the carbon support. This condition exhibited the lowest degree of platinum agglomeration and was therefore selected as the optimal microwave synthesis protocol. Minimizing agglomeration is critical for preserving active surface area and preventing Ostwald ripening, which adversely affects electrocatalytic performance.

2.5.5 Optimization of the Pre-Mixing Procedure

Following identification of the optimal microwave parameters, the precursor mixing procedure was further optimized to enhance platinum dispersion. After separate preparation of the platinum precursor solution and carbon suspension, the combined mixture was subjected to the following homogenization protocol:

- 15 minutes of magnetic stirring
- 30 minutes of sonication
- An additional 15 minutes of magnetic stirring

This enhanced pre-mixing procedure was introduced to improve precursor–support interaction and promote more uniform platinum nucleation during microwave heating.

Using this optimized mixing protocol and the selected microwave condition (120 °C, 5 minutes dwelling time), Pt/C catalysts were synthesized at 10 wt%(12.5mg Pt+45mg Carbon Black), 5 wt%(6.25mg Pt + 47.5mg Carbon Black), and 2 wt%(1.25mg Pt + 49.5mg Carbon Black) platinum loadings.

2.5.6 Real Temperature Behaviour During Microwave Synthesis

Although the microwave reactor target temperature was set to 120 C°, real-time temperature monitoring revealed a transient temperature overshoot during the initial heating phase, followed by stabilization at a slightly higher dwelling temperature.

For Pt/C catalysts, the following temperature behaviour was observed:

- 10 wt% Pt/C: initial temperature peak at 147C°, followed by stabilization at approximately 125 C°
- 5 wt% Pt/C: temperature exceeded 120C°, reaching 143C°, then stabilized at approximately 125 C°
- 2 wt% Pt/C: similar behaviour, with a peak at 143 C° and stabilization around 125 C°

A comparable trend was observed for Pt/FeNC catalysts:

- 10 wt% Pt/FeNC: temperature exceeded 120 C° and reached 142 C°, then stabilized at approximately 124 C°
- 5 wt% Pt/FeNC: temperature peak at 147 C°, followed by stabilization around 124 C°
- 2 wt% Pt/FeNC: similar behaviour to the 5 wt% sample, with a peak at approximately 147 C° and dwelling at 124 C°

This temperature overshoot is attributed to the strong microwave absorption of ethylene glycol during the initial heating stage. After this transient phase, the system self-regulates and maintains a stable dwelling temperature. Importantly, this behaviour was consistent across different platinum loadings and was similar for both carbon and FeNC supports.

2.5.7 Extension of the Optimized Microwave Protocol to FeNC Supports

Once the microwave synthesis parameters and pre-mixing procedure were optimized using Pt/C catalysts, the same protocol was applied to FeNC supports. Platinum was deposited on FeNC at 10 wt%(12.5mg Pt+45mg FeNC), 5 wt%(6.25mg Pt + 47.5mg FeNC), and 2 wt%(1.25mg Pt + 49.5mg FeNC) loadings using identical synthesis conditions.

Applying the same microwave protocol to both carbon and FeNC supports enables direct comparison between Pt/C and Pt/FeNC systems and ensures that any observed differences in structural or electrochemical performance arise from the nature of the support rather than from synthesis-related variations.

2.6 Hydrogen-Purge Thermal Deposition of Platinum on Carbon and FeNC Supports

2.6.1 Experimental Rationale

In addition to microwave-assisted synthesis, platinum deposition on both carbon and Fe–N–C supports was also carried out using a hydrogen-purged thermal reduction method. This approach was selected to provide a conventional, furnace-based synthesis route that allows comparison with the rapid microwave method and enables evaluation of the influence of synthesis atmosphere and heating profile on platinum dispersion and catalyst structure.

Hydrogen atmosphere is widely employed in catalyst synthesis due to its strong reducing capability, which facilitates the conversion of platinum precursors to metallic platinum while limiting oxide formation [31]. By applying identical platinum loadings and supports as those used in microwave synthesis, a direct comparison between the two synthesis strategies becomes possible.

2.6.2 Materials and Precursor Preparation

Hydrogen hexachloro platinate(IV) hydrate ($H_2PtCl_6 \cdot xH_2O$) was used as the platinum precursor for all hydrogen purge syntheses. Two different supports were investigated:

- Commercial black carbon for Pt/C catalysts
- Synthesized FeNC material for Pt/FeNC catalysts

Platinum was deposited at three different loadings: 2 wt%, 5 wt%, and 10 wt%, for both carbon and FeNC supports.

The required amount of platinum precursor was calculated based on the desired platinum loading relative to the mass of the support material. The platinum salt was dissolved in a suitable volume of solvent to ensure complete dissolution and homogeneous impregnation of the support. The support material was then added to the precursor solution and magnetically stirred until a uniform suspension was obtained.

The resulting slurry was dried under controlled conditions to remove the solvent and obtain a dry precursor-loaded powder prior to thermal treatment.

2.6.3 Hydrogen-Purge Thermal Treatment Procedure

The dried precursor-loaded powders were transferred into ceramic boats and placed at the centre of a tubular furnace. Prior to heating, the furnace was purged with hydrogen gas (H_2) to remove residual air and establish a reducing atmosphere.

The furnace temperature was increased at a controlled heating rate of 5 C°/min up to a target temperature of 350 C°. Once the target temperature was reached, the samples were maintained at 350 C° for a dwelling time of 2 hours under continuous hydrogen flow.

This thermal treatment enables the reduction of Pt(IV) species to metallic platinum nanoparticles and promotes their deposition onto the support surface. The relatively moderate temperature was selected to limit excessive platinum particle growth while ensuring complete reduction of the precursor.

After completion of the dwelling period, the furnace was allowed to cool naturally to room temperature while maintaining hydrogen flow to prevent oxidation of the freshly formed platinum nanoparticles.

2.6.4 Post-Treatment Handling and Sample Collection

Once cooled to room temperature, the samples were removed from the furnace and collected as fine powders. No additional washing steps were applied following hydrogen reduction, as the platinum precursor had already been converted to metallic platinum during thermal treatment.

The resulting catalysts were denoted according to their support type, platinum loading, and synthesis method. These hydrogen-purged Pt/C and Pt/FeNC catalysts were subsequently used

for physio-chemical characterization and electrochemical evaluation, alongside their microwave-synthesized counterparts.

2.6.5 Comparative Framework with Microwave Synthesis

By synthesizing Pt/C and Pt/FeNC catalysts using both microwave-assisted reduction and hydrogen-purge thermal reduction, while maintaining identical platinum loadings (2 wt%, 5 wt%, and 10 wt%), this study enables a systematic comparison of synthesis routes. Differences observed in catalyst morphology, platinum dispersion, and electrochemical performance can therefore be attributed to the synthesis method rather than compositional variations.

The influence of rapid volumetric heating under microwave irradiation versus conventional furnace heating under hydrogen atmosphere is discussed in detail in the Results and Discussion chapter.

2.7 Physio-Chemical Characterization Methods

2.7.1 Field Emission Scanning Electron Microscopy (FESEM)

Field Emission Scanning Electron Microscopy (FESEM) was employed to investigate the morphology and surface characteristics of the synthesized catalyst materials. FESEM is a high-resolution imaging technique that utilizes a field emission electron source to generate a focused electron beam, enabling detailed observation of surface features at the micro- and nanoscale.

For the analysis, catalyst powders were mounted onto aluminium sample holders using conductive carbon tape. The electron beam was scanned across the sample surface, and the emitted secondary electrons were collected to generate high-resolution images. Measurements were acquired at different magnifications to obtain both an overall view of the catalyst morphology and detailed information regarding the surface structure.

FESEM analysis provided valuable information concerning particle distribution, agglomeration behaviour, surface roughness, and morphological homogeneity. In addition, the technique allowed qualitative evaluation of the porosity and structural organization of the catalyst particles. The obtained micrographs were used to correlate morphological features with the electrochemical performance of the catalysts.

2.7.2 Thermogravimetric Analysis (TGA)

Thermogravimetric Analysis (TGA) was performed to evaluate the thermal stability and compositional characteristics of the catalyst materials. In this technique, the mass of a sample is continuously monitored while the temperature is increased under controlled conditions.

A known quantity of catalyst was placed in an alumina crucible and heated according to a predefined temperature program. The sample mass was recorded throughout the experiment as a function of temperature. The resulting thermogravimetric curve provides information regarding thermal degradation processes, removal of adsorbed species, decomposition of organic components, and oxidation or combustion phenomena occurring during heating.

The analysis enables identification of characteristic weight-loss regions associated with different physicochemical transformations. Furthermore, the residual mass remaining at elevated temperatures can provide information regarding the inorganic fraction of the material, including the presence of metal-containing species. TGA is therefore a useful tool for assessing catalyst stability and comparing the thermal behaviour of different samples.

2.7.3 Inductively Coupled Plasma (ICP) Analysis

Inductively Coupled Plasma (ICP) analysis was employed to determine the elemental composition of the catalyst materials and to quantify the metal content within the samples. This analytical technique is based on the ionization of the sample in a high-temperature plasma, followed by detection of the emitted radiation or ionized species corresponding to specific elements.

Prior to analysis, the catalyst samples were subjected to an acid digestion procedure to ensure complete dissolution of the metallic species present in the material. The resulting solutions were introduced into the plasma as a fine aerosol, where temperatures exceeding several thousand degrees Celsius promoted atomization and ionization of the elements.

The concentration of each element was subsequently determined through calibration with standard solutions of known concentration. ICP analysis provides highly sensitive and accurate quantification of trace and bulk metallic species and is widely used to verify catalyst composition, evaluate synthesis reproducibility, and determine the actual loading of active metal components. In this work, ICP measurements were used to assess the elemental composition of the synthesized catalysts and to support the interpretation of their electrochemical performance.

2.8 Electrochemical Characterization Methods

Electrochemical characterization was carried out to evaluate the oxygen reduction reaction (ORR) activity, selectivity, and kinetic behaviour of the synthesized catalysts. Both rotating ring–disk electrode (RRDE) and gas diffusion electrode (GDE) techniques were employed in order to obtain complementary information under fundamentally different mass transport regimes. While RRDE measurements provide insight under well-controlled, fully flooded conditions suitable for mechanistic analysis, GDE measurements enable evaluation of catalyst performance under gas-fed conditions that more closely resemble practical fuel cell operation.

The combined use of RRDE and GDE methodologies allows a comprehensive assessment of catalyst activity, selectivity toward the four-electron ORR pathway, and behaviour across a wide range of current densities.

2.8.1 Electrochemical Cells and Instrumentation

All electrochemical measurements were performed using a computer-controlled potentiostat (CH Instruments, Inc.)in a three-electrode configuration.

For RRDE experiments, a rotating ring–disk electrode system (Als Japan) equipped with a glassy carbon disk and a platinum ring was employed. The rotation speed was precisely controlled to regulate mass transport conditions. For GDE measurements, a dedicated half-cell (Gaskatel Flexcell) configuration was used, allowing simultaneous contact between the catalyst layer, liquid electrolyte, and gas phase. All experiments were conducted at room temperature. Prior to each measurement, electrolytes were prepared using analytical-grade reagents and deionized water.

2.8.2 Electrolytes

Two different electrolytes were employed in order to evaluate catalyst performance under both alkaline and acidic conditions:

- 0.1 M KOH for alkaline ORR studies
- 0.1 M $HClO_4$ for acidic ORR studies

For GDE measurements, more concentrated electrolytes were used to ensure sufficient ionic conductivity under high-current operation:

- 1 M KOH
- 1 M $HClO_4$

Before each experiment, the electrolyte was purged with high-purity nitrogen (N_2) or oxygen (O_2), depending on the measurement step.

2.8.3 RRDE Electrode Preparation

Catalyst inks for RRDE measurements were prepared following a standardized procedure to ensure reproducibility and uniform catalyst coverage.

For the Pt/C catalyst, 2 mg of Pt/C powder were dispersed in a solvent mixture consisting of 1585 µL of deionized water and 1585 µL of isopropanol (IPA), followed by the addition of 13.7 µL of Nafion® ionomer solution. The resulting ink was ultrasonicated to obtain a homogeneous dispersion. A catalyst loading corresponding to a platinum concentration of 0.02 mg/cm^2 was targeted. Subsequently, 10.3 µL of the ink were drop-cast onto the polished glassy carbon disk electrode and allowed to dry under ambient conditions.

For the FeNC catalyst, 2 mg of FeNC powder were dispersed in 400 µL of isopropanol (IPA), and 10 µL of Nafion® ionomer solution were added, resulting in an ionomer-to-carbon (I/C) ratio of 0.2. The mixture was ultrasonicated to ensure uniform dispersion. A catalyst loading of 0.4 mg/cm^2 was achieved by depositing 10.3 µL of the prepared ink onto the polished glassy carbon disk electrode, followed by drying under ambient conditions.

2.8.4 RRDE Measurement Strategy and Reproducibility Protocol

Initial RRDE experiments were conducted using four different glassy carbon disk electrodes. However, post-analysis revealed significant electrode-to-electrode variability, including

differences in background currents, ORR onset potentials, and ring current stability. These inconsistencies rendered the initial dataset unsuitable for reliable comparison. Consequently, a revised strategy was adopted. All RRDE experiments were repeated using a single, best-performing glassy carbon electrode selected based on surface smoothness, background current stability, and reproducibility. This electrode was used consistently for all subsequent RRDE measurements. To further ensure data reliability, each electrochemical test was repeated twice for every catalyst and electrolyte. Only datasets exhibiting strong overlap between repetitions were considered representative.

2.8.5 RRDE Electrochemical Testing Protocol

All RRDE measurements followed a fixed and rigorous multi-step protocol. Reversible hydrogen electrode (RHE) calibrations were performed using specific reference electrodes depending on the electrolyte pH: a Ag/AgCl electrode (0.19 V vs RHE) was used for acidic media, while a Hg/HgCl electrode (0.657 vs RHE) was used for alkaline media. Consequently, all potentials throughout this work are reported against the RHE scale.

Electrode Conditioning

Electrochemical cleaning and stabilization of the catalyst-coated electrode were performed by cyclic voltammetry in N_2-saturated electrolyte at a scan rate of 500 mV/s . This step removed weakly adsorbed species and ensured stabilization of the catalyst layer prior to ORR measurements between 0.05 to 1.2 V Potential range at 500 cycles.

Cyclic Voltammetry (CV)

Subsequent CV measurements were conducted in both N_2- and O_2-saturated electrolytes at a scan rate of 100 mV/s and potential range of 0-1.2 V. These scans provided information on background capacitive behaviour and the onset of ORR-related features. CVs were recorded twice for each condition to verify reproducibility.

Linear Sweep Voltammetry in N2-Saturated Electrolyte

Linear Sweep Voltammetry (LSV) measurements were performed in N_2-saturated electrolyte to establish the electrochemical background response of the catalyst in the absence of oxygen reduction. The electrolyte was purged with nitrogen prior to testing, and the measurements were conducted in the potential range of 0–1.2 V vs. RHE at a scan rate of 10 mV/s for 10 consecutive cycles. The obtained curves were used as a reference for comparison with the corresponding measurements performed in O_2-saturated electrolyte.

Linear Sweep Voltammetry (LSV)

ORR activity was evaluated by linear sweep voltammetry under O_2-saturated conditions at 10 mV/s with 10 cycles at the range of 0-1.2 V vs RHE V using rotating disk electrode (RDE) mode. Measurements were performed at rotation speeds of:

- 400 rpm
- 900 rpm
- 1600 rpm
- 2500 rpm

The use of multiple rotation speeds enabled separation of kinetic and mass transport contributions to the measured current. Each LSV was repeated twice for reproducibility.

Ring Current Measurements and Four-Electrode Analysis

During RRDE operation, disk and ring currents were recorded simultaneously. The ring electrode was held at a potential suitable for peroxide oxidation, enabling detection of hydrogen peroxide generated during ORR at 10 mV/s between 0 to 1.2 V vs RHE.

From the combined disk and ring currents, the electron transfer number (n) and peroxide yield (%) were calculated, providing insight into ORR selectivity and reaction pathway.

Koutecky–Levich (K–L) Analysis

Koutecky–Levich plots were constructed from LSV data acquired at different rotation speeds. The linearity and slope consistency of the K–L plots were analysed to confirm kinetic control and validate the calculated electron transfer numbers. The apparent electron transfer number (n) and the percentage of hydrogen peroxide produced (% H_2O_2) can be calculated by monitoring the currents at both the disk and ring (n) can be determined by [32]:

$$n = 4\left(\frac{I_d}{I_d + I_r/N}\right) \tag{2.5}$$

$$\%H_2O_2 = 200 \times \frac{I_r}{N \times (I_d + I_r/N)} \tag{2.6}$$

Electrochemical Impedance Spectroscopy (EIS)

Electrochemical impedance spectroscopy was performed to probe the interfacial properties of the catalyst layer. EIS measurements enabled determination of the ohmic resistance and charge-transfer resistance, supporting interpretation of kinetic behaviour observed in LSV and RRDE analyses between 10 mH_z to 1MH_z with AC impedance of 10 mV .

2.8.6 Gas Diffusion Electrode (GDE) Methodology

Rationale for GDE Measurements

While RRDE techniques are suitable for mechanistic investigations, they operate under fully flooded conditions and are limited in achievable current density. In contrast, the GDE configuration enables gas-phase oxygen transport through a porous gas diffusion layer, allowing operation at significantly higher current densities and under conditions closer to those encountered in real fuel cells. GDE measurements were therefore employed to complement RRDE results and to evaluate catalyst behaviour under gas-fed operation.

2.8.7 Gas Diffusion Layer and Active Area Definition

All GDE experiments employed Sigracet 28 BC carbon paper as the gas diffusion layer. This material consists of a carbon fibre substrate coated with a PTFE-containing microporous layer, providing strong hydrophobicity and preventing electrolyte flooding. Rectangular GDL pieces of 3 × 5 cm^2 were cut for cell assembly. Due to potentiostat current limitations, a reduced electrochemically active area of 0.25 cm^2 was used for all measurements. For Pt/C electrodes, the catalyst ink was deposited directly onto a 0.5 × 0.5 cm^2 area. For FeNC electrodes, ink deposition was performed over a 1 × 1 cm^2 area, after which the active area was reduced to 0.25 cm^2 using polymer tape masking.

2.8.8 GDE Catalyst Ink Preparation

Pt/C Ink for GDE

A commercial 40 wt% Pt/Vulcan carbon catalyst was used. The ink composition was:

- Catalyst: 2 mg
- Nafion® solution: 21.9 µL
- Isopropanol: 166.94 µL
- Deionized water: 131.16 µL

The ionomer-to-carbon ratio was 0.8, and the solvent composition corresponded to approximately 56 vol% IPA and 44 vol% water. A volume of 20 µL of ink was drop-cast onto the 0.25 cm^2 active area, achieving a target platinum loading of 0.20 mg Pt/cm^2.

FeNC Ink for GDE

Due to the lower intrinsic activity of non-precious catalysts, a significantly higher loading was required. The FeNC ink composition was:

- Catalyst: 30 mg
- Nafion® solution: 686 µL
- Isopropanol: 246 µL
- Deionized water: 193 µL

The ionomer-to-carbon ratio was 1.0. A volume of 150 µL of ink was deposited onto a 1 cm^2 area, corresponding to a final catalyst loading of 4 mg/cm^2 after masking. Drying was performed at 75 C° for 1 hour.

2.8.9 GDE Cell Assembly

The catalyst-coated GDL was mounted with the catalyst layer facing the liquid electrolyte and the carbon paper backing facing the gas chamber. Proper sealing was ensured using gaskets.

A three-electrode configuration was employed:

- Working electrode: catalyst-coated GDL
- Reference electrode: Ag/AgCl
- Counter electrode: Pt wire (Pt/C) or carbon rod (FeNC)

Gas streams (N_2 or O_2) were fully humidified prior to entering the cell.

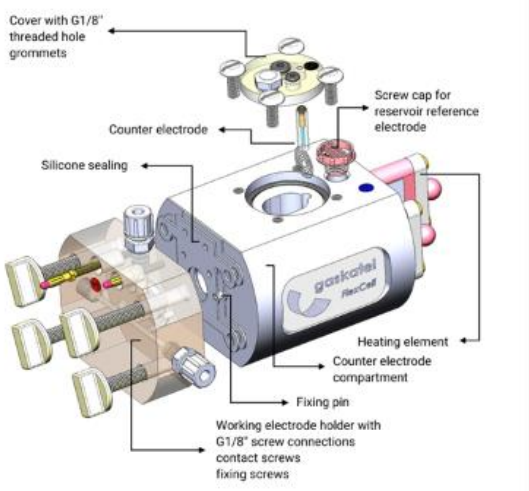

Fig. 2.1 GDE test cell assembly [26].

2.8.10 GDE Electrochemical Testing Protocol

All GDE measurements followed a standardized six-step protocol:

Electrochemical cleaning by CV in N_2 at 500 mV/s for 500 cycles at (0.05 - 1.2) V vs RHE potential range

1) CV in N_2 at 100 mV/s (10 cycles) at (0.05 - 1.2) V potential range
2) CV in N_2 at 50 mV/s (10 cycles) at (0.05 - 1.2) V potential range
3) Wetting test via open-circuit potential–time (OCPT) measurement in O_2 for 5 minutes
4) LSV in O_2 at 10 mV/s, repeated three times at (0 - 1.2) V potential range
5) EIS measurements under ORR conditions from $1mH_z$ up to $1MH_z$

2.8.11 Significance of the Electrochemical Methodology

The combined RRDE and GDE methodologies employed in this work provide a rigorous and comprehensive evaluation of ORR catalysts. RRDE measurements enable mechanistic insight, selectivity analysis, and kinetic parameter extraction, while GDE measurements allow assessment under realistic, gas-fed conditions. This dual approach ensures that observed performance trends are robust, reproducible, and relevant for practical electrochemical energy conversion applications.

Chapter 3: Physio-Chemical Properties

3.1 Physio-chemical Characterization

3.1.1 Optimization of Microwave Synthesis Parameters: Impact of Dwelling Time

To optimize the microwave-assisted synthesis before preparing hybrid catalysts, an initial parameter screening was conducted. For this control group, I synthesized 10 wt% Pt on a commercial Vulcan carbon black support (modifying a 40% Pt/C framework down to a 10% Pt target). The main objective was to evaluate the effect of the microwave isothermal dwelling time at a fixed reduction temperature boundary of 120°C by comparing two operational programs: an abbreviated 2-minute dwelling time (Protocol 1) and an extended 5-minute dwelling time (Protocol 2). Managing this localized thermal duration is vital to control nanoparticle nucleation rates and avoid extensive agglomeration of the metallic phase.

Field Emission Scanning Electron Microscopy (FESEM) was used to evaluate the microstructural distribution, spatial homogeneity, and attachment of the platinum nanoparticles across the carbon support matrices under both configurations.

The comparative microstructural outcomes between the two dwelling configurations reveal clear differences in particle distribution quality and surface localization:

2-Minute Dwelling Time (Protocol 1): The FESEM micrographs (Figure 3.1) indicate that a shorter reduction window restricts the structural uniformity of the catalyst. At lower magnifications (25k and 50k), the carbon black support displays its typical porous, spherical agglomerate morphology, but the spatial distribution of the bright platinum clusters is visibly non-homogeneous across broader sample regions. Imaging at 100k and 150k shows that while some small nanoparticles are successfully pinned to the support surfaces, they coexist with localized, larger metallic clusters and irregular spatial clearings where little to no deposition occurred. This indicates that a 2-minute window provides insufficient time for complete, uniform volumetric nucleation, causing localized precursor concentrations to form isolated, bulkier crystalline clusters rather than distributing evenly.

5-Minute Dwelling Time (Protocol 2): In contrast, extending the isothermal dwelling duration to 5 minutes significantly improves the material's morphological properties (Figure 3.2). imaging at 25k and 50k show an exceptionally homogeneous, well-spread coverage of platinum across the entire exposed surface area of the carbon black matrix, with no massive localized clustering or empty areas. Deep surface inspections at high magnifications (100k and 200k) confirm that the platinum nanoparticles are highly dispersed as tiny, discrete dots closely attached to the carbon. The 5-minute isothermal window allows the system to achieve full chemical reduction of the platinum precursor while providing sufficient time for the newly formed nuclei to arrange uniformly over the high-surface-area support. Crucially, the temperature ceiling prevents thermal migration, meaning the nanoparticles remain stable and separated rather than sintering into large, low-surface-area aggregates.

A direct comparison of these FESEM results shows that Protocol 2 (5-minute dwell) produces the most uniform nanoparticle dispersion and minimizes detrimental metal aggregation, which is essential for maximizing the electrochemically active surface area (ECSA). Consequently, the 5-minute dwelling program was selected as the foundational operational pathway for all subsequent microwave-assisted catalyst preparations in this work.

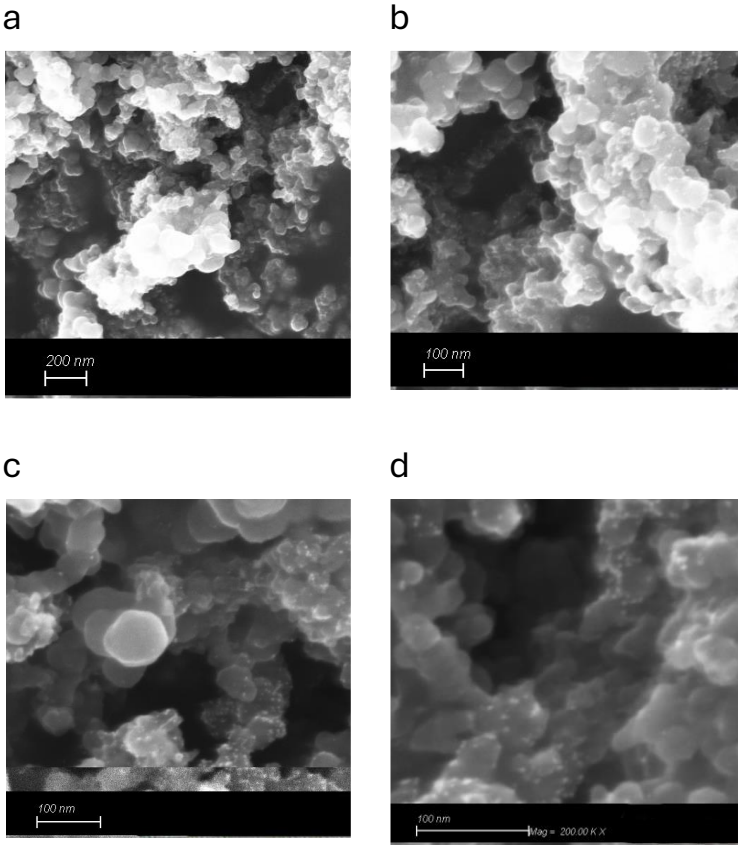

Figure 3.1. FESEM micrographs of the 10% Pt/C catalyst synthesized via microwave-assisted reduction with an abbreviated 2-minute dwelling time at magnifications of: (a) 25k, (b) 50k, (c) 100k, and (d) 200k.

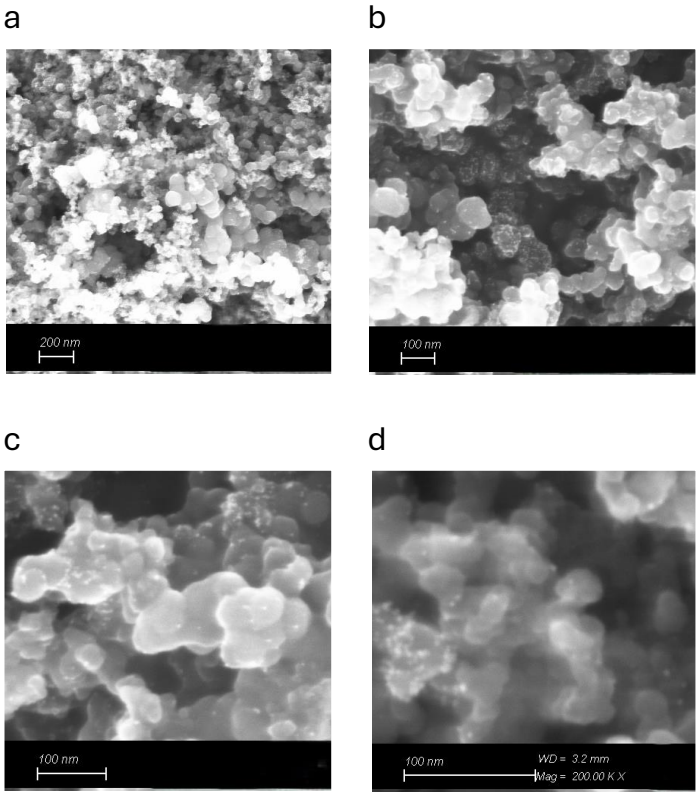

Figure 3.2. FESEM micrographs of the 10% Pt/C catalyst synthesized via microwave-assisted reduction with an optimized 5-minute dwelling time at magnifications of: (a) 25k, (b) 50k, (c) 100k, and (d) 200k.

3.2 Physicochemical and Morphological Characterization

To correlate the electrocatalytic ORR activity and transport properties with the physical features of the catalysts, a detailed physicochemical characterization was conducted. Field Emission Scanning Electron Microscopy (FESEM) was utilized to evaluate structural morphology, while Thermogravimetric Analysis (TGA) was employed under an oxidizing atmosphere to determine thermal stability and decouple the actual metal-to-carbon residual mass loading ratios across the synthesis paths.

3.2.1 Microstructural Morphology Analysis (FESEM)

The morphological evolution of the hard-templated FeNC support host upon embedding the platinum nanoparticles via microwave-assisted (MW) flash reduction was evaluated using FESEM at a magnification of 25k.

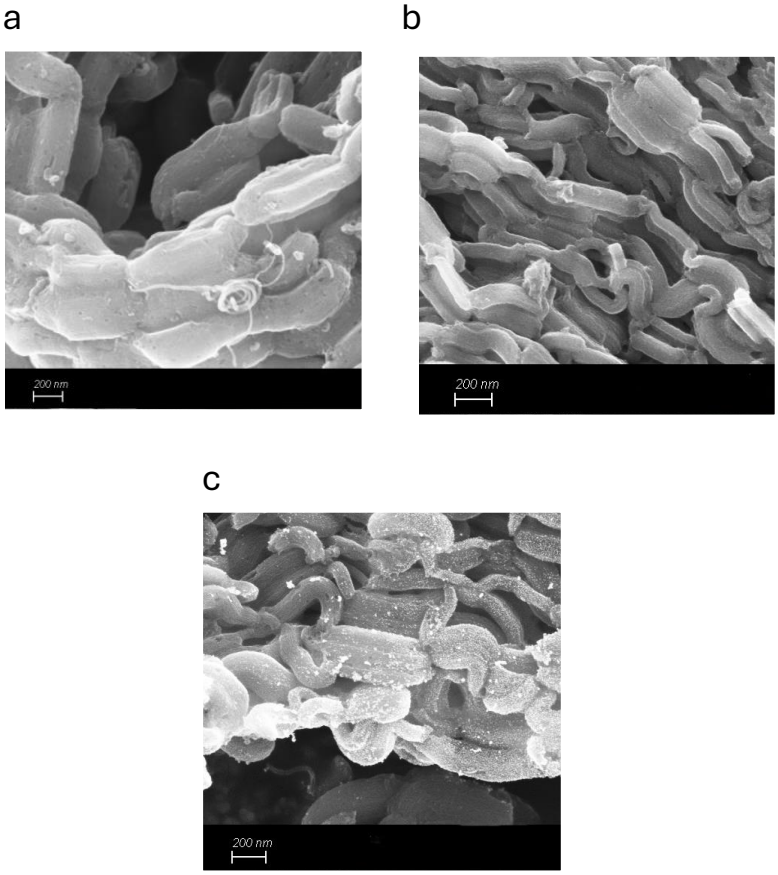

Figure 3.3. FESEM micrographs recorded at 25k magnification displaying the structural morphology of the microwave-reduced catalysts: (a) FeNC/Pt 2%, (b) FeNC/Pt 5%, and (c) FeNC/Pt 10%.

All three samples across the loading series successfully preserve the characteristic ordered, worm-like and rope-like bundled rod morphology. This structural motif confirms the precise replication of the original sacrificial SBA-15 silica hard template. This highly open carbon network accommodates rapid electrolyte infiltration and unhindered mass transport, matching the large electrochemical double-layer capacitance observed in liquid cells.

FeNC/Pt 2%: The replicated carbon rods appear distinct, clean, and highly porous. Fine carbonaceous filament extensions or interconnected nanofibers coexist with the primary macro structured replica blocks, creating open channels ideal for transport.

FeNC/Pt 5%: The ordered replication blocks remain highly intact and tightly grouped. The rod profiles exhibit excellent structural exposure, showing no signs of macroscopic particle clustering or channel clogging at this intermediate loading level.

FeNC/Pt 10%: The carbon arrays appear tightly bundled and heavily structured. A minor, uniform surface texturing or granular speckling highlights the higher concentration of platinum nanoparticles distributed along the porous carbon walls. This dense, coexisting distribution provides the vital secondary kinetic boost required to handle extreme current densities during gas diffusion cell operations.

3.2.2 Thermal Stability and Metal Loading Verification (TGA)

TGA was performed under an oxidizing airflow up to 900C°. This analysis tracks the bulk oxidation kinetics of the carbon lattice and isolates the remaining inorganic metallic residue to verify the efficiency of the synthesis methods.

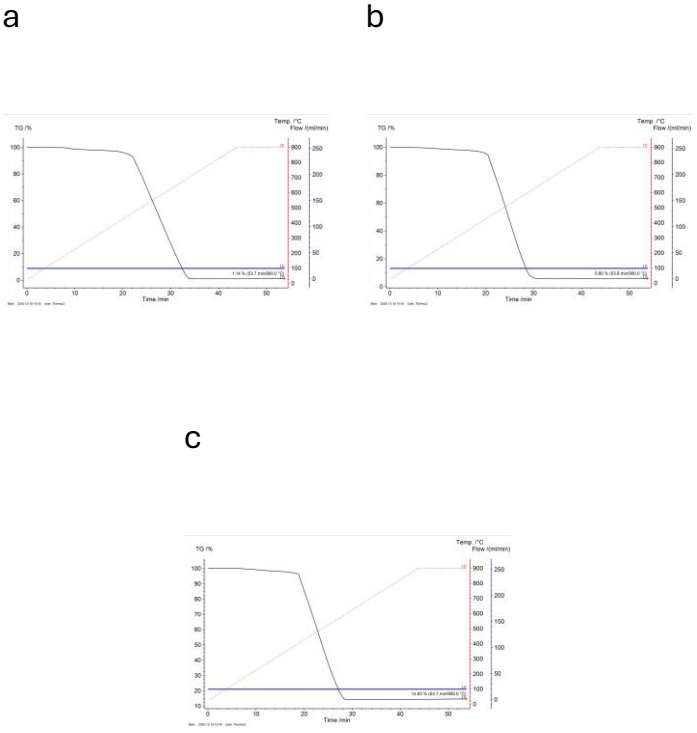

Figure 3.4. TGA mass loss (%) and temperature profiles recorded under airflow for conventional hydrogen gas reduction (H2) for: (a) Pt/C 2%, (b) Pt/C 5%, and (c) Pt/C 10%.

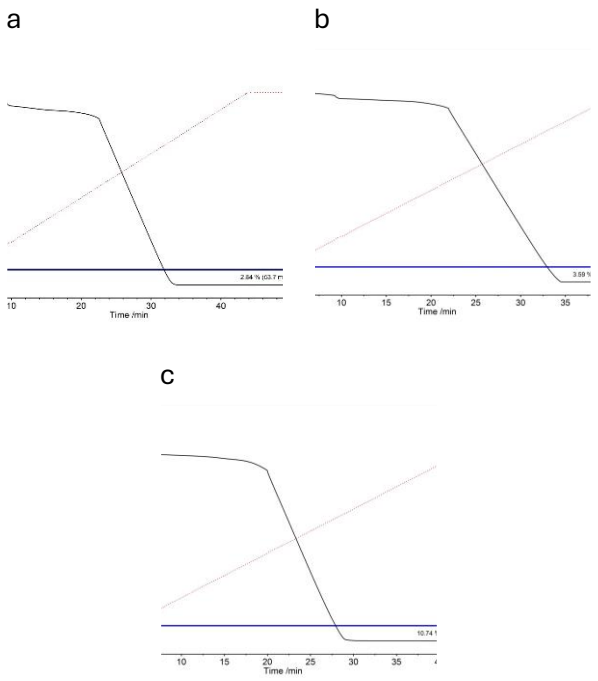

Figure 3.5. TGA mass loss (%) and temperature profiles recorded under airflow for Mw synthesis for: (a) Pt/C 2%, (b) Pt/C 5%, and (c) Pt/C 10%.

The relative residual mass fractions quantified at the conclusion of the thermal sweeps are compiled in Table 3.1:

Table 3.1. Residual metal ash fractions (%) derived from TGA oxidation profiles :

Nominal Material Target	***H2 Method***	***MW Method***
Pt/C 2wt.%	1.14%	2.84%
Pt/C 5wt.%	5.80%	3.59%
Pt/C 10wt.%	14.63%	10.74%

Thermal Decomposition Behaviour and Synthesis Coordination

Across all tested samples, a minor initial mass loss below 200C° is observed due to the evaporation of physically adsorbed moisture and volatile surface functional groups. The primary mass drop occurs sharply between 400C° and 700C°, driven by the complete combustion of the porous graphitic carbon support into gaseous CO_2, leaving behind isolated metal species.

A clear, catalyst-dependent trend emerges when comparing the two reduction methods:

Microwave-Assisted Flash Reduction (MW): This method shows exceptional accuracy for the high-loading target, yielding a final inorganic residue of 10.74% for the 10% nominal sample. The rapid microwave radiation successfully traps the metal precursors uniformly within the porous host channels, preventing volatile precursor loss during reduction and achieving the targeted composition with high precision.

Conventional Hydrogen Gas Reduction (H_2): The gas-reduced samples display an elevated relative residual mass percentage (e.g., 5.80% and 14.63% for the 5% and 10% targets,

respectively). This trend indicates that the high-temperature hydrogen gas environment induces minor gasification or early burn-off of less stable amorphous carbon walls, resulting in a slightly enriched relative metal fraction in the final isolated powder.

Furthermore, increasing the platinum nanoparticle fraction shifts the onset of bulk carbon combustion toward lower temperatures (moving from 450C° in the 2% series down to 400C° in the 10% series). This shift confirms a minor catalytic effect exerted by the densely distributed platinum sites, which lower the thermal activation energy required for the surrounding carbon matrix to undergo combustion.

3.2.3 Compositional Verification via ICP

To quantify the exact bulk chemical content and actual active metal mass fractions, Inductively Coupled Plasma (ICP) analysis was integrated into the characterization protocol.

Table 3.2. Mass composition and nominal versus experimental metal loadings determined via bulk chemical analysis.

Material	*Synthesis Pathway*	*Nominal Pt Loading (wt.%)*	*ICP Experimental Pt Loading (wt.%)*
2% Pt/C	Hydrogen Purge	2.0%	0.0072
2% Pt/C	Microwave (MW)	2.0%	-
5% Pt/C	Hydrogen Purge	5.0%	0.0082
5% Pt/C	Microwave (MW)	5.0%	0.0085
10% Pt/C	Hydrogen Purge	10.0%	0.0204
10% Pt/C	Microwave (MW)	10.0%	0.0095
2% Fe-N-C/Pt	Microwave (MW)	2.0%	0.0084
5% Fe-N-C/Pt	Microwave (MW)	5.0%	0.0189
10% Fe-N-C/Pt	Microwave (MW)	10.0%	0.0382

Chapter 4

Electrochemical Characterization: RDE and RRDE

4.1 Electrochemical Evaluation in Acidic Media ($HClO_4$)

The electrochemical behaviour and ORR kinetics of the prepared catalysts were systematically evaluated in an acidic electrolyte (0.1M $HClO_4$) using a RRDE setup. This section presents the performance metrics of the baseline platinum on carbon (Pt/C) control groups followed by the advanced platinum-modified iron-nitrogen-carbon (FeNC/Pt) composite catalysts, comparing the hydrogen (H_2) and microwave-assisted (Mw) synthesis routes.

4.1.1 Core Group Benchmarking: Pt/C Controls

voltammetric Profile Analysis (CV in N_2 and O_2)

To establish a baseline for metal surface activity, CV was executed in an N_2- saturated electrolyte at a scan rate of 100mV/s allowing a direct side-by-side comparison of both preparation methods.

Hydrogen Synthesis Series: The baseline Pt/C 40% catalyst exhibits prominent, sharp hydrogen underpotential deposition (H_{upd}) peaks in the 0.05V to 0.30V range, alongside a well-defined cathodic platinum oxide reduction peak cantered at approximately 0.70V. As the loading is reduced to Pt10(Carbon Vulcan+ 10% Pt), Pt5(Carbon Vulcan+ 5% Pt), and Pt2(Carbon Vulcan+ 2% Pt), the absolute current densities scale down proportionally. The Pt2 sample displays a heavily compressed profile with a noticeable tilt, indicating an increased relative contribution of the carbon support baseline and lower active metal surface area.

Microwave Synthesis Series: The microwave-reduced samples display highly symmetric voltametric profiles that match or exceed the peak definition of the H_2 series. Notably, for the Pt10 and Pt5 samples, the H_{upd} peaks between 0.05V and 0.25V remain well-resolved, and the cathodic oxide reduction peak remains sharp and cantered near 0.73V. Even at the lowest loading of Pt2, the profile maintains excellent current response and clear features, proving that microwave reduction successfully yields highly accessible, clean metal surface boundaries.

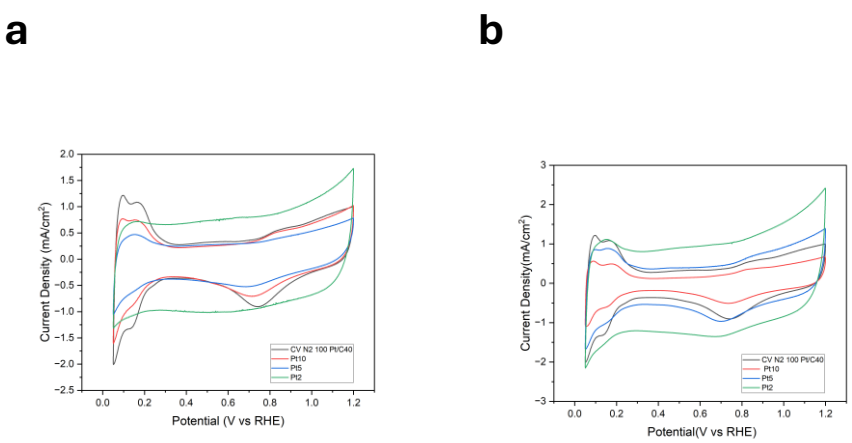

Figure 4.1. Cyclic voltammograms (CV) of synthesized Pt/C catalysts comparing the: (a)hydrogen (H2), (b) microwave-assisted (MW) techniques at varying platinum weight fractions. Measurements recorded in an N2 -saturated 0.1M HClO4 solution at a100mV/s scan rate.

When shifted to an O_2-saturated environment, the activation of the oxygen reduction reaction alters the voltametric profiles for both groups:

In the H_2 Series: The current loop drops into a distinct reduction envelope, with the lowest loading (Pt/C2%) demonstrating a sharp, intense cathodic peak reaching approximately -6.0mA/cm^2 centred near 0.48V.

In the MW Series: A highly comparable ORR response is observed. ThePt2 sample similarly shows a strong, well-defined cathodic reduction peak reaching nearly -5.2mA/cm^2 centred at approximately 0.60V. The positive shift of this peak position compared to the H_2 equivalent suggests more favourable reduction kinetics for the microwave-treated catalyst at very low loadings.

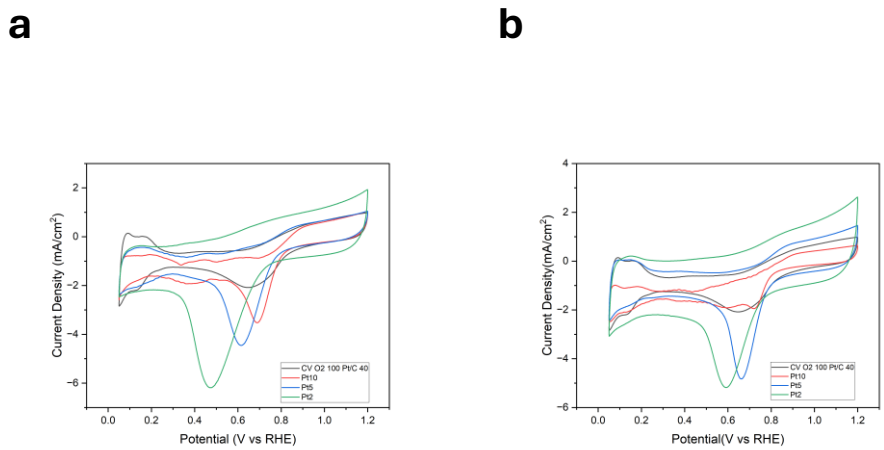

Figure 4.2. CV of synthesized Pt/C catalysts comparing the: ***(a)****hydrogen (H2synthesis),* ***(b)*** *microwave-assisted (MW) techniques at varying platinum weight fractions. Measurements recorded in an O2 -saturated 0.1M HClO4 solution at a100mV/s scan rate.*

Linear sweep voltammetry

LSV curves were recorded at 1600rpm with a scan rate of 10mV/s in an O_2 -saturated environment to isolate transport kinetics from mass transport limitations. The curves reveal a well-defined mixed kinetic-diffusion region between 0.70V and 0.90V vs. RHE, transitioning into a steady diffusion-limited plateau below 0.65V that stabilizes between -5 mA/cm^2 and -5.8mA/cm^2 for the majority of the samples.

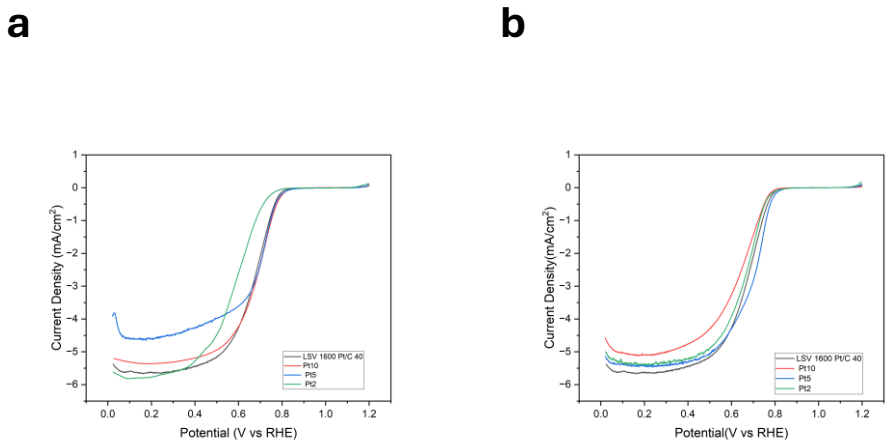

Figure 4.3. LSV curves for the Pt/C groups in an O2 -saturated 0.1M HClO4 solution at a rotation speed of 1600 rpm and scan rate of 10mV/s for the: ***(a)*** *H_2 series, and* ***(b)*** *Microwave (MW) series.*

The main performance parameters derived from these profiles are summarized in Table 4.1:

Table 4.1. parameters for Pt/C catalysts in 0.1M $HClO_4$ at 1600rpm:

Catalyst Sample	*Onset Potential (V vs. RHE)*	*Half-Wave Potential $E_{1/2}$ (V vs. RHE)*
(H_2) Series		
Pt/C 40% (Commercial Base)	0.78	0.67
Pt/C 10%	0.81	0.68
Pt/C 5%	0.80	0.70
Pt/C 2%	0.75	0.58
MW Series		
Pt/C 40% (Commercial Base)	0.78	0.67
Pt/C 10%	0.78	0.64
Pt/C 5%	0.79	0.64
Pt/C 2%	0.77	0.67

The data shows that for the lowest loading (Pt/C 2%), the microwave synthesis provides a clear kinetic advantage over the hydrogen method, shifting the half-wave potential significantly upward from 0.58 V to 0.67 V. This shift is likely driven by the rapid volumetric heating of the microwave protocol, which suppresses nanoparticle agglomeration and maximizes the electrochemically active surface area at low metal concentrations. For the intermediate Pt/C 5% and Pt/C 10% configurations, both preparation methods generate highly comparable onset thresholds. This trend indicates that increasing the platinum loading achieves higher onset potentials by providing a greater density of active catalytic sites, which eventually compensates for the synthesis method variations. Consequently, these results validate the microwave protocol as an efficient and competitive alternative.

RRDE Selectivity

the direct reaction pathway was evaluated using the RRDE measurements to trace intermediate hydrogen peroxide (H_2O_2) release and calculate the electron transfer number (n). The data points recorded at a selection potential of 0.5V vs. RHE show clear trends based on synthesis conditions:

H_2 Synthesis Series (at 0.5V): Pt/C10% yields 4.18% peroxide (n = 3.8); Pt/C 5% yields 4.24% peroxide (n = 3.3); Pt/C 2% yields 4.45% peroxide (n=3.3).

MW Synthesis Series (at 0.5V): Pt/C 10% yields 6.76% peroxide (n = 4.0); Pt/C 5% yields 0.35% (n = 3.8); Pt/C 2% yields 0.70% (n = 3.6).

The microwave-synthesized catalysts display a dramatic decrease in peroxide generation at intermediate and lower loadings (Pt/C 5% and Pt/C 2%), keeping intermediate release safely below 1%. This confirms that the microwave method drives highly selective oxygen reduction kinetics. While the hydrogen samples shift toward lower electron transfer numbers (n=3.3) as loading decreases, the microwave samples maintain high efficiency n≈3.6), supporting a direct four-electron pathway even at reduced platinum mass fractions.

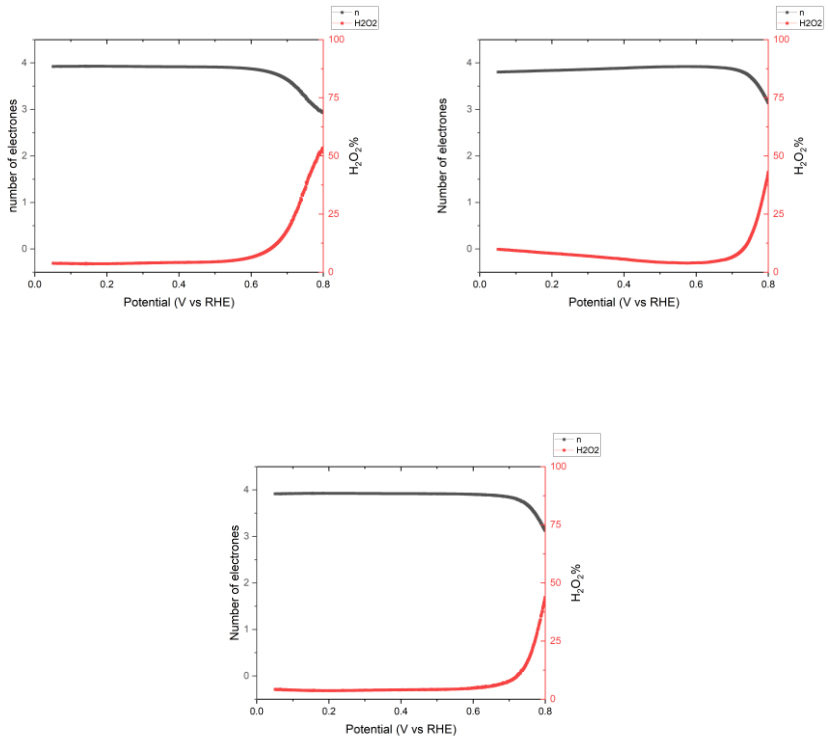

Figure 4.4. Hydrogen series catalyst selectivity curves for (a) Pt/C2%, (b) Pt/C5%, (c) Pt/C10% samples showing the calculated number of transferred electrons (n) and intermediate hydrogen peroxide yield (H2O2%) as a function of potential.

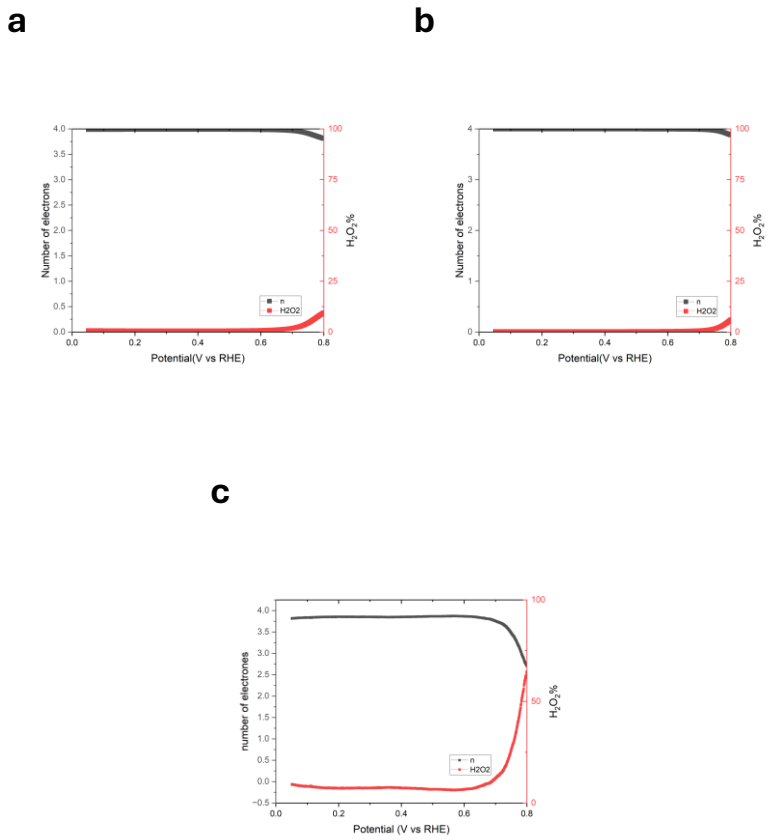

Figure 4.5. Microwave (Mw) catalyst selectivity curves for (a) Pt/C2%, (b) Pt/C5%, (c) Pt/C10% samples showing the calculated number of transferred electrons (n) and intermediate hydrogen peroxide yield (H_2O_2%) as a function of potential.

Koutecky-Levich Analysis for Pt/C Catalysts

To investigate the ORR kinetics, a Koutecky-Levich analysis was performed on hydrodynamic voltammetry data in oxygen-saturated acidic media. The experimental electron transfer numbers (n), extracted from the inverse slopes of the Koutecky-Levich plots, revealed a clear dependence on both platinum loading and the synthesis pathway.

For the catalysts prepared via conventional hydrogen thermal reduction, the 2% and 5% platinum loadings both yielded an electron transfer number of 3.3, indicating a mixed mechanism with significant parallel two-electron peroxide formation. Increasing the loading to 10% shifted the reaction toward a direct four-electron pathway, raising n to 3.8. This improvement is attributed to a higher spatial density of active platinum sites, which facilitates the rapid re-adsorption and reduction of intermediate peroxide species before they can desorb.

This kinetic trend was consistently enhanced across the microwave-assisted synthesis series, outperforming the hydrogen furnace counterparts at every equivalent loading. The microwave-synthesized catalysts exhibited electron transfer numbers scaling from 3.6 for the 2% loading to 3.7 for the 5% loading, ultimately achieving the ideal thermodynamic limit of 4.0 at 10% loading. The superior selectivity of the microwave series stems from the rapid, uniform heating intrinsic to microwave irradiation. This promotes ultrafast nucleation and high nanoparticle

dispersion, exposing optimized crystalline facets that lower the activation barrier for O-O bond cleavage and maximize direct reduction to water.

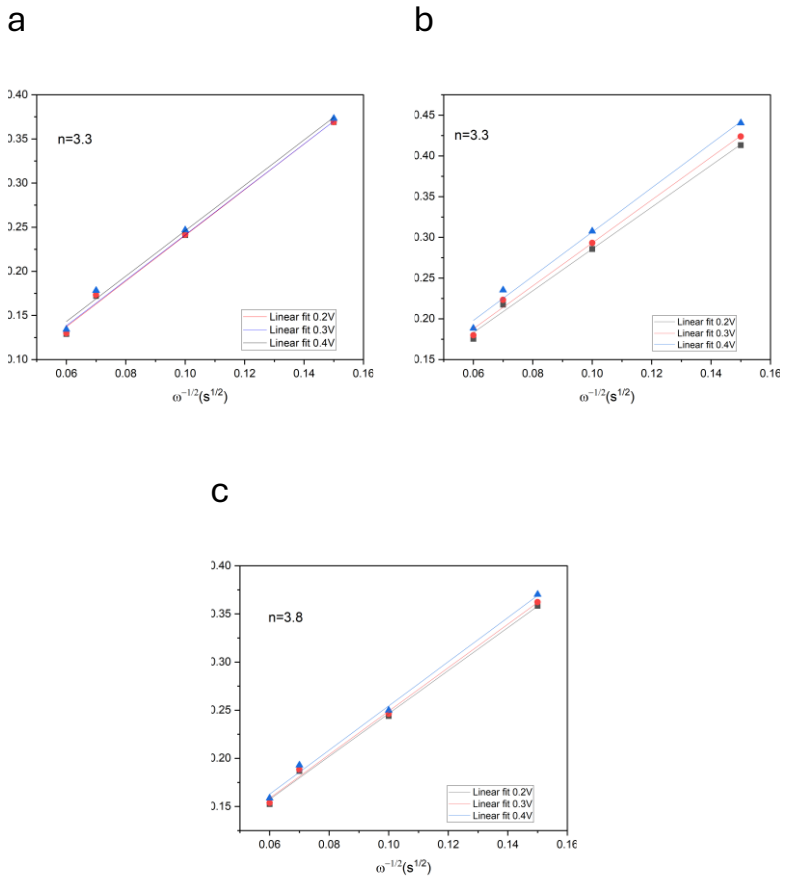

Figure 4.6. Hydrogen (H_2) synthesised catalyst K-L curves for (a) Pt/C2%, (b) Pt/C5%, (c) Pt/C10% samples showing the calculated number of transferred electrons (n) .

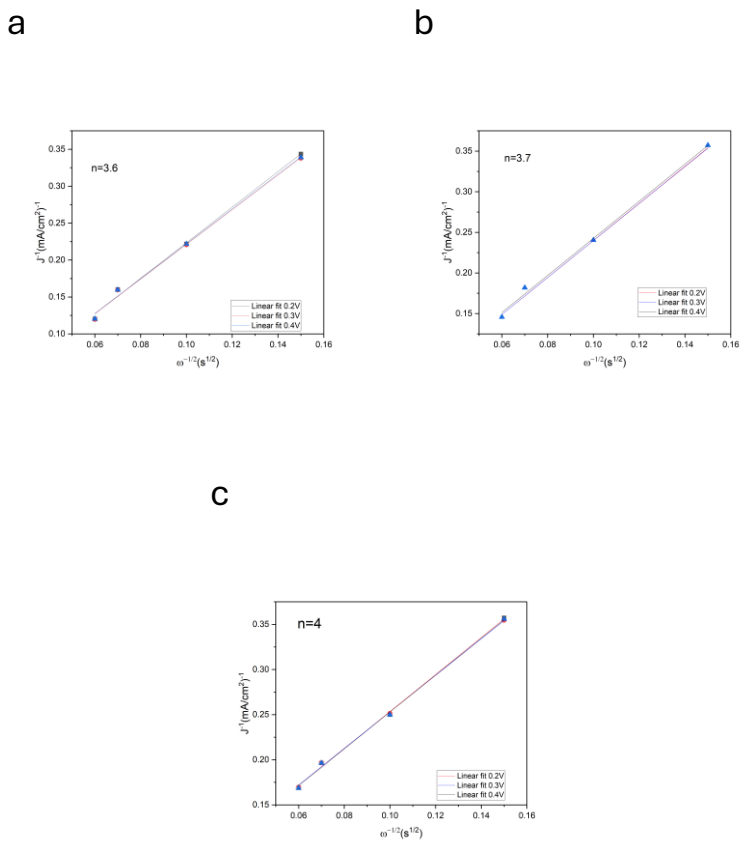

Figure 4.7. Microwave (Mw) catalyst K-L curves for (a) Pt/C2%, (b) Pt/C5%, (c) Pt/C10% samples showing the calculated number of (n) .

Electrochemical surface area(ECSA) Analysis for Pt/C Catalysts

The H_2 Purge Series (Furnace): At Pt/C 2wt%, the hydrogen underpotential deposition (H_{upd}) peaks are completely not visible. Due to the slow thermal ramping and prolonged heating in the furnace, low concentrations of platinum mobile atoms migrate freely and agglomerate or get buried in the carbon support, dropping the active area below the detection limit. As loading increases to 5% (6.43 m^2/g)and 10% (19.78 m^2/g), the ECSA rises sharply. This demonstrates that higher metal concentrations are strictly necessary in furnace synthesis to force the exposure of active crystal facets and overcome support encapsulation.

The Microwave (MW) Series: The MW series shows highly stable and elevated ECSA values across all loadings (13.57 to 16.19 m^2/g). The ultra-fast volumetric heating of the microwave drives rapid, instantaneous chemical reduction, causing a massive burst of uniform nuclei. This "flash" kinetics locks the small platinum nanoparticles onto the carbon grains before they can migrate, suppressing thermal sintering (Ostwald ripening) [33]. This ensures excellent precursor utilization and active site exposure even at ultra-low metal loadings (2%). [34] [35]

4.2. Advanced Composite Evaluation: FeNC/Pt Catalysts

Following the validation of the microwave protocol on the carbon black control group, the investigation was extended to the advanced FeNC matrix. Platinum was integrated onto the synthesized FeNC support at nominal target metal weight fractions of 2%, 5%, and 10% to evaluate the synergistic effects between the precious metal nanoparticles and the underlying non-precious single-atom/nitrogen coordination sites.

voltammetric Profile Analysis (CV in N_2 and O_2)

To probe the interfacial behaviour of the composite structures, cyclic voltammetry was conducted in an N_2-saturated 0.1M $HClO_4$ matrix at a scan rate of 100mV/s.

H_2 Synthesis Series: The baseline bare FeNC support exhibits a broad, rectangular double-layer charging profile, reflecting its highly porous, elevated surface area network. Upon the introduction of platinum via the hydrogen route, the baseline capacitance remains remarkably high. For the FeNC/Pt10 (FeNC + 10% wt. Pt) and FeNC/Pt5 (FeNC + 5%wt. Pt) variations, broad waves associated with platinum oxidation and subsequent reduction emerge super imposed on the carbon matrix loop, indicating active metallic site exposure.

Microwave Synthesis Series: The microwave-reduced composite catalysts reveal a distinct alteration in their capacitive parameters. While the bare FeNC support displays the characteristic wide rectangular charging profile, the platinum-modified samples (FeNC/Pt10, FeNC/Pt5, and FeNC/Pt2) present a more compressed capacitive envelope compared to the H_2 series. This indicates a localized reorganization of the carbon surface accessibility driven by the rapid microwave heating process. Notably, the characteristic platinum-derived peaks specifically those corresponding to hydrogen underpotential deposition (H_{upd}) are not clearly seen in the cyclic curves. This absence may be attributed to the high background double-layer capacitance of the underlying FeNC carbon support, which effectively masks the faradaic signals of the platinum surface. Despite the lower background capacitance, clear features indicating clean, accessible metallic boundaries are preserved across all loadings.

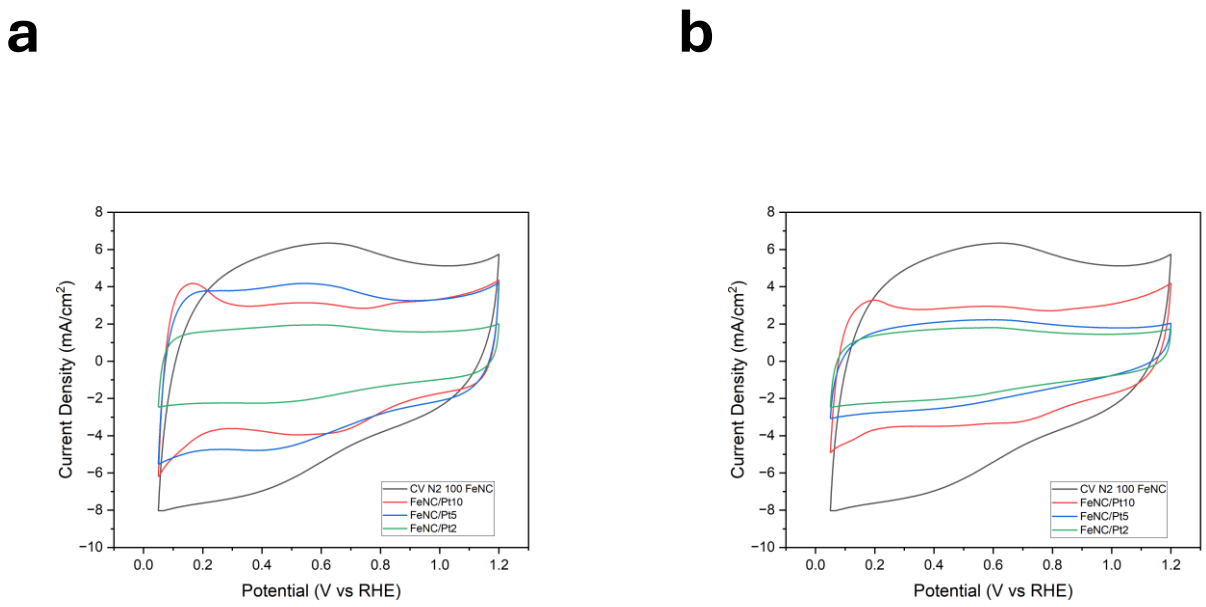

Figure 4.8. CV of synthesized FeNC/Pt composite catalysts comparing the (a) H_2 and (b) microwave-assisted (MW) techniques at 2wt.%, 5wt.%, and 10wt.% platinum loadings alongside the bare FeNC support baseline, recorded in an N2-saturated.

When the testing environment was saturated with molecular oxygen, a profound transition in the voltametric loops occurs due to the activation of the oxygen reduction reaction:

In the H_2 Series: The current profiles are dominated by intense cathodic reduction envelopes. The bare FeNC support exhibits a reduction peak cantered around 0.55V. The introduction of platinum shifts the reduction activity, with the FeNC/Pt5 sample exhibiting a deep, well-resolved cathodic peak reaching approximately -7.5mA/cm^2 near 0.60V.

In the MW Series: A highly uniform and stable ORR response is observed. The FeNC/Pt10 and FeNC/Pt5 samples demonstrate well-defined cathodic peaks cantered tightly near 0.58V to 0.60V with current densities tracking past -5.0mA/cm^2. This confirms that the microwave flash-reduction protocol successfully anchors functional platinum sites capable of driving immediate molecular oxygen reduction across the composite surface.

a

b

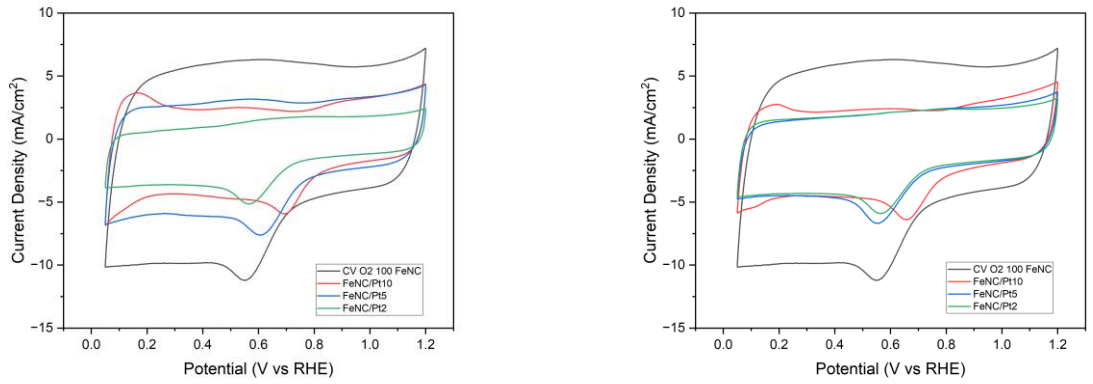

Figure 4.9. CV of synthesized FeNC/Pt composite catalysts comparing the (a) hydrogen (H_2) and (b) microwave-assisted (MW) techniques at 2wt.%, 5wt.%, and 10wt.% platinum loadings alongside the bare FeNC support baseline, recorded in an O_2-saturated

Comparative ORR Kinetics (LSV)

LSV profiles were recorded at a rotation speed of 1600 rpm. The extracted onset and half-wave potentials are consolidated below in Table 4.2.

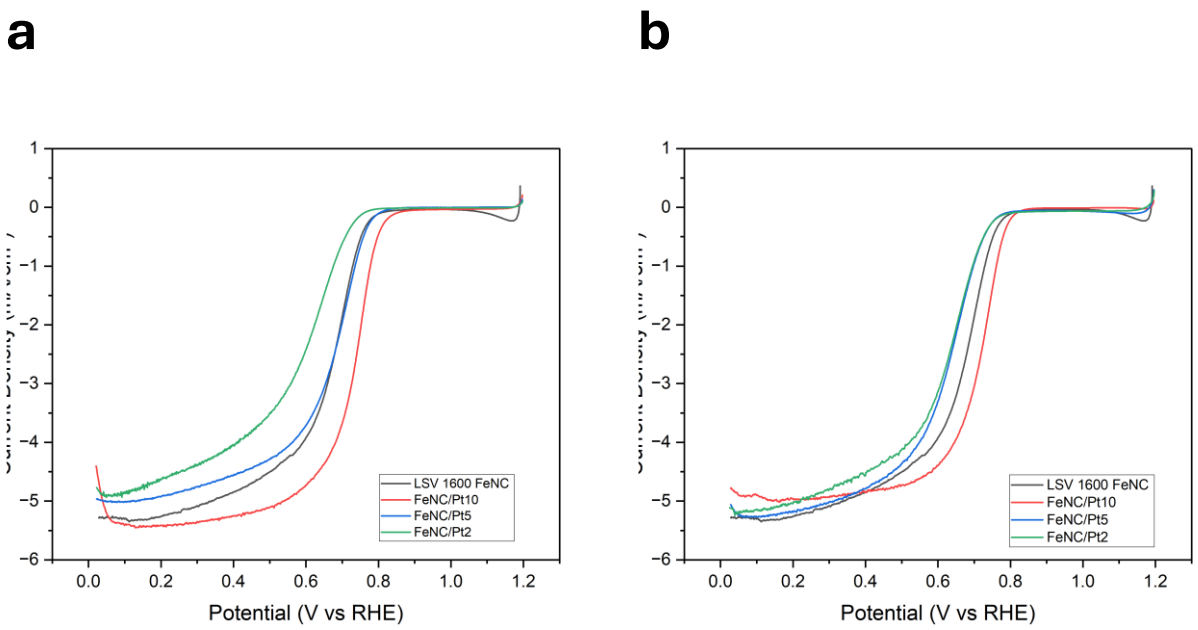

Figure 4.10. LSV polarization curves for the FeNC/Pt series and bare FeNC base support in an O_2 -saturated 0.1M $HClO_4$ solution at a rotation speed of 1600 rpm and scan rate of 10 mV/s for the: (a) H_2 synthesis series, and (b) MW synthesis series.

Table 4.2. ORR parameters for FeNC/Pt composites in 0.1M $HClO_4$ at 1600 rpm.

Catalyst Sample	***Onset Potential (V vs. RHE)***	***Half-Wave Potential $E_{1/2}$ (V vs. RHE)***
(H_2) Series		
FeNC	0.78	0.67
FeNC/Pt10	0.83	0.73
FeNC/Pt5	0.78	0.67
FeNC/Pt2	0.74	0.59
Microwave Series		
FeNC	0.78	0.67
FeNC/Pt10	0.79	0.71
FeNC/Pt5	0.75	0.63
FeNC/Pt2	0.74	0.62

The LSV data highlights an intriguing performance divergence between the two preparation methods:

H_2 Series: Within the H_2 series, the addition of 10 wt.% Pt provides an immediate kinetic boost, shifting the onset potential forward to 0.83 V and the half-wave potential to 0.73 V.

However, as the loading decreases to 5% and 2%, the kinetics decay below the level of the bare support. This decay suggests that the slow thermal ramping of the hydrogen synthesis process promotes particle agglomeration at low concentrations, which simultaneously deactivates the native FeNC active sites through physical blocking without providing enough well dispersed Pt surfaces to compensate for the loss.

Microwave Series: Within the Microwave series, a more stable mass transport plateau near approximately -5.2 mA/cm^2 is established across all samples. While FeNC/Pt10 achieves competitive kinetics (E_{onset} = 0.79V; $E_{1/2}$ = 0.71V), the lower-loading variants (FeNC/Pt5 and FeNC/Pt2) maintain significantly better half wave potential stability (0.63 V and 0.62 V, respectively) compared to the hydrogen series equivalents. This stability indicates that the uniform volumetric energy delivery of microwave radiation suppresses metal migration, yielding smaller, ultra fine Pt clusters. This optimal structural integration preserves structural synergy with the support, preventing structural collapse or active site blocking .

Selectivity Pathway and Peroxide Yields

The fundamental pathway efficiency and catalyst selectivity were verified by analysing intermediate hydrogen peroxide (H_2O_2) release via 4-electrode collection metrics. The quantitative data points extracted at a constant disk potential of 0.5V vs. RHE show critical variations in reaction mechanism:

H_2 Synthesis Composite Series (at 0.5V): FeNC/Pt10 yields 2.46% peroxide (n = 3.9); FeNC/Pt5 yields 6.26% peroxide (n = 3.8); FeNC/Pt2 yields 16.70% peroxide (n = 3.6).

MW Synthesis Composite Series (at 0.5V): FeNC/Pt10 yields 4.64% peroxide (n = 4.0); FeNC/Pt yields15.28% peroxide (n = 3.8); FeNC/Pt yields 19.64% peroxide (n = 4.0).

The selectivity profiles reveal distinct trends: the hydrogen series method maintains lower absolute peroxide yields at the intermediate 5% loading (6.26%). However, the microwave-reduced series demonstrates a powerful mechanistic advantage in terms of completion: even as the peroxide yield rises to 15.28% and 19.64% at lower metal loading scales, the calculated electron transfer number (n) remains robustly locked at 4.0 for both FeNC/Pt10 and FeNC/Pt2.

This phenomenon indicates that while the microwave-reduced samples generate a higher concentration of peroxide intermediates at lower loadings, the active sites generated by the flash microwave process remain highly effective at immediately capturing and reducing those intermediates. This ensures that the overall process proceeds through a complete, highly efficient four-electron pathway in acidic environments.

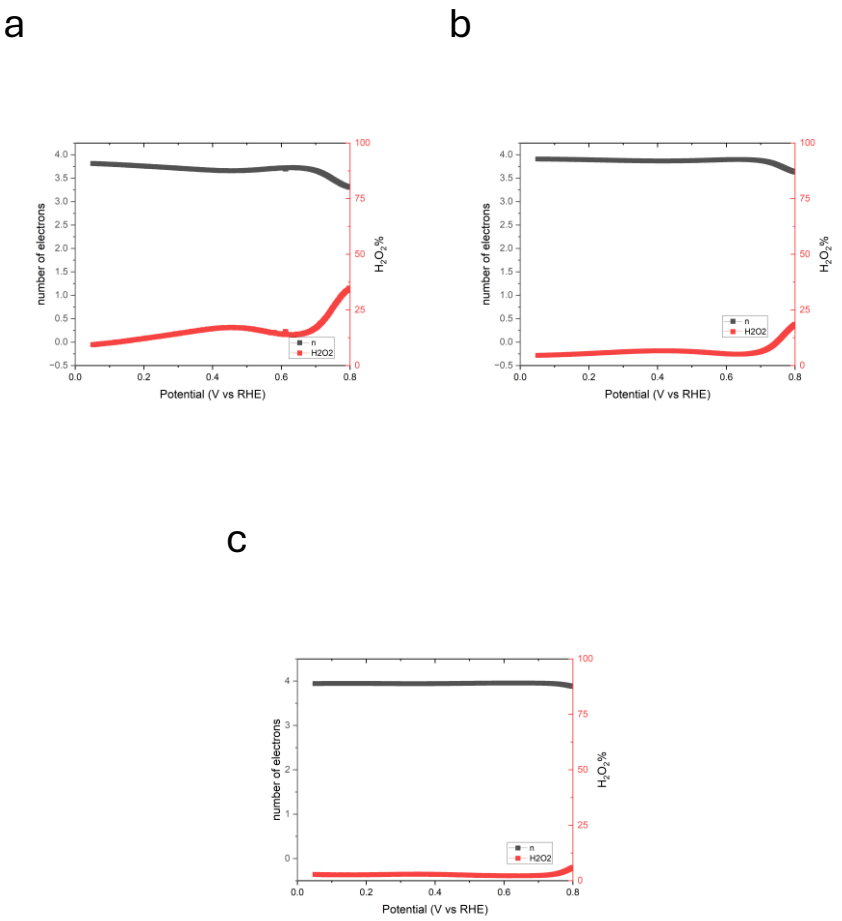

Figure 4.11. H2 composite selectivity curves showing the calculated number of transferred electrons (n) and hydrogen peroxide yield (H2O2) as a function of potential for the (a)FeNC2%, (b)FeNC/Pt5% , (c)FeNC/Pt10% in acidic media.

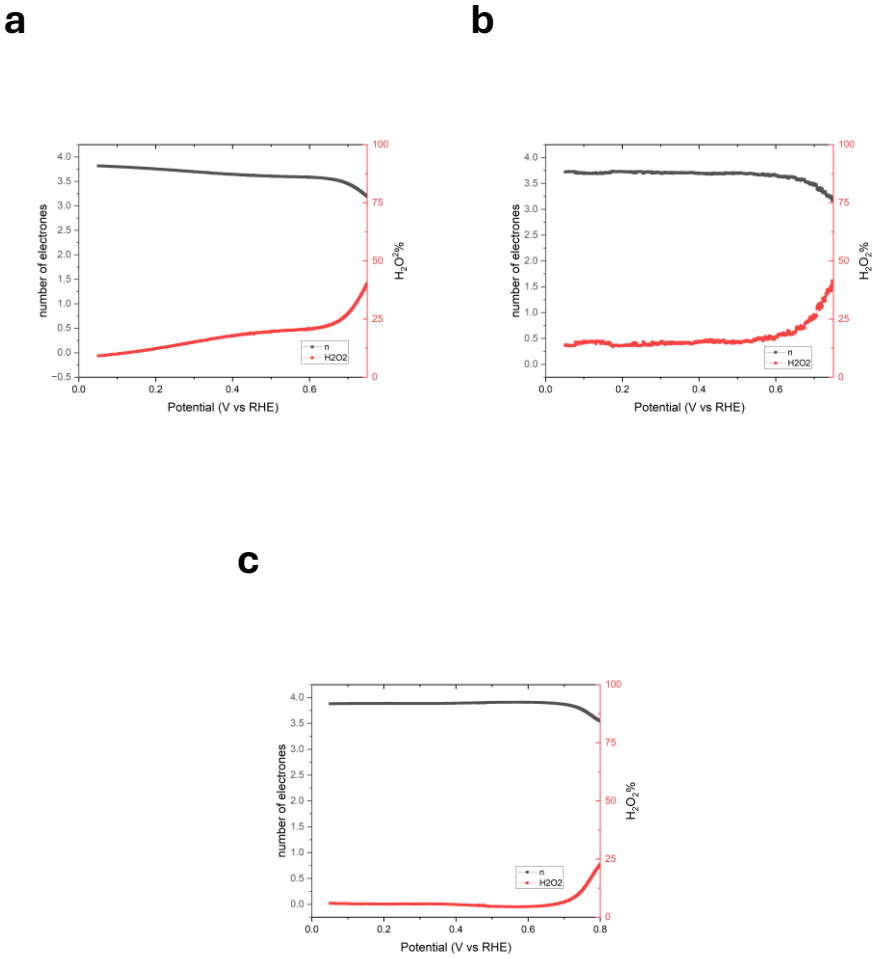

Figure 4.12. Mw composite selectivity curves showing the calculated number of transferred electrons (n) and hydrogen peroxide yield (H2O2) as a function of potential for the (a)FeNC2%, (b)FeNC/Pt5% , (c)FeNC/Pt10% in acidic media.

Koutecky-Levich Analysis for FeN/Pt Catalysts

To evaluate the oxygen reduction reaction (ORR) kinetics, Koutecky-Levich analysis was performed on the composite FeNC/Pt catalysts in oxygen-saturated acidic media. The experimental electron transfer numbers (n) revealed that the introduction of platinum nanoparticles onto the transition-metal-nitrogen-carbon matrix yielded distinct kinetic behaviors depending on the synthesis pathway.

For the conventional hydrogen thermal reduction series, a sequential mechanism shift occurred as a function of platinum loading. The low-loading FeNC/Pt 2% catalyst yielded an n of 3.2, indicating significant parallel two-electron peroxide formation. Increasing the loading to 5% shifted the mechanism toward a direct pathway ($n = 3.7$), ultimately reaching the ideal limit of 4.0 at 10% loading. This progression demonstrates that higher densities of platinum site ensembles work synergistically with the host Fe–N–C substrate to facilitate complete intermediate reduction.

Conversely, the microwave series exhibited exceptional kinetic efficiency even at the lowest loading thresholds. The microwave-treated FeNC/Pt 2% catalyst achieved an ideal four-electron transfer ($n = 4.0$), remained optimized at 3.8 for the 5% sample, and concluded at 4.0 for the 10% configuration. This highly efficient trend suggests that rapid, localized microwave heating optimizes the structural configuration and dispersion of interfacial active site junctions between the platinum clusters and the FeNC matrix. This interfacial synergy effectively lowers the activation barrier for direct O–O bond cleavage, achieving complete four-electron selectivity to water without requiring high noble metal loadings.

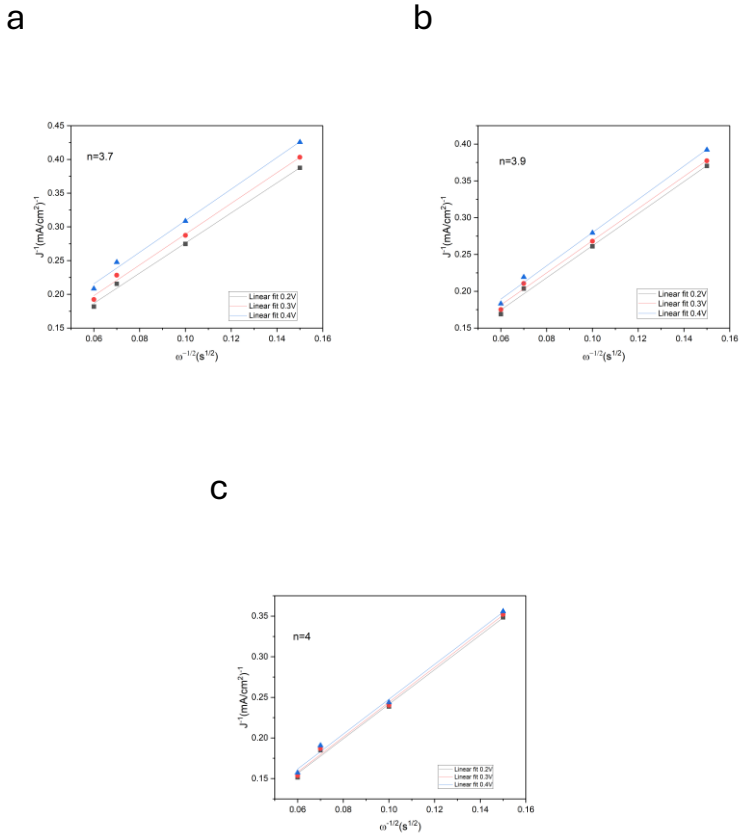

Figure 4.13. Hydrogen (H_2) synthesised catalyst K-L curves for (a) FeNC/Pt2%, (b) FeNC/Pt5%, (c) FeNC/Pt10% samples showing the calculated number of transferred electrons (n) .

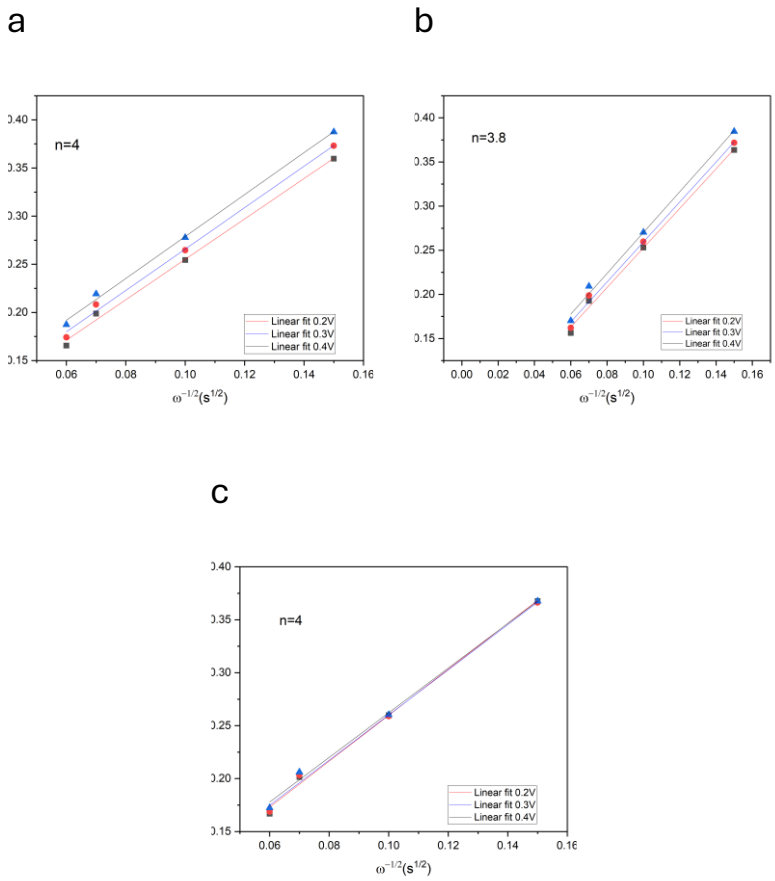

Figure 4.14. Microwave (Mw) synthesised catalyst K-L curves for (a) FeNC/Pt2%, (b) FeNC/Pt5%, (c) FeNC/Pt10% samples showing the calculated number of transferred electrons (n) .

4.3 Electrochemical Evaluation in Alkaline Media (KOH)

The evaluation of the prepared electrocatalysts was subsequently carried out in an alkaline environment (0.1M KOH) to contrast the ORR kinetics and reaction pathways against those recorded in acidic media. This section outlines the performance of the benchmark platinum on carbon control samples followed by the structural analysis of the FeNC/Pt composite catalysts under both hydrogen and microwave-assisted configurations.

4.3.1 Core Group Benchmarking: Pt/C Controls

Voltammetric Profile Analysis

CV was executed in an N_2-saturated 0.1M KOH electrolyte at a scan rate of 100 mV/s to delineate the active surface areas and interfacial transitions of the platinum sites.

Hydrogen (H_2) Synthesis Series: The baseline Pt/C 40% material registers characteristic hydrogen adsorption/desorption (H_{upd}) currents below 0.40V vs. RHE alongside a noticeable platinum oxide reduction feature centred near 0.78V in the reverse scan. Lowering the platinum fraction to 10%, 5%, and 2% suppresses the absolute current densities predictably. The Pt2 sample reflects a highly compressed profile, indicating reduced exposed metallic facets under these processing boundaries.

Microwave Synthesis Series: The microwave-reduced counterparts present exceptional current response symmetry. For the Pt10 and Pt5 loadings, the characteristic H_{upd} doublets are clearly resolved, and the cathodic oxide reduction peaks shift slightly more anodic (0.80V), denoting high active site cleanliness. Notably, the lowest loading variant (Pt2) demonstrates a significantly enhanced voltametric profile with prominent current densities that expand well beyond its H_2 series equivalent, indicating that flash microwave reduction yields superior metal nanoparticle exposure at very low weight fractions.

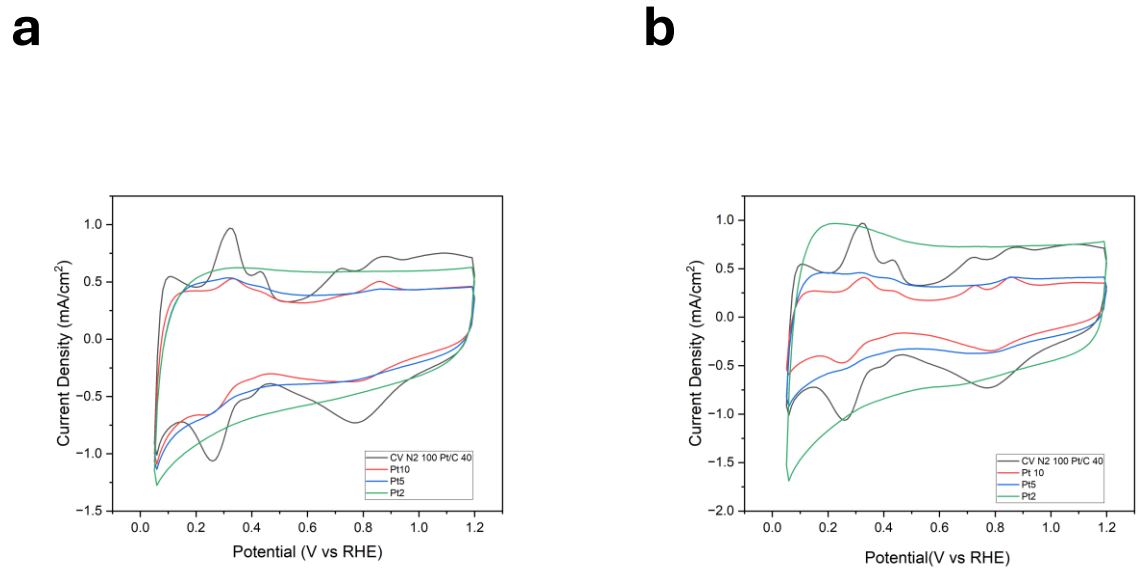

Figure 4.15. CV of synthesized Pt/C catalysts comparing the: (a) H_2, (b) microwave-assisted (MW) techniques at varying platinum weight fractions. Measurements recorded in an N2 -saturated 0.1\M KOH solution at a100mV scan rate.

Upon saturating the electrolyte with molecular oxygen the voltammetric loops are modified by the intensive cathodic contribution of the ORR:

In the H_2 Series: Intense cathodic reduction loops mask the baseline features. The Pt5 configuration registers a very sharp, steep reduction envelope centred precisely at 0.78V vs. RHE, approaching a current density near -5 mA/cm^2.

In the MW Series: The oxygen reduction profiles are highly defined. Both the Pt5 and Pt2 configurations develop exceptionally symmetrical, clean cathodic reduction envelopes centred near 0.78V and 0.76V vs. RHE, respectively. This response highlights that the microwave flash-reduction technique establishes uniform active centres ready for chemical interactions with molecular oxygen.

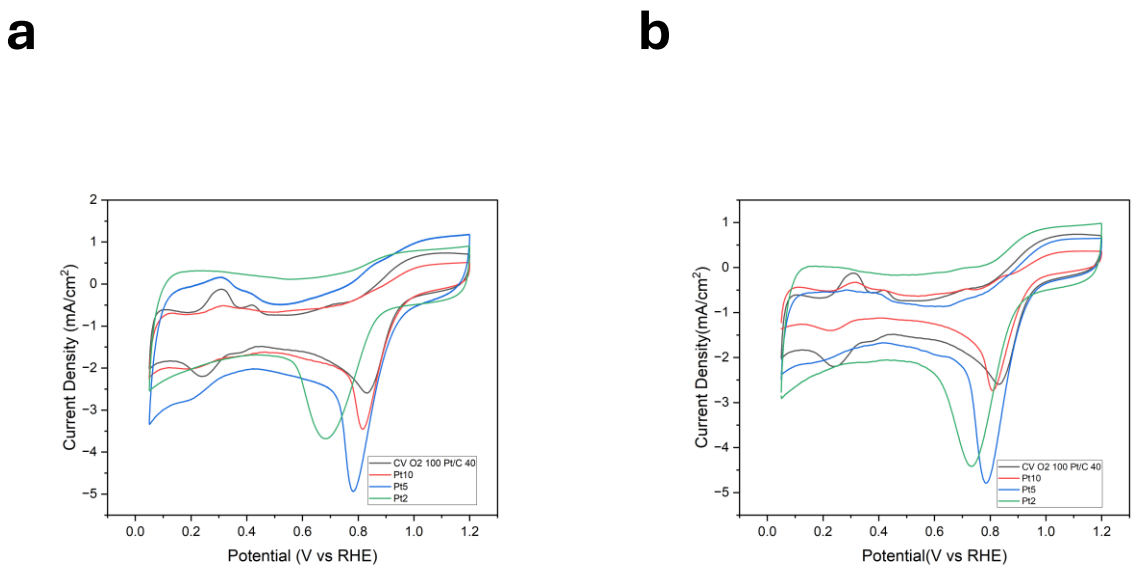

Figure 4.16. CV of synthesized Pt/C catalysts comparing the: (a)hydrogen (H_2), (b) microwave-assisted (MW) techniques at varying platinum weight fractions. Measurements recorded in an O2 -saturated 0.1\M KOH solution at a100mV scan rate.

Comparative ORR Kinetics (LSV)

To systematically isolate chemical kinetics from mass-transport constraints, LSV curves were collected using a rotating ring-disk electrode at a rotation rate of 1600 rpm and a scan rate of 10 mV/s. The resulting polarization profiles reveal an active kinetic region above 0.85 V vs. RHE that transitions sharply into a well-defined, uniform diffusion-limited plateau tracking between -5.0 mA/cm^2 and -5.5 mA/cm^2 at lower potentials.

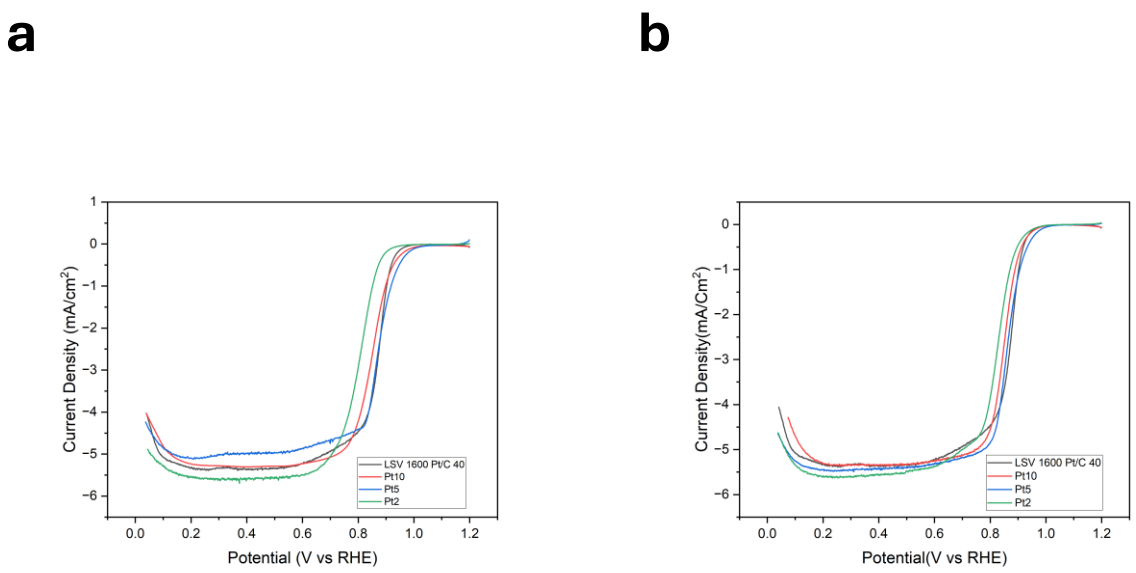

Figure 4.17. LSV curves for the Pt/C groups in an O2 -saturated 0.1M KOH solution at a rotation speed of 1600 rpm and scan rate of 10mV/s for the: (a) Hydrogen (H_2) series, and (b) Microwave (MW) series.

The essential parameters derived from these scans are catalogued in Table 4.3:

Table 4.3. ORR parameters for Pt/C controls in 0.1M KOH at 1600 rpm.

Catalyst Sample	***Onset Potential (V vs. RHE)***	***Half-Wave Potential $E_{1/2}$ (V vs. RHE)***
(H_2) Series		
Pt/C 40% (Commercial)	0.93	0.87
Pt/C 10%	0.96	0.85
Pt/C 5%	0.97	0.87
Pt/C 2%	0.89	0.80
Microwave Series		
Pt/C 40% (Commercial)	0.93	0.87
Pt/C 10%	0.92	0.83
Pt/C 5%	0.96	0.86
Pt/C 2%	0.92	0.82

The comparative data underscores a notable kinetic advantage for the microwave protocol at the lowest loading boundary (Pt/C 2%), where the onset potential shifts positively from 0.89V to 0.92V, and the corresponding half-wave potential rises from 0.80V to 0.82V. For the intermediate weight fractions (5% and 10%), the metrics generated by both synthetic paths are highly aligned, validating the microwave protocol as a competitive, high-throughput preparation approach.

RRDE Selectivity and peroxide Yields

The catalyst reaction pathway was analysed via 4-electrode measurements by evaluating intermediate peroxide generation and tracking the overall electron transfer number (n). The data metrics extracted at a constant disk potential of 0.5V vs. RHE outline distinct synthesis-dependent trends:

H_2 Synthesis Series (at 0.5V): Pt/C 10% yields 2.60% peroxide (n = 3.9); Pt/C 5% yields 1.65% peroxide (n = 4); Pt/C 2% yields 2.5% peroxide (n = 3.9).

MW Synthesis Series (at 0.5V): Pt/C 10% yields 4.08% peroxide (n = 3.9); Pt/C 5% yields 5.37% peroxide (n = 3.9); Pt/C 2% yields 2.42% peroxide (n = 3.9).

In alkaline media, both synthetic routes maintain high selectivity toward the primary four-electron reduction pathway, with electron transfer numbers consistently at or near 4.0. However, the H_2 synthesis series exhibits enhanced intermediate restraint at the 5% loading threshold, minimizing peroxide generation to 1.65% with a complete four-electron transfer (n=4). In contrast, the microwave-reduced route experiences a higher intermediate peroxide evolution at 5% loading (5.37%) before stabilizing at the 2% loading threshold (2.42%), indicating that the localized catalyst structures impact intermediate retention differently depending on the chosen synthesis route and mass loading.

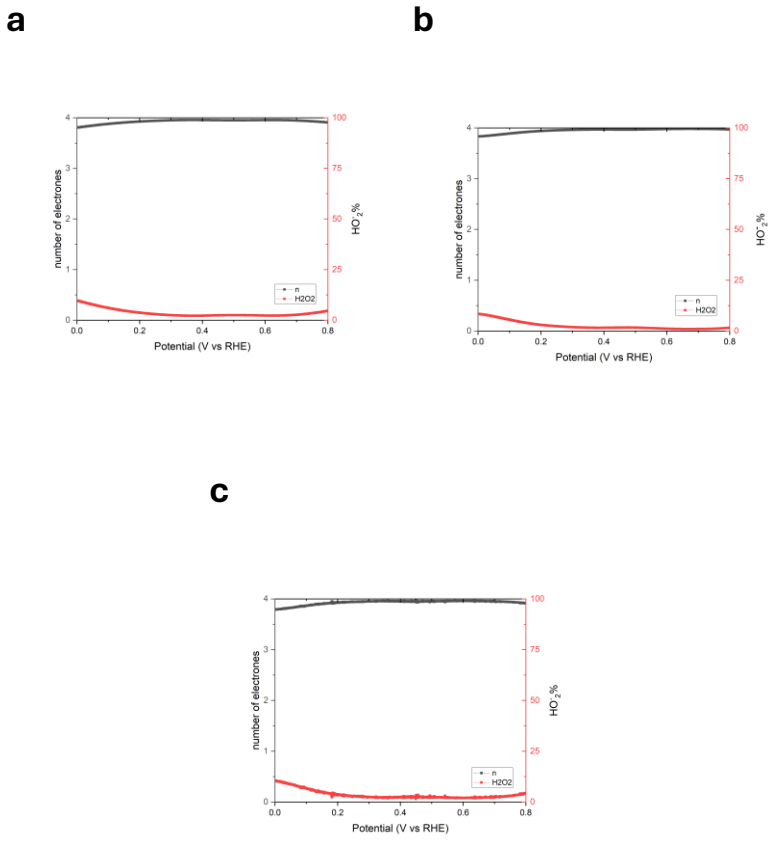

Figure 4.18. H2 catalyst selectivity profiles showing calculated electron transfer number (n) and intermediate Hydroperoxide release (HO^-_2) in alkaline media for(a)Pt/C2%, (b)Pt/C5%, (c)Pt/C10% .

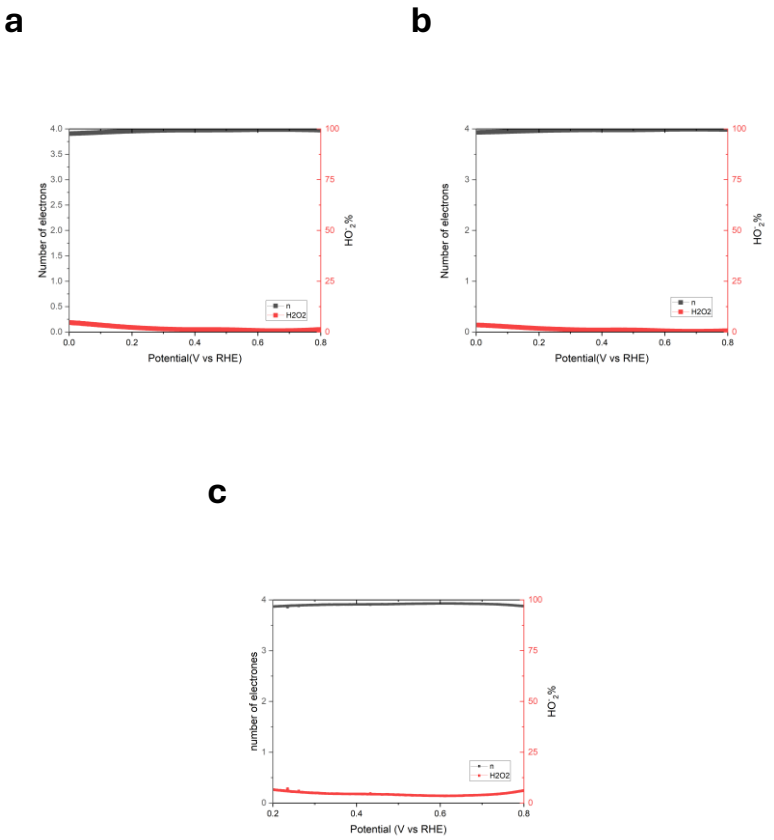

Figure 4.19. Mw catalyst selectivity profiles showing calculated electron transfer number (n) and intermediate Hydroperoxide release (HO_2^-) in alkaline media for(a)Pt/C2%, (b)Pt/C5%, (c)Pt/C10% .

Koutecky-Levich Analysis for Pt/C Catalysts

In alkaline media, the Koutecky-Levich electron transfer numbers (n) for both H_2-furnace and microwave-treated Pt/C catalysts converge almost identically, tracking from 3.4–3.5 at 2% loading to 3.8 at 10% loading. This close alignment indicates that increasing the local density of platinum sites consistently improves selectivity toward the four-electron mechanism by capturing intermediate peroxide species. Crucially, the microwave synthesis advantage observed in acidic environments is minimized here because the basic medium inherently lowers the activation barrier for direct O–O bond cleavage. Consequently, macro-scale platinum loading dictates the reaction kinetics in this environment, overriding any microstructural benefits from the alternative synthesis pathways.

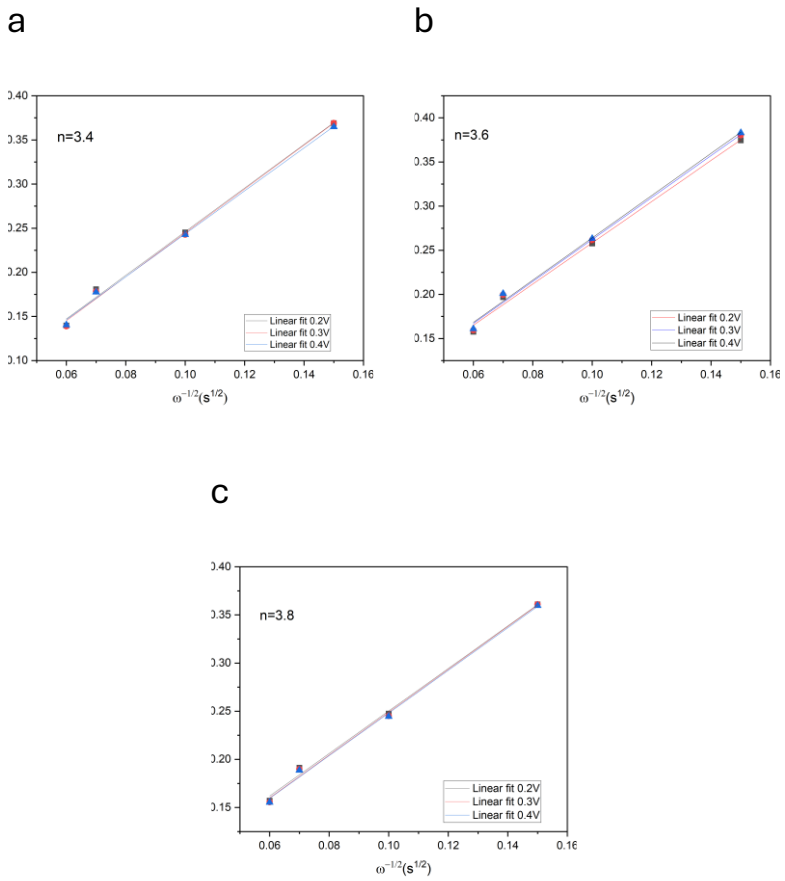

Figure 4.20. Hydrogen (H_2) synthesised catalyst K-L curves for (a) Pt/C2%, (b) Pt/C5%, (c) Pt/C10% samples showing the calculated number of transferred electrons (n) .

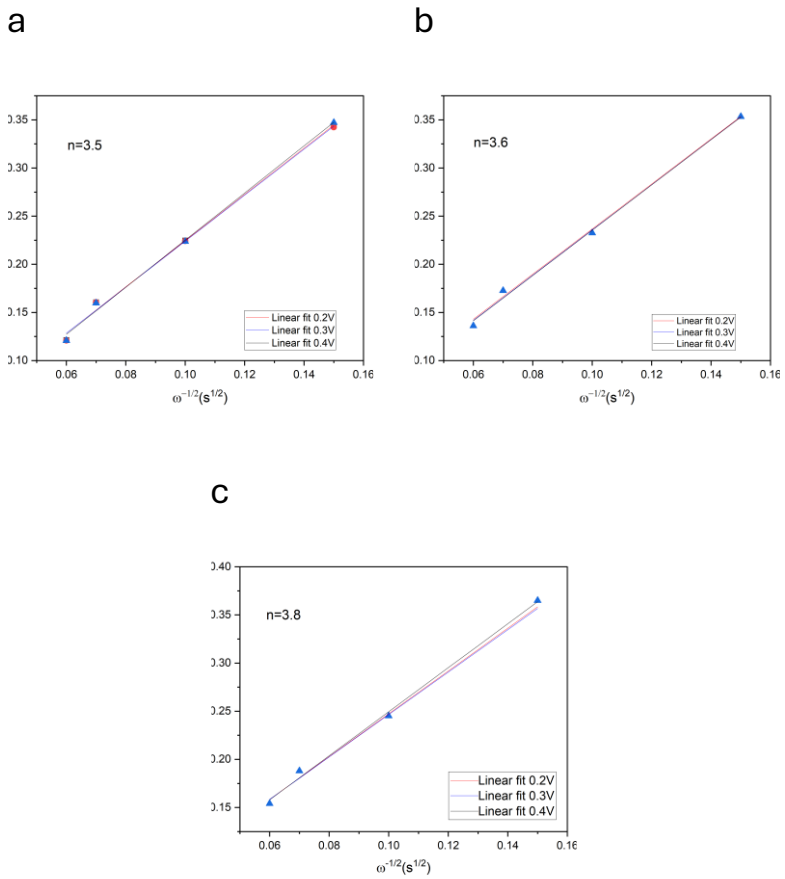

Figure 4.21. Microwave (Mw) synthesised catalyst K-L curves for (a) Pt/C2%, (b) Pt/C5%, (c) Pt/C10% samples showing the calculated number of transferred electrons (n) .

Electrochemical surface area Analysis for Pt/C Catalysts

The H_2 Purge Series (Furnace): Similar to the acidic medium, the 2wt% sample shows no visible H_{upd} features due to severe metal agglomeration. While the ECSA increases at 5% (5.95 m^2/g) and 10% (9), the overall surface area is noticeably lower than its acidic counterparts. This suppression is a consequence of modified double-layer charging dynamics in base, where slower hydrogen adsorption kinetics on agglomerated, chunky platinum clusters restricts complete monolayer formation. [36]

The Microwave (MW) Series and the 5% Peak: The microwave samples show high structural accessibility, but feature a prominent anomaly: the ECSA peaks significantly at 5wt% (25.71 m^2/g), outperforming both the 2% (11.19 m^2/g) and 10% (12.86 m^2/g) variations. At this intermediate5% threshold, the microwave flash treatment yields an idealized balance of particle size and spatial distribution. In an alkaline medium where aggressive proton-assisted surface blocking is absent this optimal inter-particle spacing allows maximum hydroxide wetting of the isolated platinum interfaces. This unmasks a massive fraction of active crystal facets that become otherwise restricted by localized channel crowding at higher loadings (10%) or severe dispersion gaps at lower loadings (2%). [36] [37]

4.3.2 Advanced Composite Evaluation: FeNC/Pt Catalysts

Following the control group baseline evaluation, the electrochemical screening was directed toward the advanced FeNC composite matrices modified with platinum weight fractions of 2%, 5%, and 10%.

Voltammetric Profile and Analysis

CV recorded in an N_2-saturated 0.1M KOH solution at 100mV/s reveal structural variations within the carbon matrix based on synthesis technique.

H_2 Synthesis Series: The baseline bare FeNC support develops a very broad, rectangular double-layer capacitance trace, reflecting its highly open, porous architecture. This classic rectangular voltammetric profile indicates ideal non-faradaic capacitive charging (C_{dl}), which directly correlates to the highly open, hierarchically porous structure of the carbon matrix. [38] The interconnected network of micro- and mesopores allows for effortless electrolyte wetting and maximum surface area exposure without any mass transport resistance. [39]

Upon loading platinum via the hydrogen route, this background capacitance profile remains broad and tightly bundled across all weight fractions, showing negligible suppression or matrix blocking.

Microwave Synthesis Series: The introduction of platinum induces a progressive compression of the broad rectangular capacitive envelope relative to the bare FeNC baseline. This loading-dependent suppression suggests that the rapid thermal input from the microwave flash-reduction method alters the carbon surface wetting properties or access boundaries, modifying double-layer charging while preserving metallic active sites.

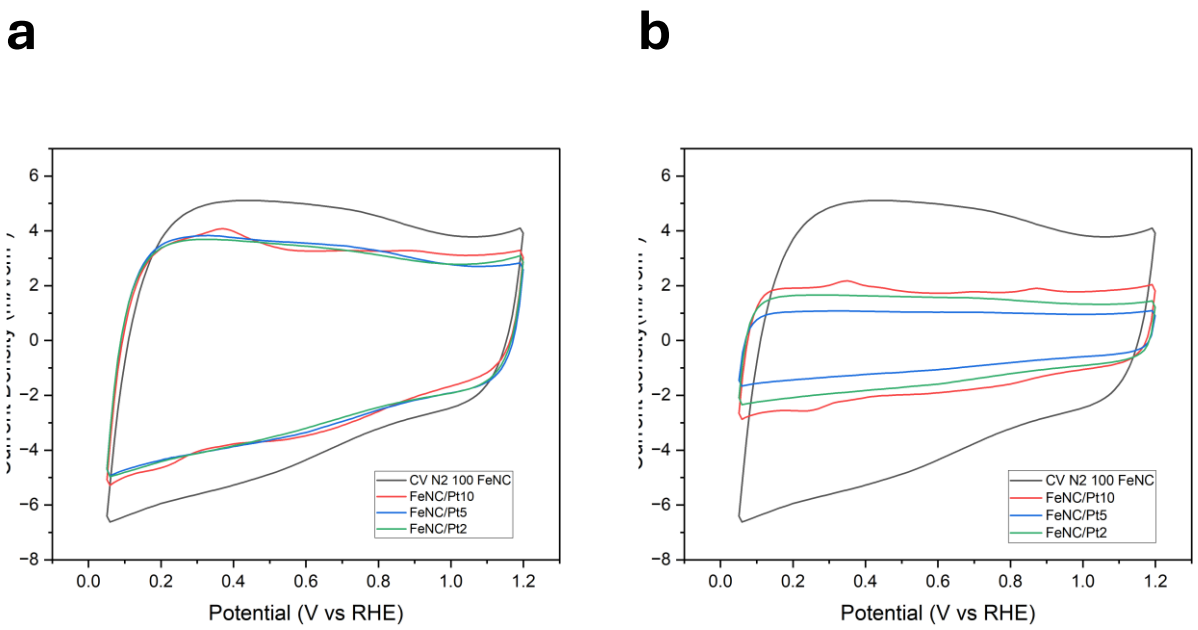

Figure 4.22. CV of synthesized FeNC/Pt catalysts comparing the: (a)hydrogen (H_2), (b) microwave-assisted (MW) techniques at varying platinum weight fractions. Measurements recorded in an N2 -saturated 0.1M KOH solution at a100mV scan rate.

When shifted to an O_2-saturated alkaline electrolyte, intensive oxygen reduction features develop:

In the H_2 Series: Distinct, highly defined oxygen reduction peaks emerge centred near 0.84 V vs. RHE across all platinum fractions, super imposing smoothly on top of the prominent carbon matrix background capacitance.

In the MW Series: The ORR cathodic peaks are sharp and well-resolved centred around 0.84 V vs. RHE (especially sharp for the FeNC/Pt10 and FeNC/Pt5 variants), coinciding with the compressed background double-layer capacitance seen in the inert scans.

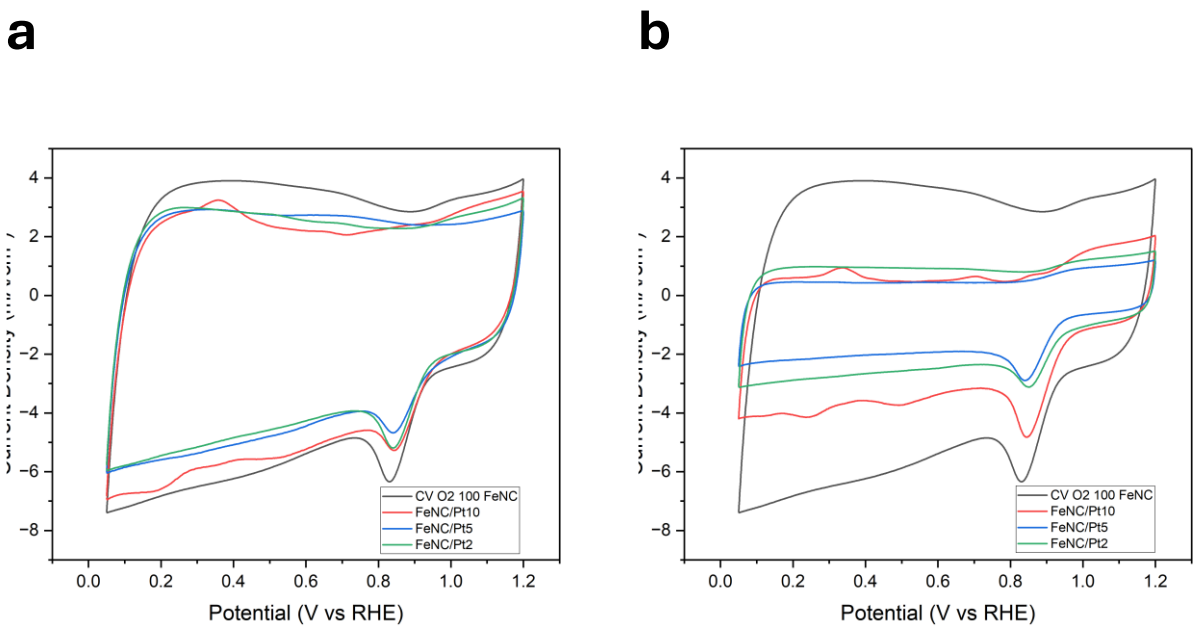

Figure 4.23. CV of synthesized FeNC/Pt catalysts comparing the: (a)hydrogen (H2), (b) microwave-assisted (MW) techniques at varying platinum weight fractions. Measurements recorded in an O2 -saturated 0.1M KOH solution at a100mV scan rate.

Comparative ORR Kinetics (LSV)

To isolate the true kinetic metrics, LSV was conducted at a rotation speed of 1600 rpm in an oxygen-saturated medium. The extracted onset and half-wave potentials are consolidated in Table 4.4.

a

b

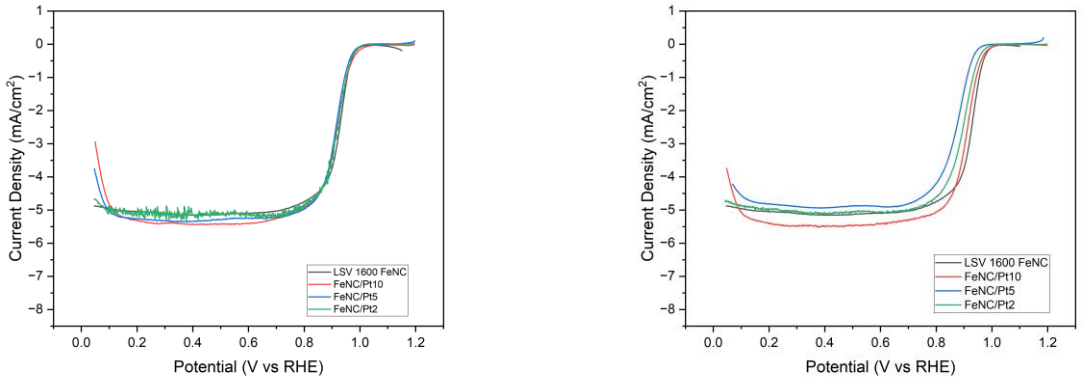

Figure 4.24. LSV curves for the FeNC/Pt groups in an O2 -saturated 0.1M KOH solution at a rotation speed of 1600 rpm and scan rate of 10mV/s for the: (a) Hydrogen (H2) series, and (b) Microwave (MW) series.

Table 4.4 ORR parameters for FeNC/Pt composites in 0.1M KOH at 1600 rpm.

Catalyst Sample	***Onset Potential (V vs. RHE)***	***Half-Wave Potential $E_{1/2}$ (V vs. RHE)***
H_2 Series		
FeNC	0.99	0.92
FeNC/Pt10	1.01	0.91
FeNC/Pt5	0.99	0.91
FeNC/Pt2	0.99	0.91
MW Series		
FeNC	0.99	0.92
FeNC/Pt10	0.97	0.90
FeNC/Pt5	0.94	0.87
FeNC/Pt2	0.96	0.89

The alkaline hydrodynamic data reveals unique behaviour compared to the acidic runs:

The bare FeNC catalyst matrix displays remarkably high standalone activity in alkaline conditions, registering an onset potential of 0.99V and a half-wave potential of 0.92V outperforming several standalone Pt/C configurations.

Within the H_2 composite series, adding10 wt.% Pt drives an exceptional anodic shift, pushing the onset potential to 1.01V while half-wave potentials stay tightly locked near 0.91V across all loading ranges.

Within the Mw composite series, the kinetics show minor fluctuations, with the half-wave potentials stepping down slightly to 0.90V, 0.87V, and 0.89V. Interestingly, the 2wt.% composite configuration (FeNC/Pt2) outperforms the intermediate 5wt.% alternative (0.89V vs. 0.87V), pointing toward a highly active interfacial alignment at that ultra-low loading boundary.

Selectivity Pathway and Peroxide Yields

Catalytic selectivity and pathway stability were tracked using 4-electrode collection techniques. The quantitative metrics extracted at a constant disk potential of 0.5V vs. RHE indicate a reversal in structural performance compared to the acidic testing runs:

H_2 Synthesis Composite Series (at 0.5V): FeNC/Pt10 yields 8.40% peroxide (n = 3.8); FeNC/Pt5 yields 5.90% peroxide (n = 3.9); FeNC/Pt2 yields 4.60% peroxide (n = 3.9).

MW Synthesis Composite Series (at 0.5V): FeNC/Pt10 yields 13.09% peroxide (n = 3.8); FeNC/Pt5 yields 19.56% peroxide (n = 3.7); FeNC/Pt2 yields 4.79%peroxide (n = 3.7).

The collection data points highlight distinct mechanistic features:

In alkaline media, the H_2 method delivers excellent selectivity at lower loading scales, suppressing intermediate peroxide generation down to 5.90% and 4.60% while maintaining a stable, high electron transfer number near 3.9

In the Microwave series, a unique structural performance is resolved: while the intermediate 5% loading records an elevated peroxide yield (19.56%), the 2% loading sample (FeNC/Pt2) demonstrates high efficiency, dropping intermediate peroxide generation back down to 4.79%. This response indicates that ultra-low metal additions processed under fast microwave heating establish a highly selective, active composite boundary layer optimized for alkaline environments.

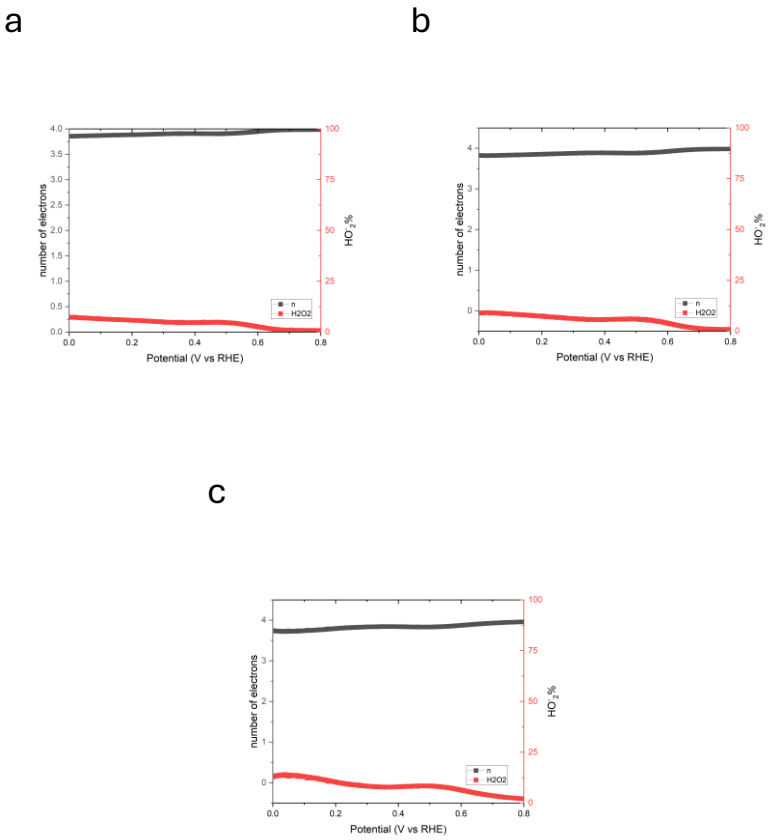

Figure 4.25. H_2 catalyst selectivity profiles showing calculated electron transfer number (n) and intermediate Hydroperoxide release (HO2 −) in alkaline media for(a)FeNC/Pt2%, (b)FeNC/Pt5%, (c)FeNC/Pt10% .

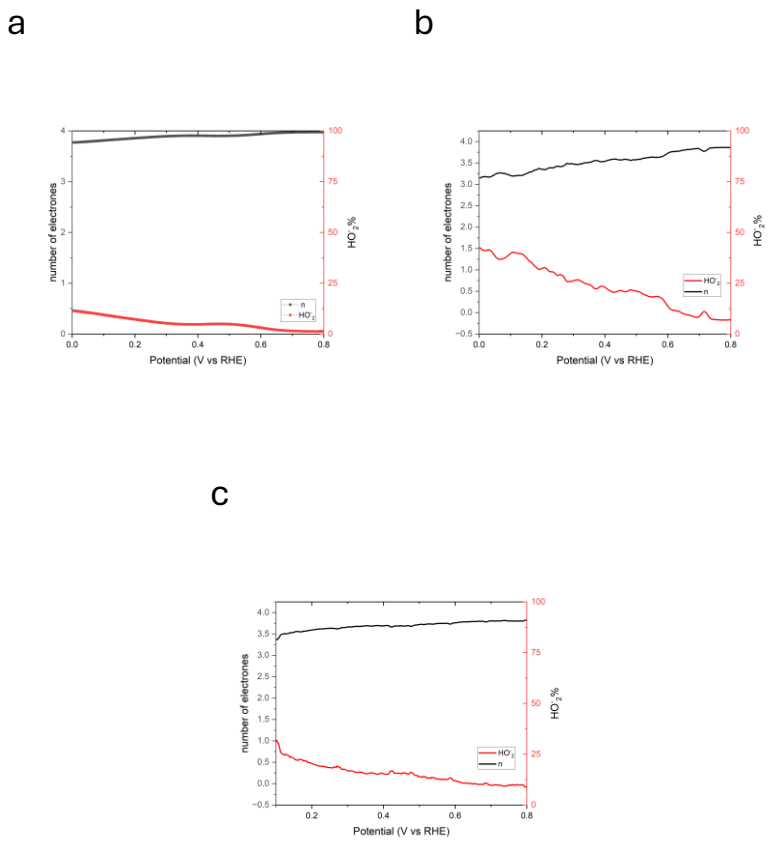

Figure 4.26. Mw catalyst selectivity profiles showing calculated electron transfer number (n) and intermediate Hydroperoxide release (HO_2^-) in alkaline media for(a)FeNC/Pt2%, (b)FeNC/Pt5%, (c)FeNC/Pt10% .

Koutecky-Levich Analysis

In alkaline (basic) solutions, the reaction behaves differently than in acid because it is naturally much easier for oxygen molecules to split apart. When evaluating the electron transfer number (n) for the FeNC/Pt catalysts, we see a surprising flip in performance: the traditional H_2-furnace method actually outperforms the microwave method.

- The H_2-furnace samples are highly efficient from the start, showing an electron transfer number of 3.9 at low loadings (2% and 5%) and hitting the perfect limit of 4.0 at 10% loading. This means they drive a clean, direct 4-electron reaction straight to water.
- The Microwave (Mw) samples lag slightly behind, staying at a lower, flat value of 3.7 for the 2% and 5% samples, and only reaching 3.8 at 10% loading.

The long, steady heating under hydrogen gas during furnace synthesis allows the platinum clusters to settle and chemically pair up perfectly with the iron and nitrogen centers on the carbon support. This unique synergy creates "dual-site" active spots that work together to completely reduce oxygen. On the other hand, the rapid flash-heating from the microwave method is too fast to form these ideal interfacial junctions on this specific

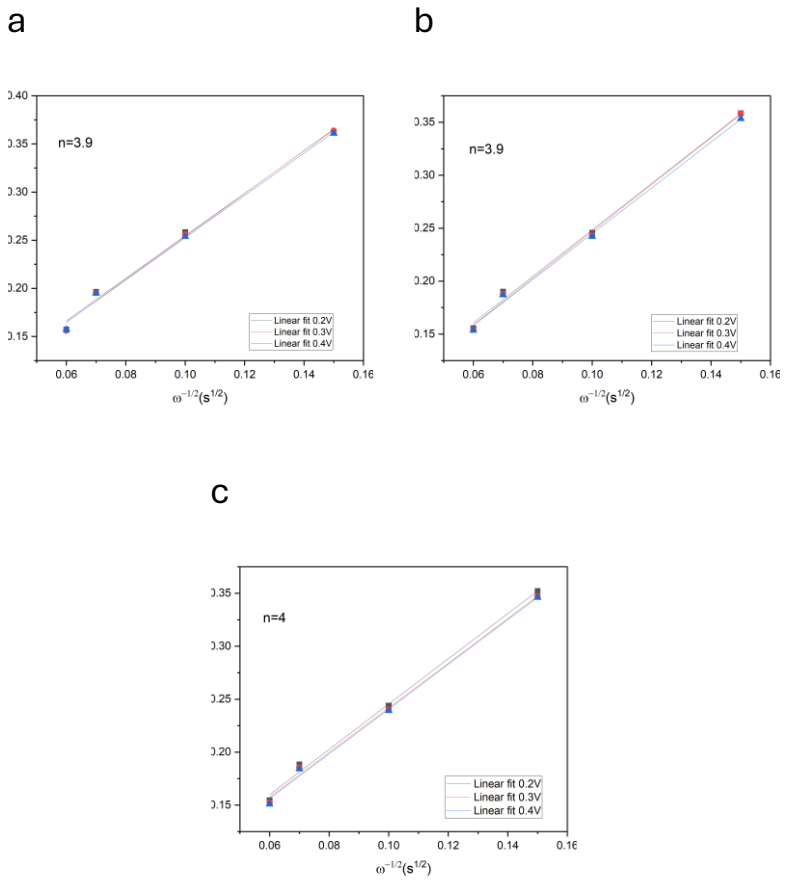

Figure 4.27. Hydrogen (H2) synthesised catalyst K-L curves for (a) FeNC/Pt2%, (b) FeNC/Pt5%, (c) FeNC/Pt10% samples showing the calculated number of transferred electrons (n) .

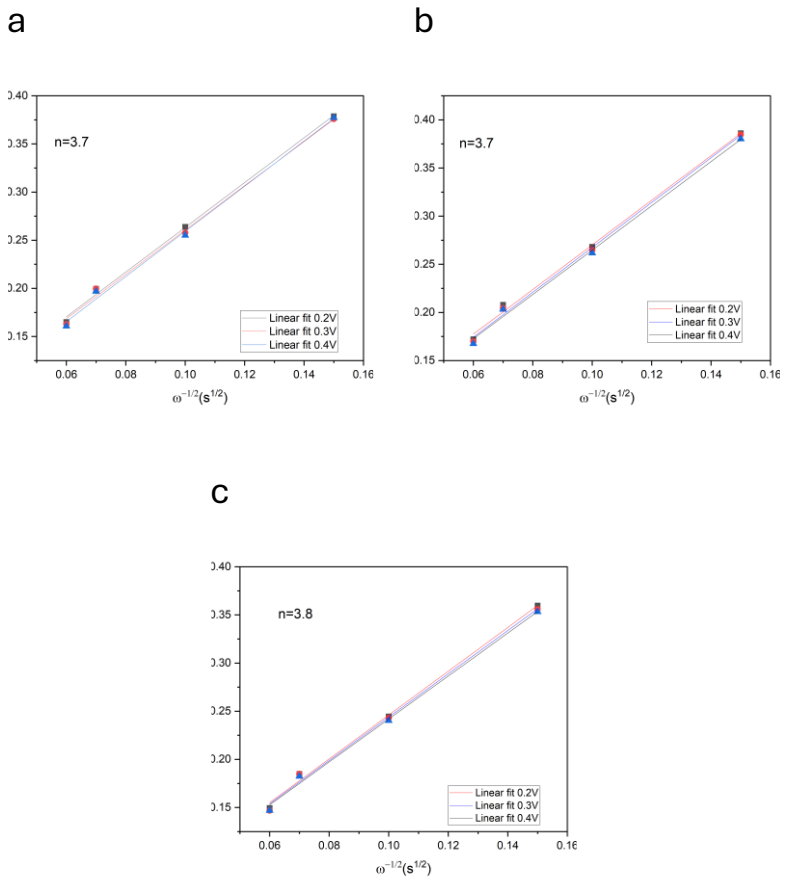

Figure 4.28. Microwave (Mw) synthesised catalyst K-L curves for (a) FeNC/Pt2%, (b) FeNC/Pt5%, (c) FeNC/Pt10% samples showing the calculated number of transferred electrons (n) .

4.4 Comparative Kinetic Evaluation: Electrolyte pH Dependence

To address the mechanism variations across different chemical environments, ORR pathways of the synthesized hybrid catalysts were compared in both acidic and alkaline media. The quantitative electron transfer numbers (*n*) extracted from the Koutecky-Levich diagnostic plots show distinct differences that are directly linked to pH-dependent interface behaviors.

Alkaline vs. Acidic Mechanics and Synthesis Impact

The Alkaline Paradigm (0.1M KOH): In basic solutions, the abundance of OH^- ions optimizes intermediate adsorption thermodynamics. The pristine FeNC matrix intrinsically demonstrates fast kinetics because the carbon framework is immune to proton attack and the active FeN_4 sites are protected against metal leaching. Any generated hydroperoxide intermediate (HO^-_2) is highly stable in base and undergoes rapid reduction at neighbouring sites, yielding high baseline selectivity (n>3.5) prior to Pt addition.

The Acidic Paradigm: In harsh acid, complete 4-electron reduction is more demanding due to volatile hydrogen peroxide (H_2O_2) generation, single-atom demetallation (iron leaching) caused by nitrogen protonation, and radical-driven carbon corrosion.

Synthesis Influence on Acid Performance: For the traditional hydrogen-purged furnace reduction series, localized thermal sintering creates larger gaps between active particles. At 2wt% and 5 wt% loadings, intermediate H_2O_2 escapes into the electrolyte before hitting a secondary active centre. It requires a high loading of 10 wt% to bring the particles close enough together to capture escaping intermediates.

Conversely, the fast volumetric energy delivery of the flash microwave synthesis (120C°, 5 min) prevents particle migration, maintaining ultra-small, tightly spaced Pt nanoclusters. This close spatial dispersion facilitates a local cascade mechanism where escaping peroxide is immediately captured by adjacent sites, raising efficiency to n=4 (2 wt%) and n=3.8 (5 wt%), and achieving an ideal direct pathway (n=4) at 10 wt% loading.

4.5 Accelerated Durability and Catalyst Degradation Analysis

To evaluate the operational lifespan and resistance to degradation of the target catalysts under conditions simulating long-term operation, accelerated stress testing (AST) was performed. The protocol consisted of subjecting the materials to 10,000 continuous electrochemical potential cycles between 0.6V and 1V vs. RHE in an oxygen-saturated environment. Based on the kinetic activity and selectivity trends established during initial screenings, the advanced composite evaluation focused on the primary winning configurations FeNC/Pt 5% and FeNC/Pt 10%. These were evaluated alongside the bare FeNC support baseline to decouple the stability of the non-precious coordination sites from precious metal degradation mechanisms.

4.5.1 Accelerated Stress Testing in Acidic Media (0.1M $HClO_4$)

Voltametric Profile Shift and Aging

The baseline changes in active site accessibility were monitored via CV in an O_2 saturated 0.1M $HClO_4$ solution by comparing the initial 0 cycle response against the post-aging 10,000 cycles profiles.

Bare FeNC Support: Initially, the bare matrix features its primary ORR cathodic peak centred at approximately 0.58 V vs. RHE. Following the 10,000 potential sweeps, the profile exhibits a significant cathodic migration, with the reduction peak shifting down to 0.48V. This marked100mV displacement indicates substantial overpotential accumulation, likely driven by proton-assisted demetallation of active FeN_x sites or surface functional group alteration.

FeNC/Pt 5% Composite: The 5wt.% composite displays a well-defined initial reduction envelope centred near 0.55V. Post-aging, the peak experiences a cathodic displacement of approximately 80mV, stabilizing at 0.47V. The background pseudocapacitive double-layer charging region (between 0.1V and 0.7V) maintains high stability, indicating structural retention of the carbon backbone.

FeNC/Pt 10% Composite: The 10wt.% loading initially records the most anodically advanced peak position at 0.61V. However, after the stability sweeps, it undergoes a pronounced negative peak shift of roughly 120mV, relocating down to 0.49V.his higher degradation rate is accompanied by a slight expansion in background double-layer capacitance, pointing toward localized carbon oxidation or severe platinum particle agglomeration. This accelerated degradation at higher metal loading is driven by the closer proximity of Pt nanoparticles, which promotes rapid Ostwald ripening during potential

cycling. Concurrently, the dense Pt clusters accelerate the electrochemical oxidation of the adjacent carbon matrix, generating oxygen-containing surface functional groups that account for the observed expansion in double layer capacitance.

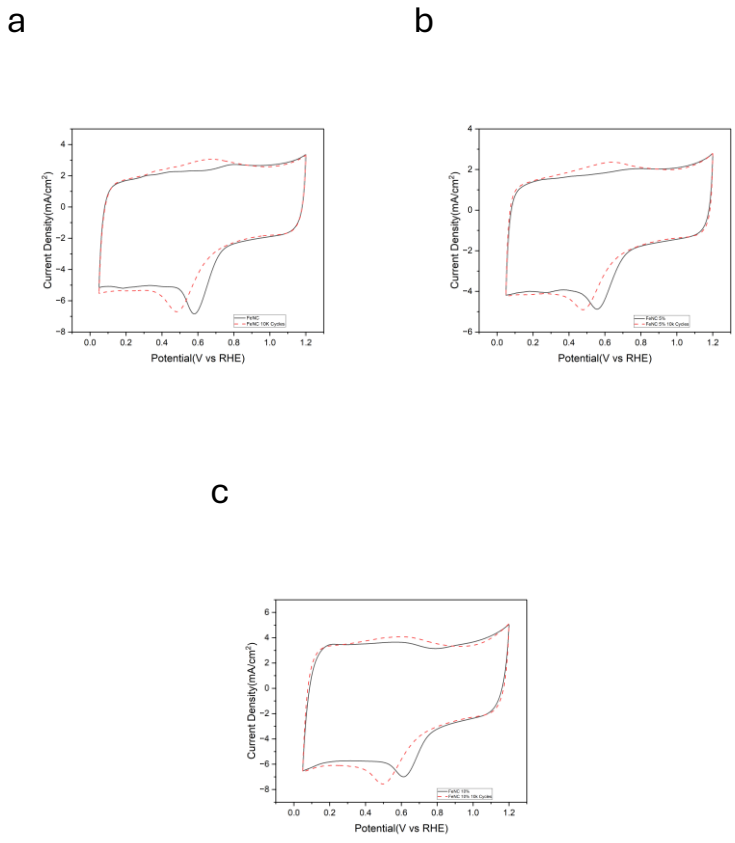

Figure 4.29. CV recorded in an O2-saturated 0.1M HClO4 solution at 100mV/s comparing the initial state (0 cycle, black solid line) and post-aging state (10,000 cycles, red dashed line) for: (a) Bare FeNC, (b)FeNC/Pt 5%, and (c) FeNC/Pt 10%.

Hydrodynamic Decay and Activity Losses

To quantify the degradation of steady-state transport kinetics, LSV curves were recorded at 1600 rpm before and after aging.

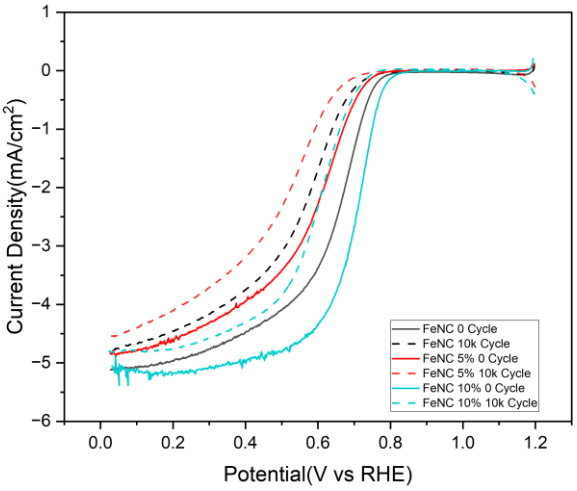

Figure 4.30. LSV curves in an O2-saturated 0.1M HClO4 solution at 1600 rpm and 10mV/s tracking the performance decay before and after 10,000 aging cycles for the bare matrix and platinum-modified composite catalysts.

The absolute potential decay values (ΔE) for both the onset and half-wave regions are summarized in Table 4.5:

Table 4.5. Kinetic potential degradation parameters after 10,000 cycles in 0.1M $HClO_4$

Material	***ΔE$_{onset}$ (V)***	***ΔE$_{1/2}$ (V)***
FeNC	0.06±0	0.09±0
FeNC/Pt 5%	0.05±0.01	0.04±0.01
FeNC/Pt 10%	0.06±0.01	0.07±0.03

The hydrodynamic metrics identify the FeNC/Pt 5% sample as the most resilient configuration. While the bare support loses 90mV at the half-wave boundary, the 5% platinum integration limits half-wave decay to just 40mV. This enhanced stability validates the presence of a protective structural synergy, where the presence of lower mass fractions of platinum nanoparticles suppresses severe carbon support oxidation and stabilizes adjacent FeN_x centres. In contrast, the 10% composite degrades more quickly ($\Delta_{E1/2}$ = 70mV), suggesting that higher local nanoparticle densities accelerate platinum dissolution and Ostwald ripening in acidic environments. Crucially, across all samples, the diffusion-limited mass-transport plateau remains steady near -5 mA/cm^2, proving that the physical film maintains excellent mechanical adherence to the disk substrate.

Pathway Resiliency and Selectivity Preservation

`The impact of catalyst aging on the underlying reaction mechanism was tracked by recording intermediate peroxide (H_2O_2) release and electron transfer shifts via hydrodynamic collection metrics.

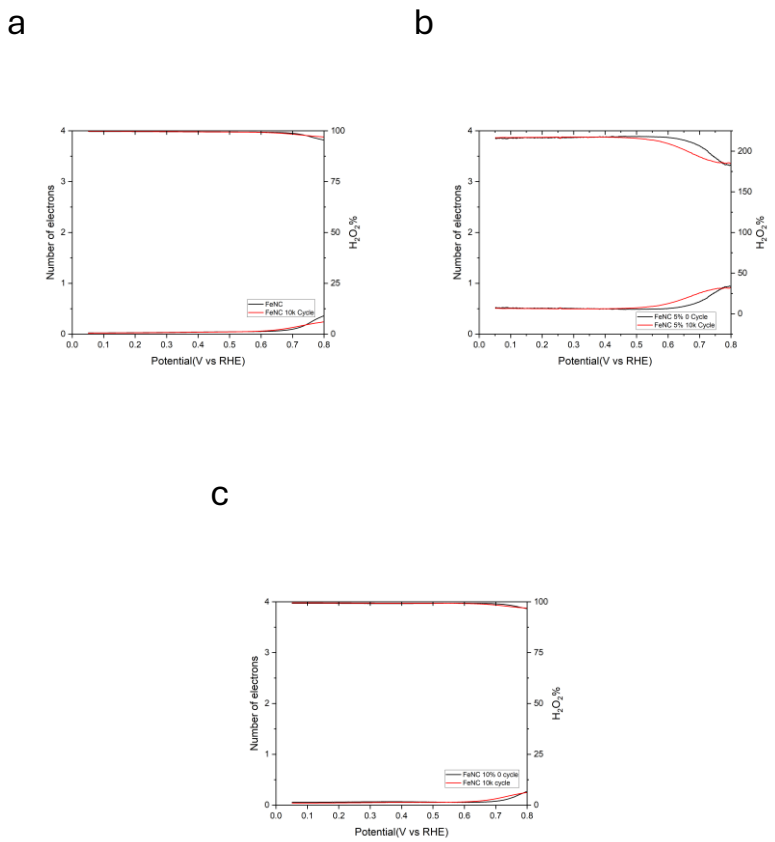

Figure 4.31. RRDE selectivity profiles showing the calculated electron transfer number (n) and hydrogen peroxide yield before and after 10k cycles in acidic media for: (a) FeNC, (b)FeNC/Pt 5%, and (c) FeNC/Pt 10%.

The total alterations in electron transfer numbers measured at a disk potential of 0.5V vs. RHE are compiled in Table 4.6:

Table 4.6. Alterations in selectivity parameters after 10k cycles at 0.5 V vs. RHE in acid.

Material	***Δ Peroxide Yield (%)***	***Δn***
FeNC	1.41±0	0.02±0
FeNC/Pt 5%	0.07±0.01	0.0±0.01
FeNC/Pt 10%	0.05±0	0±0

The collection parameters demonstrate exceptional pathway resiliency for the composite materials. The bare support displays a modest peroxide increase (Δ= 1.41%), indicating minor degradation of its high-efficiency sites. In contrast, both the 5% and 10% platinum-modified composites exhibit near-zero variance in their operational pathways (Δ Peroxide 0.07% and Δn=0). This response proves that while the active sites undergo partial surface restructuring causing the kinetic overpotentials seen in the LSV sweeps the remaining functional active boundaries continue to drive a direct, highly efficient 4-electron pathway without collapsing into an incomplete, corrosive 2-electron mechanism.

4.5.2 Accelerated Stress Testing in Alkaline Media

Voltametric Profile Shift and Aging

The active surface behaviour and interfacial reaction changes under alkaline stress conditions were evaluated by examining the CV features in an O_2 saturated 0.1M KOH electrolyte before and after the 10k potential aging sweeps.

FeNC/Pt 5% Composite: Initially, the catalyst exhibits a sharp oxygen reduction peak centred at 0.84 V vs. RHE. Following the accelerated durability protocol, the reduction envelope experiences an ultra-low cathodic shift of approximately 20mV, stabilizing at 0.82 V. The high symmetry and area retention of the double-layer capacitance plateau confirm that both the embedded metallic sites and the carbon host network maintain strong structural integrity in the alkaline medium.

FeNC/Pt 10%Composite: The 10wt.% loading sample exhibits its initial reduction peak near 0.82V. Post-aging, the position of this peak remains completely locked at 0.82V, demonstrating near-perfect active site preservation. The background pseudocapacitive charging current registers a minor compression, highlighting a highly stable configuration with minimal active boundary loss.

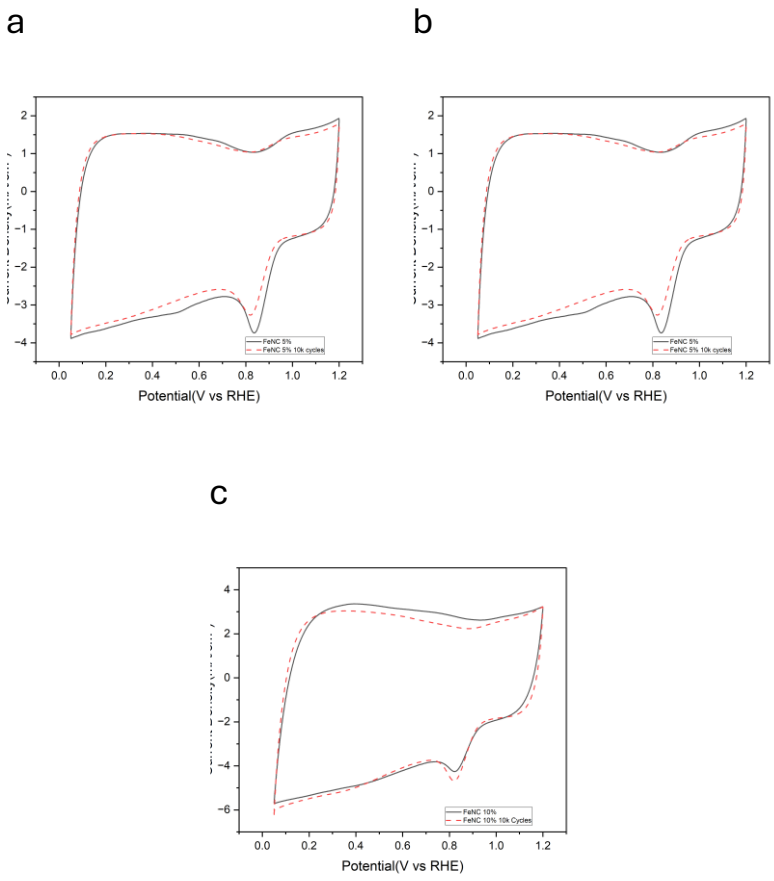

Figure 4.33. CV recorded in an O2 -saturated 0.1M KOH solution at 100mV/s comparing the initial state (0 cycle, black solid line) and post-aging state (10,000 cycles, red dashed line) for: (a) FeNC/Pt 5%, and (b) FeNC/Pt 10%.

Degradation and Activity Losses

Steady-state transport kinetics before and after the aging sweeps were recorded via LSV at a rotation speed of 1600rpm to quantify overpotential development.

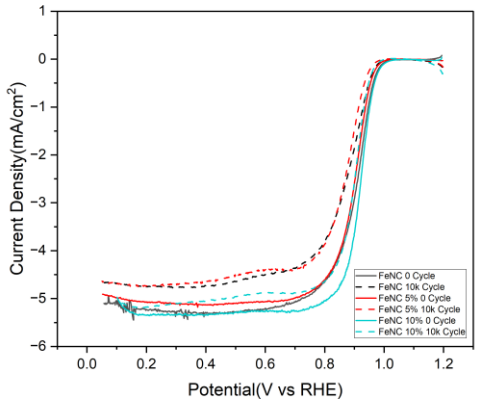

Figure 4.34. LSV curves in an O2-saturated 0.1M KOH solution at 1600rpm and 10mV/s tracking the performance profiles before and after 10k aging cycles for the bare support and platinum-modified catalysts.

The extracted degradation values (Δ_E) for both the onset and half-wave regions are compiled in Table 4.7:

Table 4.7. Kinetic potential degradation parameters after 10k cycles in 0.1M KOH.

Material	***ΔEOnset (V)***	***ΔE1/2 (V)***
FeNC	0.01	0.02
FeNC/Pt 5%	0.01	0.02
FeNC/Pt 10%	0.01	0.02

The hydrodynamic parameters reveal a highly uniform and exceptional stability profile across all tested samples. In stark contrast to the acidic environment where half-wave potentials dropped by up to 120mV all three materials exhibit an identical, ultra-low decay of just 20mV at the half-wave boundary ($E_{1/2}$) and a minor 10mV shift at the onset threshold. Because the bare FeNC support undergoes the exact same nominal shift as the platinum-loaded composites ($E_{1/2}$ = 20mV), the minor degradation observed is entirely governed by the slow surface oxidation of the carbon framework itself, rather than precious metal dissolution or active iron leaching. Furthermore, the diffusion-limited mass-transport plateaus remain tightly bundled near -5 mA/cm^2, proving that the catalytic layer avoids detachment and maintains mechanical adherence under basic operating conditions.

Pathway Resiliency and Selectivity Preservation

The impacts of structural aging on the underlying oxygen reduction pathway were monitored by measuring intermediate hydroperoxide (HO^-_2) generation metrics at the ring electrode.

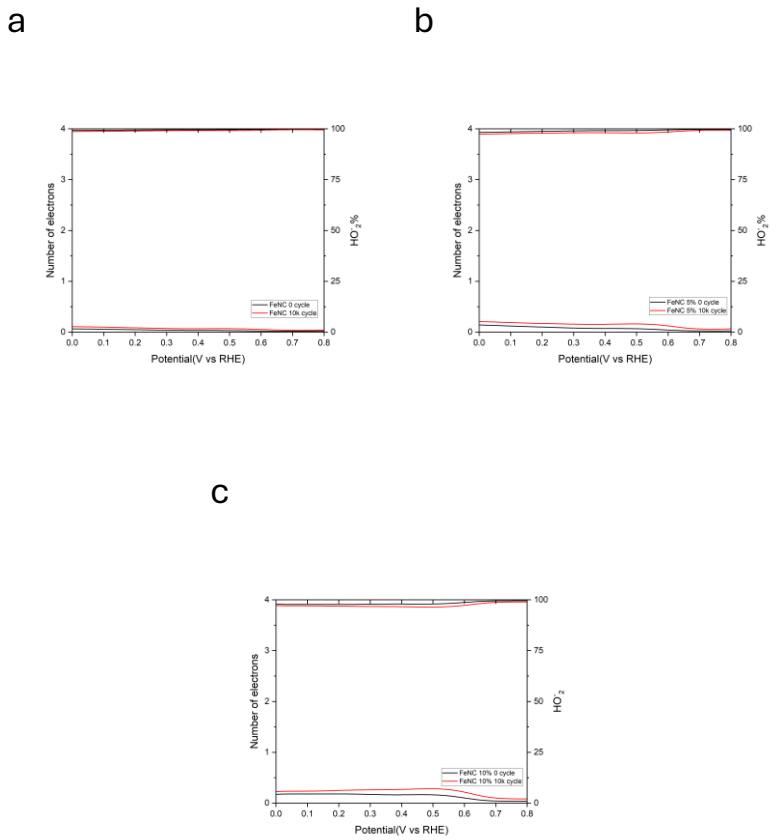

Figure 4.35. RRDE selectivity profiles showing the calculated electron transfer number (n) and intermediate hydroperoxide yield (HO^-_2) before and after 10k potential cycles in alkaline media for: (a) FeNC, (b) FeNC/Pt 5%, and (c) FeNC/Pt 10%.

The cumulative alterations (Δ) in intermediate hydroperoxide yield and electron transfer parameters extracted at a disk potential of 0.5 V vs. RHE are summarized in Table 4.8:

Table 4.8. Alterations in selectivity parameters after 10k cycles at 0.5 V vs. RHE in alkaline medium.

Material	***Δ Peroxide Yield (%)***	***Δn***
FeNC	0.75	0.02
FeNC/Pt 5%	2.00	0.04
FeNC/Pt 10%	2.75	0.05

The ring collection parameters demonstrate outstanding pathway retention post-aging. The bare carbon support exhibits near-zero alteration (Δ Peroxide=0.75%,Δn = 0.02), confirming the absolute stability of the standalone FeN_x and nitrogen coordination sites in base. For the platinum-modified composites FeNC/Pt 5% and 10%), minor increases in peroxide evolution are detected (Δ=2% and 2.75%, respectively), resulting in nominal electron transfer variations (Δn=0.05).

This minimal shift confirms that the active interfacial boundaries are highly protected within the basic matrix. By operating in the absence of aggressive, proton-assisted dissolution paths, the dual active site configuration remains functional, ensuring that the catalyst network

successfully maintains a highly selective, direct four-electron transfer pathway after long-term potential cycling.

4.6 Long-Term Steady-State Chronoamperometric Stability

While accelerated stress testing through potential cycling simulates dynamic, transient load variations, continuous steady-state operation was evaluated via long-term chronoamperometry (CA). This diagnostic test monitors the current-time (i-t) transient profiles over a continuous 4-hour operational duration under a constant cathodic overpotential bias. The evaluation was performed on the primary composite configuration FeNC/Pt 5% alongside the standalone bare FeNC support matrix to contrast the steady-state degradation modes in both acidic (0.1M $HClO_4$) and alkaline (0.1M KOH) environments.

Chronoamperometric Durability in Acidic Media

In the acidic testing environment, both electrocatalysts display a sharp initial current drop during the first 30 minutes of operation, driven by double-layer charging and the rapid initialization of surface intermediate coverage, which subsequently transitions into a gradual decay trend over the remaining test period.

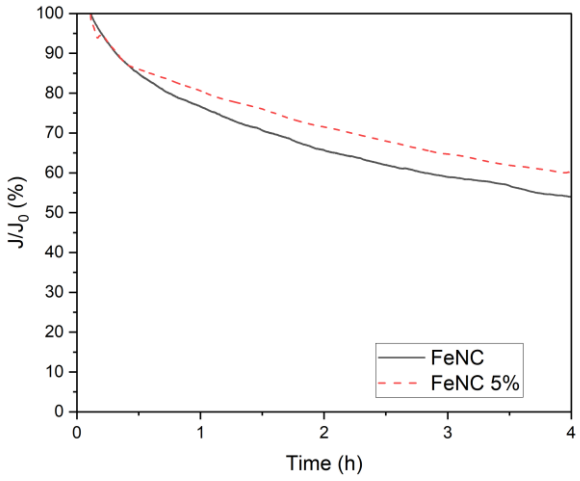

Figure 4.36. Chronoamperometric current density retention (J/J0) profiles recorded over 4 hours in an O2-saturated 0.1M HClO4 solution for the bare FeNC matrix and the FeNC/Pt 5% composite catalyst.

Plain FeNC: The baseline support experiences a continuous drop in relative current density throughout the run, retaining only 54% of its initial current value (J_0) after 4 hours of continuous polarization. This severe performance loss highlights the vulnerability of bare FeN_x and carbon active centres under continuous acidic reduction conditions, where proton-assisted demetallation and the leaching of active iron species degrade the active site population.

FeNC/Pt 5% Composite: The platinum-modified composite catalyst demonstrates superior steady-state stability, maintaining a current density retention of 60% at the 4-hour milestone.

The divergence between the two profiles highlights a protective structural synergy introduced by the 5wt.% platinum nanoparticles. By embedding the precious metal centres uniformly within the open, macrostructure carbon host network, the local charge transfer burden is shared between the coexisting active centres. This spatial distribution minimizes localized overpotential hot-spots, dampens active site leaching, and successfully mitigates the continuous structural decay encountered by the bare framework.

Chronoamperometric Durability in Alkaline Media

When shifted to the oxygen-saturated alkaline electrolyte, the steady-state current-time profiles reveal high operational durability, establishing a clear contrast with the acidic runs.

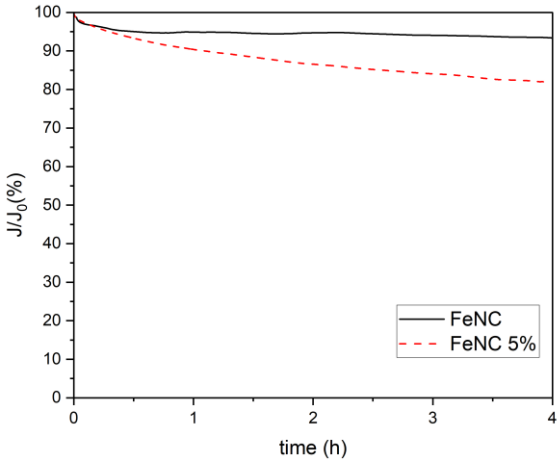

Figure 4.37. Chronoamperometric current density retention (J/J0) profiles recorded over 4 hours in an O2-saturated 0.1M KOH solution for the bare FeNC matrix and the FeNC/Pt 5% composite catalyst.

Plain FeNC: The standalone support displays outstanding steady-state resilience. Following a minor initial stabilization period, the current response flattens out, retaining an exceptional 93.5% of its initial current density at the conclusion of the 4-hour test. This remarkable retention confirms that the non-precious active centres FeN_x coordination envelopes and adjacent nitrogen-doped graphitic domains are naturally thermodynamically stable in basic operating environments, where the complete absence of corrosive hydronium ions prevents active site dissolution.

FeNC/Pt 5% Composite: The composite variant exhibits a smooth, gradual decay curve across the continuous operation period, stabilizing to retain 82% of its initial current response at the 4-hour boundary.

This steady-state alkaline response presents a unique variation from the dynamic potential cycling data. While the FeNC/Pt 5% composite was the clear stability winner under potential cycling, it encounters a slightly higher continuous current decay (82% remaining) compared to the bare carbon support matrix (93.5% remaining) during this steady-state run.

This difference indicates that under an uninterrupted, continuous cathodic overpotential bias in base, the exposed metallic platinum surfaces develop a high steady-state coverage of strongly

adsorbed intermediate hydroxyl species (OH_{ads}). This accumulation acts as a localized surface blocking layer over the platinum sites, causing a minor continuous current attenuation that is completely avoided by the bare, non-precious coordination framework.

Chapter 5

Electrochemical Characterization: GDE

5.1 Gas Diffusion Electrode (GDE) Performance

To bridge the gap between idealized liquid half-cell configurations and practical fuel cell environments, the optimal catalysts were evaluated using a Gas Diffusion Electrode (GDE) architecture. In standard RDE experiments, the ORR is heavily restricted by the low solubility and slow diffusion kinetics of molecular O_2 within flooded liquid boundaries, which artificial chokes the maximum mass-transport current density at approximately -5.5mA/cm^2.

By implementing a gas-fed cell configuration where pure gaseous O_2 is delivered directly through a porous, transport distances are minimized. This design establishes an active triple-phase boundary (coexisting solid catalyst, thin liquid electrolyte layer, and gaseous reactant), unlocking high current density streams scaling into hundreds of milliamperes per square centimetre. Testing was performed from the beginning across both highly concentrated acidic (1M $HClO_4$) and alkaline (1M KOH) media to map out performance boundaries under realistic polarization criteria.

5.1.1 Gas Diffusion Performance in Acidic Media

The interfacial characteristics and capacitive profile of the electrode assemblies within the high-concentration acidic cell were verified via CV under an inert N_2 gas stream prior to active gas-fed polarization sweeps.

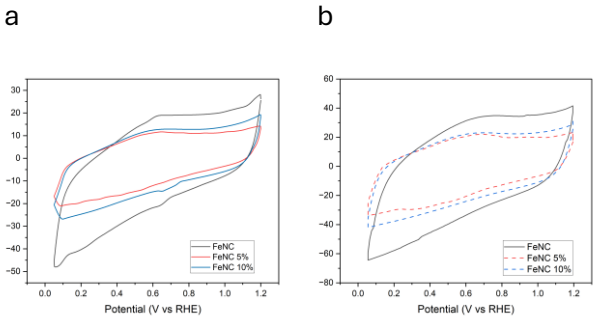

Figure 3.32. CV recorded in the GDE assembly within an N2-saturated 1M HClO4 solution comparing the bare matrix support baseline, FeNC/Pt 5%, and FeNC/Pt 10% at scan rates of: (a) 50mV/s, and (b) 100mV/s.

The voltammetric scans display predictable scan-rate scaling, with double-layer charging responses doubling exactly as the potential sweep accelerates from 50mV/s (20mA/cm^2 at 0.40 V vs. RHE) up to 100mV/s (40mA/cm^2). The bare FeNC support develops the widest open rectangular loop, indicating optimal surface area accessibility and network wetting. Introducing the precious metal fractions yields a controlled, loading-dependent compression of the capacitive baseline, indicating partial local pore modification during high-pressure ink deployment.

Steady-state transport kinetics and maximum current output under direct gas flux were subsequently mapped using LSV fed with pure O_2.

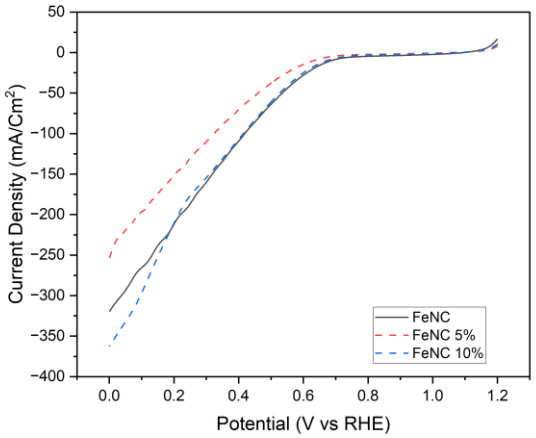

Figure 3.33. Gas-fed LSV curves recorded in an O2-saturated 1M HClO4 solution at a scan rate of 100mV/s tracking the current density profiles.

The explicit GDE kinetic onset potentials extracted from these high-concentration acidic sweeps are summarized in Table 5.1:

Table 5.1. GDE kinetic onset potential values in gas-fed.

Material	***E_{Onset} (V vs. RHE)***
FeNC	0.63
FeNC/Pt 5%	0.56
FeNC/Pt 10%	0.63

The acidic polarization trends confirm excellent high-current scaling:

Kinetic Activation Region: At low overpotentials, the bare support and the high-loading FeNC/Pt 10% composite reach an identical onset threshold of 0.63V, outpacing the intermediate 5% configuration (0.56V). This shows that the native, high-density non-precious FeN_x arrangements smoothly govern the reaction initialization pathways under gas-fed acidic streams.

Mass Transport Region: As the operational potentials drop below 0.40V, the curves bypass the transport chokes seen in liquid cells, climbing continuously into the high-current polarization regime. At 0.0 V vs. RHE, the FeNC/Pt 10% sample drives the highest absolute current output at -365mA/cm^2, followed closely by the bare support at -320mA/cm^2, while the 5% variant stabilizes at -250 mA/cm^2. The high local density of platinum in the 10% matrix provides a vital secondary kinetic boost, lowering resistance inside the triple-phase layer under harsh, high-overpotential conditions.

5.1.2 Gas Diffusion Performance in Alkaline Media

The identical catalyst series was subsequently integrated into a concentrated basic cell to contrast mass-transport performance across media. Surface wetting and active boundaries were similarly checked via inert N_2 sweeps first.

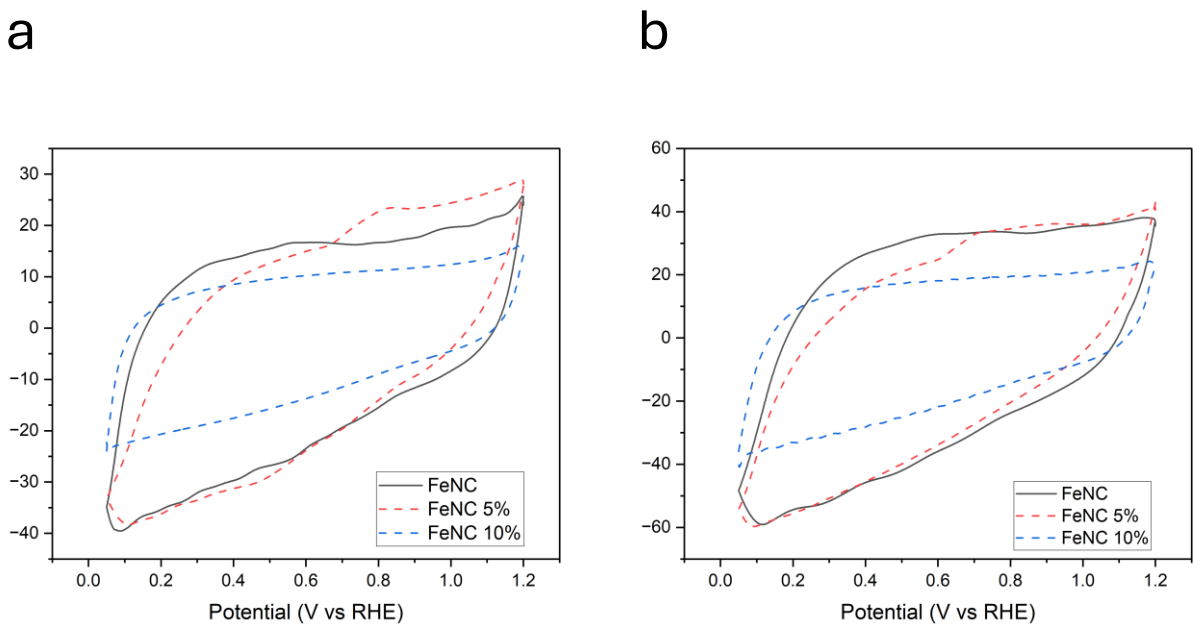

Figure 3.34. CV recorded in the GDE assembly within an N2-saturated 1M KOH solution comparing the bare matrix support baseline, FeNC/Pt 5%, and FeNC/Pt 10% at scan rates of: (a) 50mV/s, and (b) 100mV/s.

Proportional capacitive response is perfectly maintained in the basic medium. The baseline charging current loops double predictably as the scan rate shifts from 50mV/s up to 100mV/s, centred near 20 mA/cm^2 and 40mA/cm^2 at a potential of 0.60 V vs. RHE. The bare support retains the largest double-layer charging signature, confirming excellent structural preservation in basic operational testing.

Active gas-fed transport metrics were then mapped via steady-state LSV under continuous pure O_2 flow.

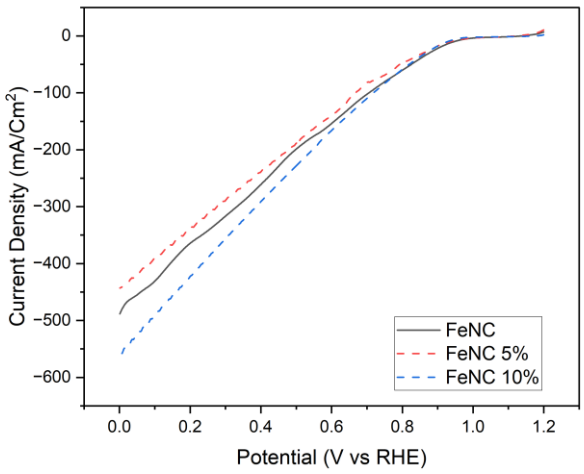

Figure3.35. Gas-fed LSV curves recorded in an O2-saturated 1M KOH solution at a scan rate of 100mV/s tracking the current density profiles.

The explicit GDE kinetic onset potentials derived from these high-concentration alkaline polarization curves are compiled in Table 5.2:

Table 5.2. GDE kinetic onset potential values in gas-fed.

Material	***E_{Onset} (V vs. RHE)***
FeNC	0.91
FeNC/Pt 5%	0.90
FeNC/Pt 10%	0.90

The basic gas-fed polarization metrics show outstanding scaling traits:

Kinetic Activation Region: The standalone FeNC records the most advanced onset potential at 0.91V, slightly leading both platinum-modified composite configurations 0.90V. This outstanding turn-on boundary provides clear proof that the native non-precious coordination sites function with high efficiency under alkaline environments, smoothly driving early-stage reduction pathways without requiring precious metal initiation.

Mass Transport Region: When pushed below 0.60V into concentration polarization zones, the direct gaseous flux allows the curves to climb continuously. At the absolute low-potential boundary (0.0V vs. RHE), the FeNC/Pt 10% composite reaches a peak current density of -560mA/cm^2. The bare support tracks remarkably close behind, generating a massive current output of -480mA/cm^2, while the 5% sample delivers a robust -440mA/cm^2.

This performance confirms that while the native non-precious network handles low overpotentials with ease, the high local density of platinum nanoparticles within the 10% composite provides a crucial secondary charge-transfer path. This coexisting site architecture successfully lowers local concentration polarization resistance, allowing the \$10\%\$ composite catalyst to lead at ultra-high operational current densities under real-world gas-fed criteria.

Chapter 6

conclusion

The structural engineering and optimization of high-efficiency electrocatalysts for the ORR represent critical milestones in advancing low-temperature fuel cell technologies. This thesis systematically investigated the synthesis, structural morphology, and multi-pH electrochemical evaluation of benchmark carbon-supported platinum (Pt/C) controls and advanced FeNC hybrid composite catalysts. By directly contrasting conventional hydrogen-purge thermal reduction with rapid, microwave-assisted volumetric flash reduction across fixed platinum weight fractions (2 wt.%, 5 wt.%, and 10 wt.%), a clear framework correlating synthesis conditions to operational kinetics, pathway selectivity, and long-term durability has been established under both RRDE and GDE setups.

A primary objective of this work was to isolate the structural influence of localized microwave reduction kinetics. Microstructural screening via Field Emission Scanning Electron Microscopy (FESEM) on Pt/C controls confirmed that managing the isothermal dwelling time is crucial for dictating nanoparticle nucleation rates. An abbreviated 2-minute dwelling window (Protocol 1) restricted spatial homogeneity, leading to localized precursor aggregation alongside un-functionalized clearings. In contrast, an optimized 5-minute dwelling block at a fixed 120°C boundary (Protocol 2) facilitated complete chemical reduction and uniform, discrete nanoparticle dispersion while successfully limiting thermal particle migration and detrimental sintering.

Extending this optimized protocol to the lab-made, hard-templated FeNC support host demonstrated exceptional structural replication. FESEM micrographs verified the preservation of highly open, porous, worm-like and rope-like bundled rod arrays dictated by the sacrificial SBA-15 silica template. Thermogravimetric Analysis (TGA) and Inductively Coupled Plasma (ICP) bulk chemical analysis verified that the flash microwave route accurately captured the high-loading target composition (yielding 10.74% inorganic residue for the 10 wt.% nominal sample). Conversely, the conventional hydrogen-purge method induced minor, early-stage gasification of unstable carbon walls, resulting in a slightly enriched relative metal ash fraction (14.63%). Furthermore, TGA confirmed a catalytic combustion effect, where increasing the platinum nanoparticle fraction lowered the thermal activation threshold of the surrounding carbon host lattice.

Hydrodynamic evaluation using RRDE testing highlighted a profound performance divergence based on the underlying solvent-support configurations:

> Acidic Media **(**0.1M $HClO_4$**):** On the carbon black (Pt/C) controls, microwave synthesis provided a distinct kinetic advantage at ultra-low metal loading boundaries, shifting the Pt/C 2% half-wave potential ($E_{1/2}$) upward to 0.67 V vs. RHE compared to 0.58 V for the hydrothermal equivalent. Within the hybrid FeNC/Pt composite matrix, the hydrogen-reduced 10 wt.% sample yielded the highest immediate kinetic acceleration (E_{Onset}=0.83 V ,$E_{1/2}$=0.73V). However, at 5 wt.% and 2 wt.% loadings, the microwave-reduced series maintained superior kinetic stability ($E_{1/2}$=0.63V and 0.62 V) over their decaying hydrothermal counterparts.

Alkaline Media **(**0.1M KOH**):** The standalone, non-precious FeNC matrix exhibited remarkable intrinsic activity, achieving an E_{Onset} of 0.99 V and an $E_{1/2}$ of 0.92 V, thus outperforming several platinum-bearing controls. While hydrogen-purge reduction pushed the composite onset to an exceptional 1.01 V (10 wt.%), the microwave-reduced 2 wt.% composite (FeNC/Pt2%) established a highly active interfacial alignment that outpaced its intermediate 5 wt.% alternative.

Four-electrode ring collection metrics demonstrated highly protected, efficient reaction pathways. In the 0.1M $HClO_4$ environment, the microwave-reduced composite series showcased a critical mechanistic advantage; despite generating elevated intermediate peroxide yields at low loading fractions, the calculated electron transfer number (*n*) remained robustly locked at 4.0 for both 10 wt.% and 2 wt.% variants, confirming a direct, complete four-electron reduction pathway. In alkaline media, the hydrogen-purge method suppressed intermediate peroxide evolution below 5% at low metal fractions (*n=3.9*), while the microwave series highlighted a unique structural optimization at the 2 wt.% threshold, dropping peroxide release to 4.79%.

Accelerated Stress Testing (AST) via 10,000 continuous dynamic potential cycles (0.6 V to 1.0 V vs. RHE) mapped unique durability patterns under operating stress:

In Acidic Media**,** the FeNC/Pt 5% composite emerged as the most resilient configuration. While the bare support suffered a severe 90 mV $E_{1/2}$ decay, the 5 wt.% platinum addition limited half-wave degradation to just 40 mV. This performance exposes a powerful structural synergy where lower precious metal fractions actively suppress carbon matrix oxidation and stabilize adjacent FeN_x centres. In contrast, higher local nanoparticle densities (10 wt.%) accelerated metal dissolution and Ostwald ripening ($\Delta E_{1/2}$=70mV).

In Alkaline Media**,** all catalyst architectures exhibited exceptional, uniform stability, experiencing an identical, ultra-low $E_{1/2}$ loss of only 20 mV. This confirms that basic operational conditions bypass corrosive hydronium-driven active iron leaching and platinum dissolution, tying minor losses strictly to the slow surface oxidation of the graphitic host carbon matrix.

Continuous 4-hour steady-state Chronoamperometric (CA) polarization highlighted a subtle divergence from the dynamic cycling runs. In acid, FeNC/Pt 5% maintained superior current retention (60%) over the bare matrix (54%), validating shared interfacial charge transfer. However, in alkaline media, the plain FeNC matrix was the absolute durability champion, retaining an exceptional 93.5% of its initial current density (J_0) compared to 82% for the 5 wt.% composite. This steady-state current attenuation on the platinum-modified surface is attributed to the accumulation of strongly adsorbed hydroxyl species (OH_{ads}) that induce localized surface blocking—a degradation mechanism completely avoided by the naturally stable, non-precious coordination framework in base.

To bridge the gap to practical applications, evaluation within a Gas Diffusion Electrode (GDE) half-cell unlocked massive current density streams by constructing a functional triple-phase boundary:

Acidic GDE Streams (1M $HClO_4$)**:** The native non-precious FeN_x configurations governed early-stage activation, matching the 0.63 V kinetic onset of the high-loading composite. Driven past mass-transport limitations, the 10 wt.% matrix yielded the highest current

density output of -365 mA/cm^2 at 0.0 V vs. RHE, followed by the bare support at -320 mA/cm^2.

Alkaline GDE Streams (1M KOH): The plain FeNC support led the activation region with a highly advanced kinetic onset potential of 0.91 V. At the absolute mass-transport boundary (0.0 V vs. RHE), the high local density of platinum nanoparticles within the 10 wt.% composite provided a crucial secondary charge-transfer network, lowering concentration polarization resistance to reach a peak current density of -560 mA/cm^2, with the bare support trailing closely behind at a massive -480 mA/cm^2.

In conclusion, this thesis demonstrates that the rational integration of low-weight-fraction platinum nanoparticles with highly porous, hard-templated FeNC matrices offers a viable, future-proof pathway toward reducing precious metal usage without compromising performance.

For acidic systems, a clear sweet-spot is isolated at an intermediate 5 wt.% loading processed via microwave reduction, which maximizes the structural synergy needed to shield the carbon support and maintain a direct 4-electron pathway.

For alkaline applications, the extraordinary standalone performance of the native FeNC matrix minimizes the necessity for precious metal additions at low overpotentials, though ultra-low metal boundaries (2 wt.% microwave or 10 wt.% GDE configurations) provide essential secondary charge-transfer pathways required to sustain extreme current densities.

References

[1] “Climate change due to increasing concentration of carbon dioxide and its impacts on environment in 21st century; a mini review.,” *Journal of King SaudUniversity- Science, 35(5):102693, 2023..*

[2] M. a. W. Eberhardt., “A simple model for the prediction of co2 concentrations in the atmosphere, depending on global co2 emissions.,” *European Journal of Physics, 45(2):025803, ,* feb 2024..

[3] B. K. S. O. O. S. M. M. a. A. R. Cem I¸sık, “The volatility of global energy uncertainty: Renewable alternatives.,” *Energy, 297:131250, 2024..*

[4] A. C. Lewis., “Optimising air quality co-benefits in a hydrogen economy:a case for hydrogen-specific standards for nox emissions. Environ.,” *Sci.:Atmos., 1:201–207, 2021..*

[5] E. Society., “Fuel cells: Proton exchange membrane fuel cells(pemfcs),” *https://knowledge.electrochem.org/encycl/art-f04-fuel-cells-pem.htm, n.d. Accessed: 2024-10-08..*

[6] V. V. a. J. K. N. Heine A. Hansen, “Unifying kinetic and thermodynamic analysis of 2 e– and 4 e– reduction of oxygen on metal surfaces.,” *The Journal of Physical Chemistry C, 118(13):6706-6718, 2014..*

[7] G. L. Y. Z. Q. L. T. Z. G. S. M. a. Ruguang Ma, “A review of oxygen reduction mechanisms for metal-free carbon-based electrocatalysts.,” *Nature, 5(78), 2019..*

[8] E. P. M. L. a. J.-P. D. F. Jaouen, “"Recent advances in non-precious metal catalysis for oxygen reduction in PEM fuel cells," .,,” *Energy Environ. Sci,* Vols. vol. 4, no. 1, pp. 114–130, Jan. 2011, doi: 10.1039/C0EE00011F..

[9] S. S. K. B. S. a. F. T. W. H. A. Gasteiger, “"Activity benchmarks and requirements for Pt, Pt-alloy, and non-Pt oxygen reduction catalysts for PEMFCs,",” *Appl. Catal. B Environ.,,* Vols. vol. 56, no. 1-2, pp. 9–35, Mar. 2005, doi: 10.1016/j.apcatb.2004.07.012..

[10] J. K. Nørskov et al., “"Origin of the Overpotential for Oxygen Reduction at a Fuel-Cell Cathode,",” *J. Phys. Chem. B,,* Vols. vol. 108, no. 46, pp. 17886–17892, Nov. 2004, doi: 10.1021/jp047349j..

[11] “J. C. Meier et al., "Design criteria for stable Pt/C fuel cell catalysts," Beilstein J. Nanotechnol., vol. 5, pp. 44–67, Jan. 2014, doi: 10.3762/bjnano.5.5.”.

[12] “A. Zitolo et al., "Identification of catalytic sites in cobalt-nitrogen-carbon materials for the oxygen reduction reaction," Nature Mater., vol. 14, no. 9, pp. 937–942, Sep. 2015, doi: 10.1038/nmat4306.”.

[13] “U. A. Paulus, T. J. Schmidt, H. A. Gasteiger, and R. J. Behm, "Oxygen reduction on a high-surface area Pt/Vulcan carbon catalyst: a rotating disk electrode study," J. Electroanal. Chem., vol. 495, no. 2, pp. 134–145, Jan. 2001, doi: 10.1016/S0022-0728(00)”.

[14] “J. J. Pinaud et al., "Liquid Asymmetric Electrochemical Cell for High-Mass-Transport Gas Diffusion Electrode Electrocatalysis Evaluation," J. Electrochem. Soc., vol. 164, no. 4, pp. F321–F333, Mar. 2017, doi: 10.1149/2.0591704jes.”.

[15] “M. Inaba et al., "Effect of Hydrogen Peroxide on Degradation of Nafion Membranes," Electrochim. Acta, vol. 51, no. 26, pp. 5746–5753, Aug. 2006, doi: 10.1016/j.electacta.2006.03.018.”.

[16] “A. J. Bard and L. R. Faulkner, Electrochemical Methods: Fundamentals and Applications, 2nd ed. New York, NY, USA: John Wiley & Sons, 2001.”.

[17] “J. Li et al., "Atomically dispersed Fe-N-C catalysts for proton exchange membrane fuel cells: Glow and fade," ACS Catal., vol. 11, no. 7, pp. 3910–3940, Apr. 2021, doi: 10.1021/acscatal.1c00216.”.

[18] “X. Wang et al., "Oxygen Reduction Catalyzed by Pt Nanoparticles Confined in Mesoporous Carbon Supports Doped with Single Fe Atoms," ACS Appl. Nano Mater., vol. 6, no. 18, pp. 16550–16558, Sep. 2023, doi: 10.1021/acsanm.3c03016.”.

[19] “D. Zhao et al., "Nonionic Triblock Copolymer Synthesis of Oligomeric Silica with Large Cylindrical Mesoporous Channels," Science, vol. 279, no. 5350, pp. 548–552, Jan. 1998, doi: 10.1126/science.279.5350.548.”.

[20] “Y. Wan and D. Zhao, "On the controllable soft-templating approach to mesoporous silicates," Chem. Rev., vol. 107, no. 7, pp. 2821–2860, Jul. 2007, doi: 10.1021/cr068020s.”.

[21] “M. Lefèvre, E. Proietti, F. Jaouen, and J.-P. Dodelet, "Iron-Based Catalysts with Improved Oxygen Reduction Activity in Polymer Electrolyte Fuel Cells," Science, vol. 324, no. 5923, pp. 71–74, Apr. 2009, doi: 10.1126/science.1170051.”.

[22] “E. Antolini, "Carbon supports for low-temperature fuel cell catalysts," Appl. Catal. B Environ., vol. 40, no. 1, pp. 1–37, Jan. 2003, doi: 10.1016/S0926-3373(02)00142-1.”.

[23] F. B. M. T. M. T. J. a. F. K. Remy Guillet-Nicolas, “ Selectively tuned pore condensation and hysteresis behavior in mesoporous sba-15 silica: Correlating material synthesis to advanced gas adsorption analysis. The Journal of Physical Chemistry C121(44):24505–24526, 2017.”.

[24] S. S. a. P. A. José H. Zagal, “Mapping transition metal-mn4 macrocyclic complex catalysts performance for the critical reactivity descriptors. Current Opinion in Electrochemistry, 27:100683, 2021.”.

[25] H. L. C. L. L. Z. C. L. J.-O. W. S. L. Y. H. L. G. J. Q. a. D. W. Yu Xiong, “Single-atom fe catalysts for fenton-like reactions: Roles of different n species.,” *Advanced Materials, 34(17):2110653.*.

[26] G. Gianola, *Advanced FeNC Catalysts for Oxygen Reduction Reactions in PEM Fuel Cells: Synthesis and Performance Evaluation,* Turin: Poilitecnico di Torino, 2025.

[27] A. Z. T. V. S. F. M. a. D. S. Ulrike I. Kramm, “On the structural composition and stability of fe–n–c catalysts prepared by an intermediate acid leaching.,” *Journal of Solid State Electrochemistry, 20(4):969–981, oct 2015.*.

[28] G. Gianola, *Advanced FeNC Catalysts for Oxygen Reduction Reactions in PEM Fuel Cells: Synthesis and Performance Evaluation,* Turin: Politecnico di Torino, 2025.

[29] G. J. l. O. M. Y. S.-H. e. a. P. J. Ferreira, “"Instability of Pt/C Electrocatalysts in Proton Exchange Membrane Fuel Cells: A Mechanistic Investigation,"," *J. Electrochem. Soc., vol. 152, no. 11, pp. A2256–A2271, Sep. 2005, doi: 10.1149/1.20505.*

[30] C. Feldmann, “"Polyol-Mediated Synthesis of Nanoscale Functional Materials,"," *Adv. Mater., vol. 15, no. 12, pp. 1014–1018, Jun. 2003, doi: 10.1002/adma.200301639..*

[31] J. P. Pinheiro et al., “"Effects of the gaseous atmosphere during the thermal preparation of Pt/C electrocatalysts,"," *J. Solid State Electrochem., vol. 18, no. 5, pp. 1245–1255, May 2014, doi: 10.1007/s10008-013-2310-7..*

[32] Y. C. a. M. W. K. Xiaoquan Min, “Alkaline o2 reduction on oxide-derived au: high activity and 4e selectivity without (100) facets.,” *Phys. Chem. Chem. Phys., 16:13601–13604, 2014..*

[33] Y. W. F. L. J. C. a. S. M. A. R. Sharma, “"Particle size-controlled growth of carbon-supported platinum nanoparticles (Pt/C) through water-assisted polyol synthesis,"," Vols. ACS Omega, vol. 4, no. 13, pp. 15711–15720, Aug. 2019, doi: 10.1021/acs.

[34] J.-J. W. a. M.-C. T. K.-Y. Shih, “"One-step microwave-assisted synthesis of PtNiCo/rGO electrocatalysts with high electrochemical performance for direct methanol fuel cells,"," *Nanomaterials,* Vols. , vol. 11, no. 9, p. 2206, Aug. 2021, doi: 10.3390/nano1109220.

[35] H. Zhao et al., “"Rapid preparation of platinum catalyst in low-temperature molten salt using microwave method for formic acid catalytic oxidation reaction,"," *Molecules, ,* Vols. vol. 29, no. 21, p. 5128, Oct. 2024, doi: 10.3390/molecules29215128..

[36] V. S. M. L. G. L. C. L. a. B. W. L. Strandberg, “"Comparison of oxygen adsorption and platinum dissolution in acid and alkaline solutions using electrochemical quartz crystal microbalance,"," *ChemElectroChem, ,* Vols. vol. 9, no. 18,.

[37] E. L. S. H. S. M. a. Q. J. L. Jiao, “"Compressive strain reduces the hydrogen evolution and oxidation reaction activity of platinum in alkaline solution,"," *ACS Catalysis, ,* Vols. vol. 11, no. 13, pp. 8165–8173, Jun. 2021, doi: 10.1021/acscatal.1c017.

[38] M. C. a. D. C. J. Li, “ "Atomically dispersed Fe-N-C catalysts for proton exchange membrane fuel cells: Progress and perspectives,"," *Energy & Environmental Science, ,* Vols. vol. 14, no. 1, pp. 50–78, Jan. 2021, doi: 10.1039/D0EE02737C..

[39] Y. Shao et al., “"Design and synthesis of hierarchically porous Fe-N-C catalysts for highly efficient oxygen reduction reaction,"," *Journal of Materials Chemistry A, ,* Vols. vol. 8, no. 33, pp. 16701–16715, Aug. 2020, doi: 10.1039/D0TA04561D..